RISK-BASED METHODOLOGY FOR STRUCTURAL EVALUATION OF BRIDGE-SIZED CULVERTS

TECHNICAL REPORT DOCUMENTATION PAGE

1. Report No. https://archives.pdx.edu/ds/psu/43838	2. Government Accession No.	3. Recipient's Catalog No.
4. Title and Subtitle Risk-Based Methodology for Structural Evaluation of Bridge-Sized Culverts		5. Report Date February 7, 2025 6. Performing Organization Code:
7. Author(s) David Y. Yang (ORCID: 0000-0003-0959-6333) Portland State University Kevin White (ORCID: 0000-0002-2902-2524) E.L. Robinson Engineering of Ohio Timothy A. Wood (ORCID: 0000-0002-3926-7314) The Citadel, The Military College of South Carolina		8. Performing Organization Report No.
9. Performing Organization Name and Address Portland State University Department of Civil and Environmental Engineering 1920 SW 4th Avenue, Suite 200 Portland, OR 97201 DUNS: 052226800		10. Work Unit No. 11. Contract or Grant No. 693JJ321C000036
12. Sponsoring Agency Name and Address Office of Bridges and Structures Federal Highway Administration 1200 New Jersey Ave SE Washington, DC 20590		13. Type of Report and Period 14. Sponsoring Agency Code
15. Supplementary Notes FHWA Technical Manager: Lubin Gao, Ph.D., P.E. FHWA Contracting Officer Representative (COR): Tuonglinh (Linh) Warren, P.E. Technical Advisory Panel: Jason Hastings, DelDOT; Yihong Gao, MnDOT; Ruben Boehler, Illinois DOT; Biniam Aregawi, TxDOT; Josh Beakley, ACPA; Tony Zhang, Caltrans; Matt Farrar, Idaho Transportation Department (retired); Murugesu Vinayagamoorthy, Caltrans (retired); David Garber, FHWA; Thomas Saad, USDOT		
16. Abstract This report presents the results of the project sponsored by the Federal Highway Administration (FHWA), "Risk-Based Methodology for Structural Evaluation of Bridge-Sized Culverts". The goal of this project was to develop general methodology to (a) quantify uncertainty, especially live load uncertainty, unique to bridge-sized RC box culverts and (b) analyze and calibrate reliability of culverts rated under different rating loads. Over 344 combinations of culvert designs and backfill depths were analyzed based on the AASHTO Manual for Bridge Evaluation as well as the three-dimensional finite element models (FEMs) of the soil-culvert systems. For each combination, a wide range of vehicle loads was examined including axle groups detected in weight-in-motion (WIM) data, the HL93 design loads, the AASHTO legal loads, and the FAST Act emergency vehicles as surrogate loads. The methodology laid out in this project was illustrated with analyses on the top slab of culverts, primarily focusing on the positive bending moment at midspan.		
17. Key Words Bridge-sized culverts; Load rating; Uncertainty quantification; Reliability analysis	18. Distribution Statement No restrictions.	

19. Security Classif. (of this report) Unclassified	20. Security Classif. (of this page) Unclassified	21. No. of Pages	22. Price

Form DOT F 1700.7 (8-72) Reproduction of completed page authorized.

SI* (MODERN METRIC) CONVERSION FACTORS

APPROXIMATE CONVERSIONS TO SI UNITS

Symbol	When You Know	Multiply By	To Find	Symbol
		LENGTH		
in	inches	25.4	millimeters	mm
ft	feet	0.305	meters	m
yd	yards	0.914	meters	m
mi	miles	1.61	kilometers	km
		AREA		
in^2	square inches	645.2	square millimeters	mm^2
ft^2	square feet	0.093	square meters	m^2
yd^2	square yard	0.836	square meters	m^2
ac	acres	0.405	hectares	ha
mi^2	square miles	2.59	square kilometers	km^2
		VOLUME		
fl oz	fluid ounces	29.57	milliliters	mL
gal	gallons	3.785	liters	L
ft^3	cubic feet	0.028	cubic meters	m^3
yd^3	cubic yards	0.765	cubic meters	m^3
		NOTE: volumes greater than 1000 L shall be shown in m^3		
		MASS		
oz	ounces	28.35	grams	g
lb	pounds	0.454	kilograms	kg
T	short tons (2000 lb)	0.907	megagrams (or "metric ton")	Mg (or "t")
		TEMPERATURE (exact degrees)		
^oF	Fahrenheit	5 (F-32)/9 or (F-32)/1.8	Celsius	^oC
		ILLUMINATION		
fc	foot-candles	10.76	lux	lx
fl	foot-Lamberts	3.426	candela/m^2	cd/m^2
		FORCE and PRESSURE or STRESS		
lbf	poundforce	4.45	newtons	N
lbf/in^2	poundforce per square inch	6.89	kilopascals	kPa

APPROXIMATE CONVERSIONS FROM SI UNITS

Symbol	When You Know	Multiply By	To Find	Symbol
		LENGTH		
mm	millimeters	0.039	inches	in
m	meters	3.28	feet	ft
m	meters	1.09	yards	yd
km	kilometers	0.621	miles	mi
		AREA		
mm^2	square millimeters	0.0016	square inches	in^2
m^2	square meters	10.764	square feet	ft^2
m^2	square meters	1.195	square yards	yd^2
ha	hectares	2.47	acres	ac
km^2	square kilometers	0.386	square miles	mi^2
		VOLUME		
mL	milliliters	0.034	fluid ounces	fl oz
L	liters	0.264	gallons	gal
m^3	cubic meters	35.314	cubic feet	ft^3
m^3	cubic meters	1.307	cubic yards	yd^3
		MASS		
g	grams	0.035	ounces	oz
kg	kilograms	2.202	pounds	lb
Mg (or "t")	megagrams (or "metric ton")	1.103	short tons (2000 lb)	T
		TEMPERATURE (exact degrees)		
^oC	Celsius	1.8C+32	Fahrenheit	^oF
		ILLUMINATION		
lx	lux	0.0929	foot-candles	fc
cd/m^2	candela/m^2	0.2919	foot-Lamberts	fl
		FORCE and PRESSURE or STRESS		
N	newtons	0.225	poundforce	lbf
kPa	kilopascals	0.145	poundforce per square inch	lbf/in^2

TABLE OF CONTENTS

LIST OF FIGURES

LIST OF TABLES

LIST OF ABBREVIATIONS AND SYMBOLS

2D, 3D	two-dimensional, three-dimensional
AASHTO	American Association of State Highway and Transportation Officials
CDF	cumulative distribution function
CFR	Code of Federal Regulations
CIP	cast-in-place
COV	coefficient of variation
DC	dead load (effect) of structural and nonstructural components
DOF	degree of freedom
DOT	Department of Transportation
EH	horizontal earth pressure load (effect)
ES	earth surcharge load (effect)
EV	vertical earth pressure load (effect)
FAST Act	Fixing America's Surface Transportation Act (Pub. L.114-94)
FEM	finite element model
FHWA	Federal Highway Administration
FORM	first order reliability method
FOSM	first order second moment
GDF	girder distribution factor
GVW	gross vehicle weight
iHLRF	improved Hasofer-Lind-Rackwitz-Fiessler (algorithm)
IM	vehicular dynamic load allowance
LL	vehicular live load (effect)
LLDF	live load distribution factor
LS	live load surcharge load (effect)
LRFD	load and resistance factor design
LRFR	load and resistance factor rating

MBE	Manual for Bridge Evaluation
MPF	multiple presence factor
NCHRP	National Cooperative Highway Research Program
RC	reinforced concrete
RF	rating factor
STD	standard deviation
UQ	uncertainty quantification
WIM	weigh-in-motion
$\alpha_R, \alpha_{DL}, \alpha_{LL}$	sensitivity factors of resistance, permanent, and live load effects
β, β_T	reliability index, target reliability index
γ_{DL}, γ_{LL}	load factors for permanent and live load effects
$\gamma_{DC}, \gamma_{EV}, \gamma_{EH}$	load factors for DC, EV, and EH
ϕ	resistance factor
Φ	CDF of standard normal distribution
p_f	failure probability
D	backfill depth
l_t, w_t	length (along traffic direction) and width of tire patch
R, DL, LL	resistance (load-carry capacity), permanent, and live load effects
S, H, T, U	clear cell span, clear cell height, slab thickness, and wall thickness
S_g, L	girder spacing, girder span
s_a	spacing between two axles
s_w	spacing between two wheels in one axle
V_{coef}	COV of soil pressure coefficient
V_{data}	COV due to limited WIM data
$V_{density}$	COV of soil density
V_{depth}	COV of backfill depth

V_{site}	COV to reflect site-to-site variation
V_{soil}	COV of the load distribution model due to uncertainty in soil property
$\bar{X}$, X_n	mean and nominal values of a random variable X
σ_X, V_X, b_X	STD, COV, and bias factor of random variable X

RISK-BASED METHODOLOGY FOR STRUCTURAL EVALUATION OF BRIDGE-SIZED CULVERTS

SUMMARY

This report presents the results of the project sponsored by the Federal Highway Administration (FHWA), "Risk-Based Methodology for Structural Evaluation of Bridge-Sized Culverts". The goal of this project is to develop general methodology to (a) quantify uncertainty, especially live load uncertainty, unique to bridge-sized RC box culverts and (b) analyze and calibrate reliability of culverts rated under different rating loads. To this end, over 300 combinations of culvert designs and backfill depths were analyzed based on the American Association of State Highway and Transportation Officials (AASHTO) Manual for Bridge Evaluation[1] (AASHTO, 2018) as well as the three-dimensional finite element models (FEMs) of the soil-culvert systems. For each combination, a wide range of vehicle loads was examined including axle groups detected in weigh-in-motion (WIM) data, the HL-93 design loads, the AASHTO legal loads, and the Fixing America's Surface Transportation (FAST) Act emergency vehicles as surrogate loads. The methodology laid out in this project is illustrated with analyses on the top slab of culverts, primarily focusing on the positive bending moment at midspan. Nonetheless, the work can be extended using the same general procedures to other cross sections, load effects, and types of culverts.

For uncertainty quantification, the project delineated and quantified the unique characteristics of the uncertainties in culvert resistance, the permanent load effect, and the vehicular live load effect. Based on the project results, distinct differences between culverts and bridges are summarized as follows:

- For permanent load effects, the predominant components in culverts are the load effects due to vertical and horizontal earth pressure, which are not present in bridge superstructure. Based on existing literature on soil property uncertainties and analysis results in this project, the permanent load effect has a quantified coefficient of variation (COV) ranging from 8.1% to 14.9%, averaging at 10.3%. This variation is slightly higher than the dead load effect due to the self-weight of reinforced concrete (8-10%) but lower than that due to the self-weight of wearing surfaces (around 25%).
- For live load effects, culverts differ more significantly from bridges. The total COV of the midspan bending moment in culverts is around 25%, while for bridges this value is around 13% to 19% (NCHRP Reports 454 and 700). More specifically, the analyses targeted two major sources of uncertainties unique to culverts:
  - The load effects in culverts are predicted based on a live load distribution model through the backfill soil and a two-dimensional frame analysis. The current load and resistance factor design (LRFD) live load distribution model results in very conservative load effects, on average 44.68% higher than the load effects estimated with FEMs. Moreover, the level of conservatism varies significantly with respect to the clear cell span of culverts, ranging from 11% for culverts with short-span cells to 73% for culverts with long-span cells. The uncertainty contrasts with that associated with the line beam analysis and girder

[1] The Manual for Bridge Evaluation, 3rd Edition (2018), is incorporated by reference in 23 CRF 650.317.

distribution factors, which are less conservative and exhibit more uniform conservatism across different girder spans and spacings.

- Due to the relatively short span of culverts, most culverts are controlled by the weight and configuration of axle groups instead of those of vehicles (as for bridges). The project found that when the load spectrum is constructed with axle group statistics, the load effect under one heavy axle passage shows slightly greater variation, with COV averaging at 45%, than that for bridges under one heavy truck, with average COV around 35% (NCHRP Report 368, Fig. B-12). Nonetheless, the projected maximum in a reference period at one specific WIM site is similar, both with around 3% COV, due to the greater number of axle groups than vehicles. However, the site-to-site variation of the projected maximum, averaging around 17% in terms of COV, is noticeably higher than that for bridges, which ranges from 5% to 10%.

The distinct uncertainties associated with culverts influence the structural reliability and the value of the necessary live load factors that can meet the target reliability. Based on the uncertainty quantification results, the reliability of culverts differs from that of bridges due to the increased live load COV, the conservatism associated with the LRFD load distribution model, as well as the greater permanent load effects compared to bridges. Using the first order reliability method implemented with the improved Hasofer-Lind-Rackwitz-Fiessler (iHLRF) algorithm, the project examined the culvert reliability and the existing live load factors for load rating. A new approach was developed for calibrating the live load factors to match the target reliability index. The following findings are highlighted:

- For load rating under design loads, the existing live load factor for the inventory level (1.75) yields an average reliability index of 3.75 for culverts analyzed in the project. This is higher than the target reliability index of 3.5. The existing live load factor for the operating level (1.35) corresponds to an average reliability index of 3.29, which is higher than the target reliability index of 2.5. Hence, the live load factor for operating rating was calibrated. The calibrated load factor decreases with increasing cell spans and backfill depths. It ranges from 0.54 to 1.42, averaging at 0.90 and with most values below the existing value of 1.35. The resulting average reliability index is 2.56, and the reliability level exhibits less variation.
- With a live load factor of 2.0, the AASHTO legal loads result in an average reliability index of 2.95, higher than the target reliability index of 2.5. Additionally, the reliability level of all culverts shows a great amount of variation, with values as low as 1.35 for culverts with small cell spans and shallow backfills. The high variation and low extremes can be attributed to the axle configuration and lower axle weight of AASHTO legal loads, which cause a lower nominal load effect than the expected maximum load effect in 5 years. With calibration, the variation can be significantly reduced while maintaining an average reliability index of 2.53. The calibrated live load factor averages at 1.54 and varies between 0.92 and 2.42, and it also decreases with cell spans and backfill depths.
- For load rating under the FAST Act emergency loads, a live load factor of 2.0 was examined. This live load factor results in an average reliability index of 4.27, which is significantly higher than the target reliability index of 2.5. This is primarily due to the heavy weights of axle groups in the emergency vehicles. With calibration, the average reliability index can be adjusted to 2.51 using a backfill- and cell span-dependent live load factor. The calibrated load factor ranges from 0.52 and 1.35, averaging at 0.86. The calibrated factors are consistently lower than 2.0

used for AASHTO legal loads and also mostly smaller than the live load factor of 1.30 used for bridges.

CHAPTER 1

INTRODUCTION

1.1 BACKGROUND AND RESEARCH PROBLEM STATEMENT

Culverts are important components of the transportation infrastructure. Among the entries in the National Bridge Inventory (NBI), bridge-sized culverts (i.e., with total span greater than 20 ft) account for more than 20% of all bridge assets (Mlynarski et al., 2019). There are also many smaller culverts in service with a total span below 20 ft.

To load rate culverts, the AASHTO Manual for Bridge Evaluation[1] (hereafter referred to as the MBE) (AASHTO, 2018) specifies a set of live load factors originally developed using girder bridges (Mlynarski et al., 2011; Moses, 2001; Nowak, 1999). This implies a similar level of uncertainties between girder bridges and culverts. However, the load effect in culverts differ considerably from those in bridges in the following aspects:

- **Estimation of load effects:** Unlike bridges, culverts are buried structures with backfill soil that complicates the estimation of loads on the surface of culverts. The AASHTO LRFD Bridge Design Specifications[2] (hereafter referred to as the LRFD Specifications) (AASHTO, 2020), referenced by the MBE for rating, include a practical method to estimate the distribution of wheel load through backfill soil. However, this load distribution model results in very conservative estimation of load effect compared to both load testing results (Ulger et al., 2020) and the previous load distribution model used in the load factor design and rating (Miller and Durham, 2008).
- **Dominating load pattern:** due to the relatively short span of culverts compared to girder bridges, the load effects in culverts are primarily controlled by the weight and configuration of axle groups instead of the gross vehicle weight and vehicle configuration considered for bridge design and evaluation. As a result, the load spectrum for culverts is different from that for bridges, which in turn may result in different uncertainty characteristics of maximum load effects within a reference period.

Due to these differences, both the uncertainty in the live load effects and the resulting structural reliability are re-examined, and the live load factors for load rating culverts are calibrated if suggested from the reliability results. The goal of this project is to conduct analyses and investigations with the following objectives:

- To quantify uncertainties of the live load effects that account for the unique characteristics of culverts and their design and evaluation;
- To evaluate structural reliability of culverts in terms of reliability indices considering the unique uncertainty models of culvert live load effects;

[1] The Manual for Bridge Evaluation, 3rd Edition (2018), is incorporated by reference in 23 CFR 650.317.

[2] AASHTO LRFD Bridge Design Specifications, 8th Edition (2017), is incorporated by reference in 23 CFR 625.4(d)(1)(v).

- To enable calibration of live load factors used for load rating culverts based on the target reliability index and live load uncertainties.

By fulfilling these objectives, the results from this project form a general methodology for risk-based structural evaluation of bridge-sized culverts.

1.2 PROJECT SCOPE

This project focuses on the analysis of reinforced concrete (RC) box culverts, which accounts for a large proportion of all bridge-sized culverts. Nonetheless, the general methodology developed in this project can be extended to other types of culverts.

Compared to recent efforts on culvert evaluation, e.g., NCHRP Project 15-54 (Mlynarski et al., 2019), the present project does not intend to propose new or refine existing analytical models for loads on culverts. Rather, the focus is on the systematic quantification of various uncertainties arising from the variety of culvert parameters (e.g., geometries and backfill depths), vehicle loads, and the biases introduced by design simplifications and assumptions including the live load distribution model and the two-dimensional (2D) frame analysis.

For reliability analysis and calibration, this project focuses on the reliability of Strength I limit state that is typically analyzed for load rating. Given the focus on the live load effects, the uncertainties of resistance and permanent load effects are quantified based on existing studies. The resistance factor and the permanent load factor are adopted from the MBE for the reliability analysis. If deemed necessary, only the calibration of live load factors is conducted. The following subsections further clarify the scope of the project.

1.2.1 Sources of Uncertainties Unique to Culvert Live Load Effects

For both bridges and culverts, the uncertainties of live loads and live load effects can be attributed to the random vehicle loads on a structure and the estimation of live load effects with structural analysis. The sources of these uncertainties can be further traced back to (a) the conversion from live loads to load effects at critical cross sections, (b) the limited number of vehicle records available at each site and the variation from site to site, (c) the maximum load effects statistically projected to a long reference period, and (d) the dynamic effect of a moving vehicle.

Among these sources, the uniqueness of culverts is elaborated as follows:

- **Uncertainty of estimating load effects in culverts:** For girder bridges, the load effects in a girder are commonly estimated based on a line beam analysis and girder distribution factor (GDF). The corresponding uncertainty was quantified for the calibration of live load models and load factors (Nowak, 1999). By contrast, the load effects in culverts are estimated based on a load distribution model and a 2D frame analysis.
- **Uncertainty of the projected maximum load effects:** Culverts are more affected by axle groups than the entire vehicles. This creates discrepancies in load frequency, weight, and configurations on a culvert compared to those on a girder bridge. Previous analysis also indicates that the site-to-site variation decreases with an increase in the span length of a

structure (Sivakumar et al., 2011). Additionally, side-by-side statistics and structural behavior under side-by-side loading are also different between culverts and girder bridges.

- **Uncertainty of dynamic effects:** Dynamic effects refer to the potential amplification of vehicle loads due to the interaction between the structure and the moving vehicle. For both bridges and culverts, they are considered by a dynamic allowance factor in the LRFD Specifications. However, due to the existence of the backfill soil, the dynamic effect in culverts is considerably dampened (Bugher et al., 2020; Kadivar et al., 2018).

The project primarily targets the first two uncertainty sources unique to culverts. For dynamic effects, the damping effect of backfill soil is considered based on the LRFD Specifications, and the bias and the coefficient of variation (COV) of the dynamic allowance are assumed to be identical between culverts and bridges. This assumption is primarily due to the limited availability of dynamic results for culverts in the literature. More details of this uncertainty are presented in Chapter 2 with other uncertainty models and uncertainty quantification (UQ) techniques used in this project.

1.2.2 Critical Cross Sections and Load Effects

In general, the load demands in a culvert should be estimated for all cross sections, including top and bottom slabs as well as side and internal walls, and for all load effects, including flexure, shear, and thrust. The load distribution model and the 2D frame analysis described in the LRFD Specifications do not consider the continued load attenuation along the height of a culvert, which results in significantly overestimated load effects in the bottom slab and side walls (Wood et al., 2016). Since this project does not aim to provide refined load distribution models, only the cross sections of the top slab where load effects can be reasonably estimated are analyzed.

Among all load effects, thrust does not normally control the design of RC box culverts, especially for culverts with shallow to moderate backfills. Additionally, the existence of thrust generally benefits the flexural capacity, albeit marginally in RC box culverts. Hence, it is not considered in this project. Between the bending moment and shear force, only the bending moment is considered at different locations in the top slab. This focus stems from the general belief that RC slabs have sufficient shear capacities when designed properly for the flexural limit state (Mlynarski et al., 2019). This is further justified by the field observations in NCHRP Project 15-54 (Mlynarski et al., 2019) as well as several experimental studies on RC box culverts (Abolmaali and Garg, 2008; Cristelo et al., 2019; Ghahremannejad et al., 2019). For instance, Abolmaali and Garg (2008) conducted load tests on full-scale culverts and found that the structural members consistently failed in flexure before developing shear cracks.

Based on the previous discussion, this project investigates the bending moments at three cross sections of the top slab, as shown in Figure 1.1. It should be noted that the reinforcement layout in Figure 1.1 is merely an illustration; actual layouts may vary depending on the construction era and the standard plans in different States. In this project, instead of relying on a specific layout, the load-carrying capacity (i.e., structural resistance) is back-calculated based on the factored load demand, as elaborated later in Section 2.2.1. In summary, the cross sections and load effects under consideration include:

- Negative bending moment at the left end of the top slab (denoted as Section S1);

- Positive bending moment at the midspan of the first cell (denoted as Section S2);
- For multi-cell culverts, negative bending moment above the leftmost internal wall (denoted as Section S3).

Note that only sections in the leftmost (first) cell are considered due to (a) symmetry with the rightmost (last) cell and (b) reduced bending moments in internal cells.

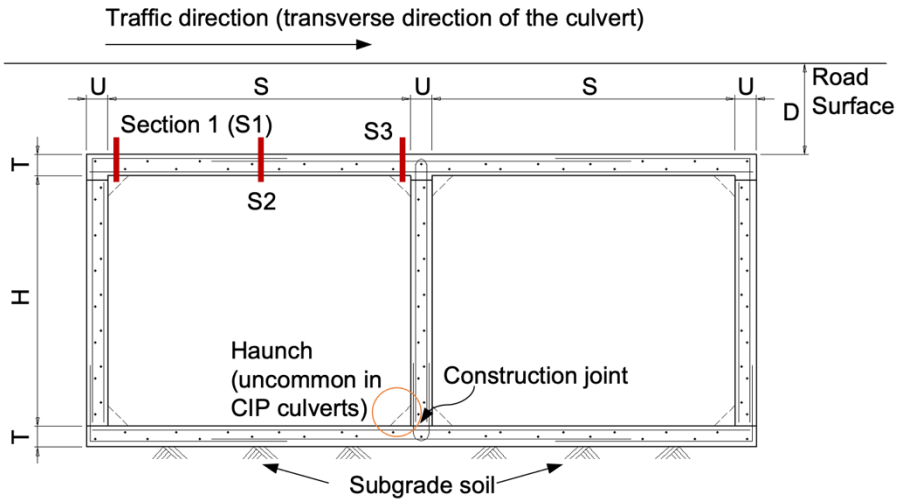

Figure 1.1 Cross sections of interest (S3 not considered in single-cell culverts)

The uncertainties due to the load distribution model and the 2D frame analysis are analyzed for all three cross sections. The results presented later in Section 3.4 indicate that only Section S2 (i.e., the positive bending moment) exhibits a level of uncertainty suitable for meaningful reliability analysis. This is because the load distribution model is commonly developed and verified with respect to the peak positive moment at or near Section S2 (Abdel-Karim et al., 1990; Orton et al., 2015; Petersen et al., 2010). Instead of reliability assessment, specific load distribution models are used for different load effects at Sections S1 and S3, which have been investigated in recent studies (Okeil and Jafari, 2024) but are beyond the scope of this project. Therefore, only the reliability related to the positive bending moment at Section S2 is analyzed and calibrated in this project. Nonetheless, a similar methodology and procedure can be implemented for other cross sections and load effects when more refined distribution models are proposed in future studies.

1.2.3 Load Rating Levels and Vehicles

This project focuses on the load and resistance factor rating (LRFR) approach to load rating. Two distinct load rating levels are investigated, including the operating rating using the design loads and the legal rating using the AASHTO legal vehicles and the FAST Act emergency vehicles as surrogate loads. For the design loads, the design lane load is not considered for culverts based on the LRFD Specifications. Therefore, the maximum load effect is determined from the more critical pattern between the design truck and the design tandem shown in Figure 1.2.

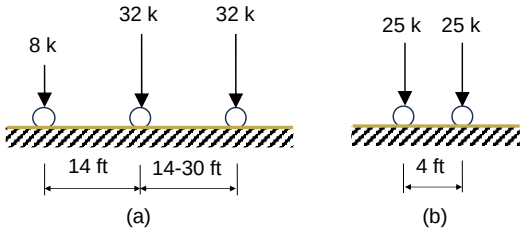

Figure 1.2 Design loads: (a) design truck and (b) design tandem

The AASHTO legal loads considered in this project include the three AASHTO trucks, i.e., Type 3 truck (T3), Type 3S2 truck (T3S2), and Type 3-3 truck (T3-3), the notional rating load (NRL), and the four single-unit specialized hauling vehicles, i.e., SU4, SU5, SU6, and SU7 trucks. For the same reason as the design lane load, the lane-type legal loads are not considered. Figure 1.3 shows the AASHTO legal loads analyzed in this project.

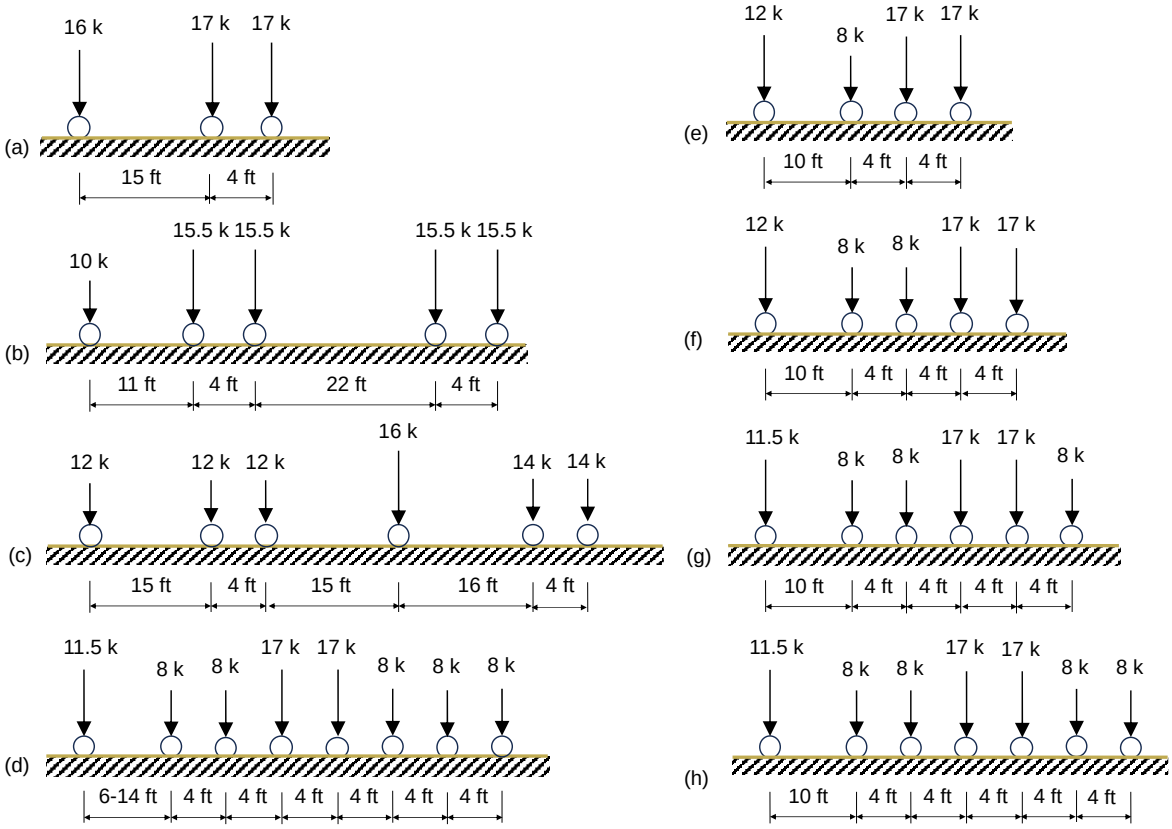

Figure 1.3 AASHTO legal loads: (a) Type 3 Truck, (b) Type 3S2 Truck, (c) Type 3-3 Truck, (d) Notional Rating Load (NRL), (e) Single-Unit SU4 Truck, (f) SU5 Truck, (g) SU6 Truck, and (h) SU7 Truck

The FAST Act emergency vehicles are encompassed by two configurations, i.e., EV2 and EV3, that are included in load ratings to facilitate unobstructed passage of emergency vehicles on bridges and culverts. Figure 1.4 shows the EV2 and EV3 loads. They not only have higher axle weights than the AASHTO legal loads, but also axle groups not complying with the Federal Bridge Formula B (FHWA, 2016). Therefore, they are included in this project as a separate load case but solely serve as surrogate load models in the calibration and reliability analysis with the WIM data.

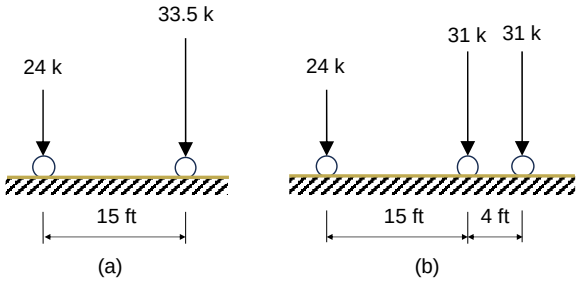

Figure 1.4 FAST Act emergency vehicles as surrogate loads: (a) EV2 and (b) EV3

1.3 TYPICAL CULVERTS

Both the backfill properties (e.g., depth, density, and stiffness) and the culvert designs (e.g., dimensions, reinforcement, and material properties) can affect the loads on culverts (Lou et al., 2018; Seo et al., 2017; Wood et al., 2017, 2016). To systematically assess the uncertainty, it is important to collect a wide range of culverts with diverse properties. Among various backfill properties, previous studies (Chen and Sun, 2013; Ramadan and Naggar, 2022; Ulger et al., 2020) indicate that the backfill depth is the predominant factor influencing load distribution for rigid culverts like RC boxes. Therefore, four backfill depths, i.e., 2 ft, 4 ft, 6 ft, and 8 ft, are considered in this project. The upper bound (8 ft) represents a realistic limit for moderately buried culverts due to largely diminished live load effects compared to the permanent load effects. However, this is not the limit to neglect live load effects entirely. The backfill of 2 ft is analyzed to investigate the transition between shallow and moderate backfill. Pavement is not considered herein due to the wide variety of pavement properties and its general benefit in reducing loads on culverts (Wood et al., 2017).

For different culvert designs, existing designs suitable for different backfill depths are reviewed based on standard plans used by different State DOTs as well as existing studies in the literature. Table 1.1 summarizes the sources of these culvert designs. Both the number of cells and the cell dimensions are considered. To include all critical sections while reducing the number of typical culverts, the present study focuses primarily on the analysis of single- and double-cell culverts. This scope is similar to the choices made during the development of the LRFD Specifications for girder bridges, where only simply supported and two-span continuous bridges were analyzed (Nowak, 1999). For each cell, relevant dimensions include cell span and height as well as slab and wall thickness. The haunch at wall-slab joints is not considered to reflect conditions in cast-in-place (CIP) culverts and provide conservative load effect estimations for precast culverts.

Table 1.1 Reviewed culvert designs

Source	Year[a]	Number of culvert designs		
		Single-cell	Double-cell	Multi-cell
Acharya et al. (2016b)	2016	1	-	-
Alamo River culvert (Caltrans)	1969	-	1	-
Standard plans (Caltrans)	1952-2010	87	166	106
Strong Creek culvert (Caltrans)	1960	1	-	-
Han et al. (2013)	2013	2	-	-
Kadivar et al. (2018)	2018	2	-	-
McGrath et al. (2005)	2005	4	4	-
Standard plans (MnDOT)	1940-2019	80	19	25
Mlynarski et al. (2019)	2019	2	1	-
Orton et al. (2015)	2015	-	8	2
Ulger et al. (2020)	2020	-	1	7
Standard plans (TxDOT)	1934-2020	21	183	732

Note: (*a*) column represents release year of culvert plans or publication year of the paper or report, except for Almo River and Strong Creek culverts, which are their years of construction.

Overall, 34 culvert designs are established for the subsequent analysis and summarized in Table 1.2. They include 16 single-cell and 18 double-cell culverts. For single-cell culverts, the clear span ranges from 10 ft to 16 ft with a 2 ft interval. For double-cell culverts, the clear span ranges from 6 ft to 14 ft with a 2 ft interval. Given each clear span, different clear heights are selected from existing designs reviewed in Table 1.1. For each combination of the cell span and height, a slab thickness is determined based on the slab thickness for a 2-8 ft backfill. Lastly, the wall thickness is decided based on the most frequent thickness in existing designs given the cell span, height, and slab thickness. Each culvert design is analyzed for the different backfill depths mentioned above. It should be noted that the typical designs listed in Table 1.2 include culverts with a total span less than 20 ft (but greater than 10 ft). Although the MBE does not consider those as bridge-sized culverts, some States do load rate culverts of this size. Therefore, they are also included in this project.

Table 1.2 Typical culverts for UQ and validation

Culvert	Number of cells, *N*	Cell clear span, *S* (ft)	Cell clear height, *H* (ft)	Slab thickness, *T* (in)	*Wall thickness, U* (in)
1	1	10	4	9	8
2	1	10	6	9	8
3	1	10	8	9	8
4	1	10	10	9	8
5	1	12	6	10	8
6	1	12	8	10	8
7	1	12	10	10	9
8	1	12	12	10	9
9	1	14	8	12	10
10	1	14	10	12	10
11	1	14	12	12	12
12	1	14	14	12	12
13	1	16	6	12	10
14	1	16	8	12	10
15	1	16	10	12	12
16	1	16	12	12	12
17	2	6	2	8	6
18	2	6	4	8	6
19	2	6	6	8	6
20	2	8	4	9	6
21	2	8	6	9	7
22	2	8	8	9	7
23	2	10	4	9	8
24	2	10	6	9	8
25	2	10	8	9	8
26	2	10	10	9	8
27	2	12	6	10	8
28	2	12	8	10	9
29	2	12	10	10	10
30	2	12	12	10	10
31	2	14	8	12	10
32	2	14	10	12	10
33	2	14	12	12	12
34	2	14	14	12	13

1.4 REPORT OUTLINE

The subsequent chapters of this report are organized as follows. Chapter 2 introduces the methods used and developed for the uncertainty quantification and reliability analysis of the typical culverts. Chapter 3 focuses on the uncertainty quantification related to the use of the LRFD load distribution model and the 2D frame analysis. Chapter 4 investigates the uncertainty associated with the unique load spectrum of culverts as well as the statistics and structural behavior associated with the side-by-side loading. Based on the quantified uncertainties, Chapter 5 analyzes the reliability indices

of typical culverts under different rating loads. An approach to calibrating live load factors and its effect on structural reliability are also explained in Chapter 5. Finally, Chapter 6 summarizes the findings and suggests future research activities.

CHAPTER 2

METHODOLOGIES FOR UNCERTAINTY QUANTIFICATION AND RELIABILITY ANALYSIS

2.1 INTRODUCTION

For Strength I and Strength II limit states, the reliability of a culvert is determined with respect to the following performance function:

$$g(\boldsymbol{X}) = R - DL - LL$$

Equation 2.1 Performance function

where $g(\mathbf{X})$ = performance function involving random variables **X**; R = structural resistance; DL and LL = load effects under permanent loads and live loads, respectively. Both the structural resistance and the load effects can be modeled as individual random variables, thereby forming the vector **X.** Alternatively, each can be expressed as a function of other primary random variables. In this project, the first option is adopted due to its prevalent use in LRFD calibration. The limit state equation refers to the case when the performance function equals to 0, i.e., $g(\mathbf{X}) = 0$. If $g(\mathbf{X}) < 0$, it is said that failure occurs for a specific limit state. The failure probability can be converted to the so-called reliability index (and vice versa) via the following expression:

$$\beta = \Phi^{-1}(1 - p_f)$$

Equation 2.2 Reliability index and failure probability

where β = reliability index; p_f = failure probability, i.e., $p_f = Pr[g(X) < 0]$; Φ = cumulative distribution function (CDF) of a standard normal distribution.

Given uncertainties involved in structural resistance and load effects, the failure probability of a structure is always greater than zero. To ensure the failure probability is sufficiently small, the LRFD Specifications uses the following simplified format for reliable structural design:

$$\phi R_n \geq \gamma_{DL} DL_n + \gamma_{LL} LL_n$$

Equation 2.3 LRFD format (simplified with one typical load combination)

where ϕ = resistance factor; γ_{DL} and γ_{LL} = load factors for permanent and live load effects, respectively; R_n, DL_n, and LL_n = nominal values for resistance, permanent load effect, and live load effect, respectively. The nominal values are deterministic values calculated following the LRFD Specifications. The load and resistance factors are so calibrated that given a reference period (i.e., the design service life), the average reliability index across a wide range of typical structures closely matches a predefined value known as the target reliability index, β_T. Following the LRFD format, the rating factor (RF) associated with LRFR can be expressed as follows:

$$RF = \frac{\phi R_n - \gamma_{DL} DL}{\gamma_{LL} LL}$$

Equation 2.4 LRFR expression (simplified with only one combined permanent load effect)

If a structure has an RF equal to one, the reliability index on average should match the target reliability index. Load rating is based on different target reliability indices and reference periods. This difference is reflected by unique live load factors used for different rating levels and rating loads. Table 2.1 summarizes the target reliability indices used for design and rating levels considered in this project. The lower target reliability index is attributed to (a) shorter reference periods and (b) costly actions to improve resistance for existing structures compared to new structures during design (Sykora et al., 2017).

Table 2.1 Target reliability indices and reference periods

Design or rating level	Target reliability index	Reference period
Design	3.5	75 years
Design load rating, inventory level	3.5	75 years
Design load rating, operating level	2.5	5 years
Legal load rating	2.5	5 years

The load and resistance factors currently used for load rating RC box culverts are summarized in Table 2.2. These factors were calibrated mainly based on the uncertainty characteristics of girder bridges (Mlynarski et al., 2011; Moses, 2001; Nowak, 1999). The following subsections describe methods and models used for quantifying the uncertainties of resistance and load effects suitable for culverts. The method used for reliability analysis is then described based on the quantified uncertainties.

Table 2.2 Factors used for LRFR

Load and resistance factor	Inventory rating	Operating rating	Legal rating
Flexural resistance, ϕ	0.9	0.9	0.9
Dead load, γ_{DC}	1.25	1.25	1.25
Vertical earth pressure, γ_{EV}	1.30	1.30	1.30
Horizontal earth pressure, γ_{EH}	1.35	1.35	1.35
Vehicular live load, γ_{LL}	1.75	1.35	2.00

2.2 UNCERTAINTY QUANTIFICATION

Following the convention in structural reliability analysis, two-parameter random variables are used to model all uncertainties in structural resistance, permanent load effects, and live load effects. Although different sets of parameters can be used to describe a probability distribution, the uncertainty is quantified by a distribution type, a mean, and a COV. The mean value can be further described by a nominal value, i.e., a deterministic value calculated following the MBE, and a bias factor, defined as the ratio between the mean and the nominal value.

2.2.1 UQ of Structural Resistance

Uncertainties of structural resistance can be attributed to the material properties (such as concrete and steel strengths), construction and geometry imperfections, and analytical models to predict resistance (Nowak, 1999). For the flexural resistance of RC members, the uncertainty models used in previous reliability and calibration studies are summarized in Table 2.3. To stay consistent with prior studies on bridge reliability, the lognormal distribution is used in this project. Compared to beams, the bias and the COV associated with the resistance of bridge deck is deemed more appropriate to represent the resistance of RC box culverts. Therefore, this project considers a bias factor equal to 1.13 and a COV equal to 0.13 for the flexural resistance of culverts.

Table 2.3 Uncertainty models for flexural resistance of RC members

Reference	Bias	COV	Distribution	Note
Ellingwood et al. (1980)	1.12	0.19	Normal	One-way simply supported slabs in buildings with a thickness ranging from 4 to 8 inches
NCHRP Report 368	1.14 (1.12)	0.13 (0.135)	Lognormal	Based on results of RC T-beams, two sets of values were reported in Table 3 and page C-9 of the reference. Both are presented herein.
NCHRP Report 454	1.12	0.10	Normal	Based on results of composite steel beams used in NCRHP Report 368.
NCHRP Report 700	1.13	0.13	Lognormal	RC bridge deck; used in this project

Besides the bias factor and the COV, it is also essential to know the nominal value of resistance in order to fully quantify the resistance uncertainty. Based on the LRFD and LRFR formats, the nominal resistance can be back-calculated as follows from the factored load effects:

$$R_n = \frac{\gamma_{DC} DC_n + \gamma_{EV} EV_n + \gamma_{EH} EH_n + \gamma_{LL} LL_n}{\phi}$$

Equation 2.5 Minimum nominal resistance based on LRFD

where DC_n, EV_n, EH_n, and LL_n = nominal values of load effects due to dead load of structural components, vertical earth pressure, horizontal earth pressure, and vehicular live load, respectively. They are calculated based on the MBE. The nominal resistance obtained from Equation 2.5 should lead to an average reliability index close to the target reliability.

2.2.2 UQ of Permanent Load Effects

The permanent load effects in a culvert are attributed to (a) the self-weight of the structural elements (termed in the LRFD Specifications as DC), (b) the vertical and horizonal earth pressures (EV and EH, respectively), and (c) the earth surcharge due to pavement beyond culvert sidewalls (ES). Figure 2.1 illustrates the load pattern of these permanent loads.

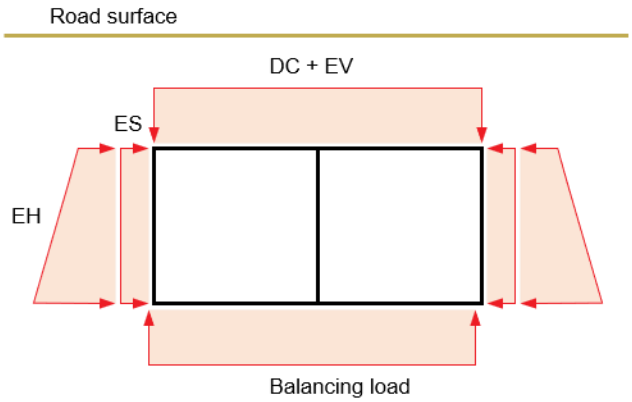

Figure 2.1 Permanent loads on a culvert

The uncertainty due to culvert self-weight is considered identical to that in bridges due to the same materials used in both. In particular, the distribution and statistics for cast-in-place RC members in NCHRP Report 368 (Nowak, 1999) are adopted to describe the uncertainty in the load effects due to DC.

EV and EH are unique to culverts. In this project, the COV of the load effect under EV, V_{EV}, is calculated by the following equation:

$$V_{EV} = \sqrt{V_{density}^2 + V_{depth}^2} = \sqrt{0.10^2 + 0.05^2} = 0.112$$

Equation 2.6 COV of load effects under EV

where $V_{density}$ = 0.10 = COV of soil density (Phoon and Kulhawy, 1999); V_{depth} = 0.05 = COV of backfill depth, assumed to following the same COV as other geometry imperfections (Ellingwood et al., 1980). The uncertainty in EH is related not only to backfill depth and soil density, but also the at-rest lateral earth pressure coefficient, which is controlled by the friction angle of soil. Based on Duncan (2000), the latter has a COV equal to 0.10. Therefore, the total COV of the load effect under EH, V_{EH}, is expressed as follows:

$$V_{EH} = \sqrt{V_{density}^2 + V_{depth}^2 + V_{coef}^2} = \sqrt{0.10^2 + 0.05^2 + 0.10^2} = 0.15$$

Equation 2.7 COV of load effects under EH

where V_{coef} = 0.10 = COV of the at-rest lateral earth pressure coefficient (Duncan, 2000). The mean values of EH and EV are assumed to be the same as the nominal values calculated based on the LRFD Specifications. Due to the focus on live load effects in this project and the lack of reliable data, the following uncertainties are not considered in the UQ of total permanent load effects:

- The vertical soil pressure is subjected to soil-structure interaction (SSI), which is modeled by an interaction factor F_e in the LRFD Specifications. The uncertainty of this factor is ignored due to the limited effect of SSI for the typical culverts and backfill depths considered in this project.

- The 2D frame model and the idealized load patterns shown in Figure 2.1 can introduce epistemic uncertainty when the loads are converted to the load effects in structures. This uncertainty is also neglected herein.
- Since pavement is not considered, the load effects due to the pavement self-weight and the earth surcharge are not included in the analysis.

Table 2.4 summarizes the uncertainty model for the load effects under DC, EV, and EH, respectively. Based on Table 2.4, the mean, $\overline{DL}$, and the COV, V_{DL}, of the total permanent load effect are obtained using the following equation:

$$\overline{DL} = DC_n b_{DC} + EV_n + EH_n$$
$$\sigma_{DL}^2 = \sigma_{DC}^2 + \sigma_{EV}^2 + \sigma_{EH}^2$$
$$V_{DL} = \frac{\sigma_{DL}}{\overline{DL}}$$

Equation 2.8 Uncertainty model of total permanent load effect

where b_{DC} = bias factors of the load effect under DC; σ_{DC}, σ_{EV}, and σ_{EH} = standard deviations (STDs) of the load effects under DC, EV, and EH, respectively, which are obtained by multiplying the means and the COVs; σ_{DL} = STD of the total permanent load effect. Given all components of the total permanent load effect follow normal distributions, the permanent load effect itself also follows a normal distribution. Based on the previous discussion and Table 2.4, the quantified uncertainties of DL are presented in Appendix A for all typical culverts.

Table 2.4 Uncertainty models for components of total permanent load effect

Load effect	Bias	COV	Distribution
DC	1.05	0.10	Normal
EV	1.0	0.112	Normal
EH	1.0	0.15	Normal

2.2.3 UQ of Live Load Effects

The uncertainty of the live load effect of a culvert can be attributed to (a) the load distribution through the backfill soil, (b) the random traffic on a culvert, and (c) the dynamic effect of a moving vehicle. Hence, the following expression of random variables is used to represent the live load effect of a culvert:

$$LL = LL_{FR} \cdot \lambda_{NET} \cdot \lambda_{LDS} \cdot \lambda_{BF} \cdot \lambda_{DYN}$$

Equation 2.9 Live load effect in a culvert

where LL_{FR} = maximum live load effect in a reference period; it is obtained based on a load distribution model, 2D frame analysis, load spectrum, and statistical projection ; λ_{NET} = random variable considering the site-to-site variation and the limited data for the derivation of LL_{FR} (Sivakumar et al., 2011); it is defined as the ratio of LL_{FR} derived from a random site in a network to LL_{FR} derived in this project; λ_{LDS} = random variable representing the ratio of the "actual" load effect to the estimated load effect LL_{FR}; the "actual" load effect refers to that from field measurement or a refined structural analysis model, e.g., a finite element (FE) model of soil-culvert

systems; λ_{BF} = random variable to account for uncertainties of backfill properties and backfill depth; finally, λ_{DYN} = random variable representing the ratio of the dynamic load effect due to moving vehicles to the static load effect. Assuming statistical independency of these random variables, the mean and the COV of the live load effect can be estimated by the following equations:

$$\overline{LL} = \overline{LL}_{FR} \cdot \bar{\lambda}_{NET} \cdot \bar{\lambda}_{LDS} \cdot \bar{\lambda}_{BF} \cdot \bar{\lambda}_{DYN}$$
$$V_{LL}^2 = V_{FR}^2 + V_{NET}^2 + V_{LDS}^2 + V_{BF}^2 + V_{DYN}^2$$

Equation 2.10 Mean and COV of live load effect

where $\overline{LL}_{FR}$, $\bar{\lambda}_{NET}$, $\bar{\lambda}_{LDS}$, $\bar{\lambda}_{BF}$, and $\bar{\lambda}_{DYN}$ = means of LL_{FR}, λ_{NET}, λ_{LDS}, λ_{BF}, and λ_{DYN}, respectively; V_{FR}, V_{NET}, V_{LDS}, V_{BF}, and V_{DYN} = COVs of LL_{FR}, λ_{NET}, λ_{LDS}, λ_{BF}, and λ_{DYN}, respectively. Since the live load effect is a maximum value within a reference period, both LL and LL_{FR} are considered to follow Gumbel distributions.

For the uncertainty related to the backfill, NCHRP Project 15-29 (Petersen et al., 2010) indicates that the bias of the load distribution model has an around 5% COV due to changing elastic moduli of backfill soil. As mentioned for the permanent load effect, a 5% COV is assumed for the backfill depth to represent construction imperfection. Since the live load is distributed in both longitudinal and transverse directions, the COV for the distributed load on a culvert is proportional to the COV of the square of the backfill depth. Combining the modulus uncertainty and the depth uncertainty gives the overall uncertainty related to the backfill, expressed as follows:

$$V_{BF} = \sqrt{V_{soil}^2 + \left(2V_{depth}\right)^2} = \sqrt{0.05^2 + (2 \times 0.05)^2} = 0.112$$

Equation 2.11 COV related to backfill soil

where V_{soil} = COV due to different soil moduli; V_{depth} = COV of backfill depth. It is also assumed that the mean value $\bar{\lambda}_{BF}$ is 1.0.

For the dynamic effect, it is assumed that the mean value $\bar{\lambda}_{DYN}$ decreases with the backfill depth based on the following equation:

$$\bar{\lambda}_{DYN} = 1 + 0.15 \times (1.0 - 0.125D) \geq 1$$

Equation 2.12 Mean of dynamic effect

where D = backfill depth in ft. Equation 2.12 combines the mean dynamic allowance, 0.15, derived for girder bridges and the backfill-related reduction model in the LRFD Specifications. Due to the lack of culvert-specific data, the COV, V_{DYN}, is determined based on the COV of dynamic allowance in bridges, which equals 0.8 based on previous studies (Nowak, 1999). As a result, V_{DYN} is expressed by the following equation:

$$V_{DYN} = \frac{0.15 \times (1.0 - 0.125D) \times 0.8}{\bar{\lambda}_{DYN}}$$

Equation 2.13 COV of dynamic effect

The current project focuses on the UQ of remaining random variables in Equation 2.9, including LL_{FR}, λ_{LDS}, and λ_{NET}. The specific methods are presented below.

2.2.3.1 Uncertainty due to load distribution through soil (λ_{LDS})

Culverts are buried structures that can interact with the surrounding soil. The uncertainty associated with a simplified load distribution model can be quantified by the ratio λ_{LDS} between the actual load effect and the load effect obtained from the load distribution model under consideration. This ratio reflects the uncertainty related to the simplifications made to facilitate structural analysis, including the simplified load pattern and the 2D frame analysis for a fundamentally three-dimensional (3D) loading (since the vehicle load is not present along the entire lay-length of culverts). Conceptually, this uncertainty can be compared to the uncertainty involved in the GDFs used in bridge design and evaluation.

The actual load effect can be obtained from either field measurement or a more sophisticated numerical model. If field measurements are used, additional uncertainty may arise from measurement errors and the methods used to infer load effects from the measurement (e.g., the error in the bending moment estimated from displacement or strain gauge values). If FE results are used, the FE model may contain its own model bias and uncertainty, though they should be less than the 2D frame analysis. It has been shown that FE analysis of the soil-culvert system can be used to effectively capture the structural behavior and accurately predict the load effects in culverts (Abuhajar et al., 2016). To analyze all typical culverts, FE models are used in this project to provide the actual live load effects. To reduce the bias and uncertainty related to the FE analysis, 3D FE models are developed based on the modeling techniques and suggestions presented in NCHRP Report 647 (Petersen et al., 2010). Chapter 3 provides specifics about the FE models of soil-culvert systems used in this project.

Previous investigations comparing 2D FE and frame results indicate that the bias of the 2D frame analysis varies considerably with culvert geometries, especially the clear cell span (Wood et al., 2016). As a result, if the ratio λ_{LDS} is treated as one single random variable by combining results from culverts with different geometries, the random variable would have a very large COV. Therefore, in this project, the variance of λ_{LDS} observed in the typical culverts is first reduced using regression analysis, taking into account various potential explanatory variables. Only the unexplained variance is then modeled as a random variable. Chapter 3 describes in detail the methods used in this process and the UQ results for λ_{LDS}.

2.2.3.2 Uncertainty due to culvert load spectrum (LL_{FR} and λ_{NET})

To quantify the uncertainty of LL_{FR}, a spectrum of a live load effect is constructed based on the loading events characterized by the weight and the configuration of axle groups. These samples of axle groups can be obtained from either weight surveys (Nowak, 1999) or weigh-in-motion (WIM) data (Sivakumar et al., 2011). Herein, a load spectrum refers to a normal probability plot for samples of the load effect under consideration. Figure 2.2 is an illustrative example of the positive bending moment spectrum of a culvert. Each sample is obtained using the load distribution model and the 2D frame analysis matching those used during the UQ of λ_{LDS}. The ordinate indicates the normal theoretical quantile (theoretical quantile for short) that can be calculated using the following equation:

$$z = \Phi^{-1}(x)$$

Equation 2.14 Theoretical quantile of a sample

where x = empirical CDF value of a sample (Burati et al., 2003 Appendix H), which can be calculated using Filliben's estimate (SciPy Community, 2024). The theoretical quantile can also be computed below for a reference period:

$$z_T = \Phi^{-1}\left(1 - \frac{1}{N_T}\right)$$

Equation 2.15 Theoretical quantile associated with a reference period

where N_T = number of loading events within the reference period T.

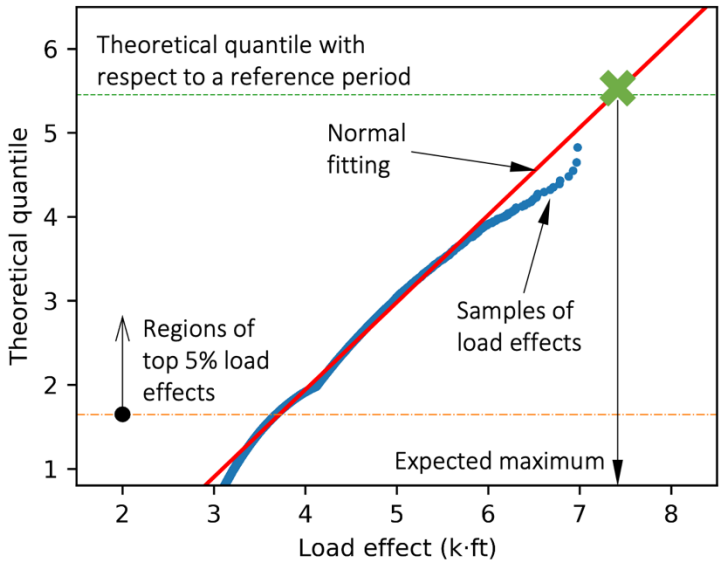

Figure 2.2 Example load spectrum

Figure 2.2 also illustrates the normal fitting of the top 5% samples and the expected maximum load effect in a reference period. The specific steps to obtain a load spectrum and to project the uncertainty of LL_{FR} associated with a reference period are summarized below based on the descriptions in NCHRP Reports 368 and 683 (Nowak, 1999; Sivakumar et al., 2011):

1. Collected statistics for the weights and configurations of axle groups from preprocessed WIM data (see NCHRP Report 683 protocol Steps 1-6 and Step 9 for details). The statistics should include axle configurations, event counts, and axle weight mean and COVs.
2. Generate samples of live load effects consistent with the load statistics. This can be achieved by the following sub-steps:
    a. Generate a sample axle weight and configuration based on the statistics in step 1;
    b. Distribute the road surface load to the culvert using the load distribution model and the 2D frame model investigated in the UQ of λ_{LDS};
    c. Identify the most critical load effect with moving load analysis;
    d. Repeat a-c to generate sufficient load effect samples

3. Fit the top 5% load effect samples to a normal distribution[1] with mean μ_{upper} and standard deviation σ_{upper}. This normal distribution represents the probability distribution of one heavy loading event (i.e., axle passage).
4. Project the load effect in one heavy loading event to the maximum load effect within a reference period. This is achieved with extreme value theory and Gumbel distribution. For instance, if the reference period is 5 years, the number of heavy loading events in five years is N, the maximum load effect is a Gumbel distribution with the following mode, u_N, and dispersion, α_N, parameters (Sivakumar et al., 2011):

$$u_N = \mu_{upper} + \sigma_{upper}\left[\sqrt{2\ln(N)} - \frac{\ln(\ln(N)) + \ln(4\pi)}{2\sqrt{2\ln(N)}}\right]$$

$$\alpha_N = \frac{\sqrt{2\ln(N)}}{\sigma_{upper}}$$

Equation 2.16 Mode and dispersion parameter of a Gumbel distribution

5. Finally, the mean and the COV of LL_{FR} can be converted from the mode and the dispersion parameters with the following expression:

$$\overline{LL}_{FR} = u_N + \frac{0.5772}{\alpha_N}$$

$$V_{FR} = \frac{\pi}{\sqrt{6}\alpha_N} \cdot \frac{1}{\overline{LL}_{FR}}$$

Equation 2.17 Mean and COV of a Gumbel distribution

The procedure described above is used in Chapter 4 for the UQ of LL_{FR}. By considering multiple WIM sites, the site-to-site variation that controls λ_{NET} is also quantified. More details of the method and the UQ results are presented in Chapter 4.

2.3 RELIABILITY ANALYSIS

Based on the quantified uncertainties, the reliability index associated with the performance function in Equation 2.1 can be computed using different methods. One common method is the first order second moment (FOSM) method, which only uses the first two statistical moments (e.g., mean and variance) for reliability calculation. It assumes that (a) all random variables in the performance function follow normal distributions and (b) the performance function is, or can be reasonably approximated by, a linear function. When either of the two assumptions is violated, the reliability index obtained with the FOSM method can no longer accurately reflect the failure probability using Equation 2.2. Since structural resistance and live load effects are often modeled as non-Gaussian random variables, other analysis methods have been used to better estimate the reliability index and the failure probability, including the iterative procedure described below.

[1] The mean value is the intersection of the fitted line with the x-axis (i.e., load effect corresponding to the zero theoretical quantile), and the STD is the inverse of the slope.

When full probabilistic information is available (i.e., both the distribution type and the parameters), an improved first order reliability method (FORM), termed the improved Hasofer-Lind-Rackwitz-Fiessler (iHLRF) algorithm (Zhang and Der Kiureghian, 1995), can be used to calculate the reliability of structures. Compared to the FOSM method, the iHLRF algorithm considers the distribution types of all random variables. This is achieved by converting random variables of specific types to standard normal variables (known as a standard normal parametric space). During this process, a linear performance function such as Equation 2.1 may become nonlinear. To this end, the iHLRF method linearizes the performance function in the standard normal parametric space at the so-called "design point", which is the most likely point located on the limit state equation. The distance from the design point to the origin of the standard normal parametric space becomes the reliability index, and the failure probability can be similarly obtained using Equation 2.2. Due to linearization, the iHLRF algorithm may still introduce error in the estimated failure probabilities, albeit low even for some highly nonlinear performance functions (Rackwitz and Fiessler, 1978). One advantage of the iHLRF algorithm compared to FOSM is that the byproduct from finding the design point can facilitate the calibration of load and resistance factors. For this reason, the iHLRF algorithm is selected to compute the reliability indices of representative culverts. Note that the same approach was utilized in NCHRP Report 368 for LRFD calibration (Nowak, 1999).

The connection between FORM and LRFD calibration is explained as follows. In particular, the design point located with the iHLRF algorithm directly provides the design values of random variables. Take, for example, a simple performance function $g = R - S$, where R and S = resistance and load effect, respectively. Assuming normal distributions for both R and S, Figure 2.3 shows the limit state equation with $g = 0$ in the original and standard normal parametric space, respectively. The origin of the standard normal parametric space (denoted Point "O" in Figure 2.3) is located at the mean values of S and R in the original parameter space. The design point can be directly identified in the figure and denoted as Point "P". Thereby, the design values of resistance and load effect (i.e., the factored resistance and load effect) can be expressed by the coordinates of the design point as follows:

$$R_d = \bar{R} + \alpha_R \beta \sigma_R = \bar{R}(1 + \alpha_R \beta V_R)$$
$$S_d = \bar{S} + \alpha_S \beta \sigma_S = \bar{S}(1 + \alpha_S \beta V_S)$$

Equation 2.18 Design values of resistance and load effects (both follow normal distributions)

where R_d = design (i.e., factored) resistance; S_d = design (i.e., factored) load effect; $\bar{S}$, σ_S, and V_S = mean, STD, and COV of the load effect, respectively. The α_R and α_S are called sensitivity factors of resistance and load effect, respectively (Melchers and Beck, 2018). In Figure 2.3, these sensitivity factors can be represented by the direction cosines of vector "OP" in the standard normal parametric space along U_R and U_S directions, respectively. In general, the sensitivity factor for resistance is negative, while that for load effect is positive (Der Kiureghian, 2022). Therefore, the design resistance is smaller than the mean resistance, while the load effect is larger than the mean. The extents of these differences are related to the reliability index. The resistance and load factors can then be obtained by taking the ratio of factored to nominal values.

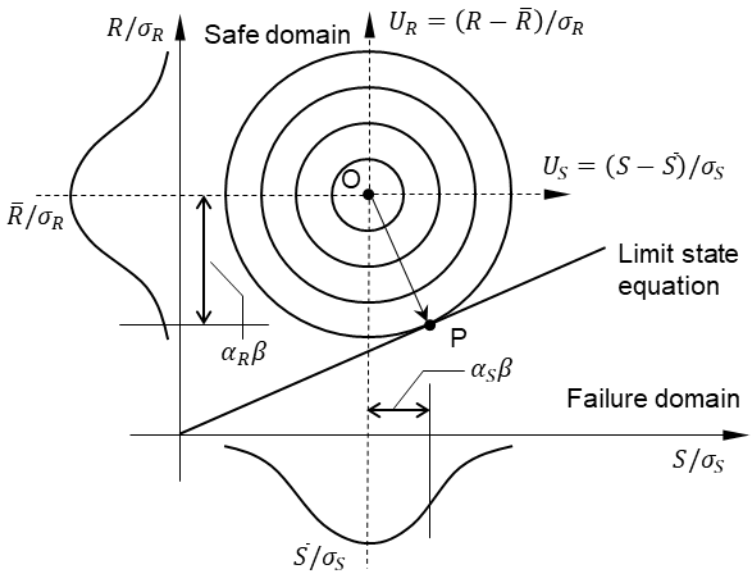

Figure 2.3 Illustration of reliability index and design point

For a general performance function, the vector ($\boldsymbol{\alpha}^*$) containing the sensitivity factors with respect to all random variables in the performance function can be expressed as

$$\boldsymbol{\alpha}^* = \left.\frac{-\nabla G(\boldsymbol{u})}{\|\nabla G(\boldsymbol{u})\|}\right|_{\boldsymbol{u}=\boldsymbol{u}^*}$$

Equation 2.19 Sensitivity vector associated with a general performance function

where $\mathbf{u}$ = variables of the performance function in the standard normal parametric space; $\mathbf{u}^*$ = design point in the standard normal parametric space; $G(\mathbf{u})$ = performance function transformed into the standard normal parametric space; $\nabla G(\mathbf{u})$ = gradient of $G(\mathbf{u})$. Given a target reliability index and the sensitivity factors of random variables, the design values can be determined using relationships similar to those in Equation 2.18. In particular, for the performance function in Equation 2.1 and the distribution types for R, DL, and LL mentioned in Section 2.2, the factored resistance, permanent and live load effects can be determined using the expressions in Table 2.5 (CEN 1990, 2002).

Table 2.5 Design values for random variables

Distribution	Design value	Notes
Normal	$\mu + \alpha\beta_T\sigma$	μ and σ = mean and STD; α = sensitivity factor associated with the variable; β_T = target reliability index
Lognormal	$\mu \exp(\alpha\beta_T V)$	V = COV, applicable for $V < 0.2$
Gumbel	$u - \frac{1}{a}\ln\{-\ln[\Phi(-\alpha\beta_T)]\}$	$a = \frac{\pi}{\sigma\sqrt{6}}$ and $u = \mu - \frac{0.577}{a}$

The expressions in Table 2.5 are the theoretical basis for calibrating partial factors in Eurocodes (CEN 1990 2002), wherein the sensitivity factors for resistance and the dominant load effect are

conservatively estimated as −0.8 and 0.7, respectively. When more than one load effect is present, the subdominant load effect is assumed to have a sensitivity factor of 0.7×0.4=0.28. Although not directly referring to the iHLRF algorithm and the design point, NCHRP Project 12-28 (Moses and Verma, 1987) adopted an equivalent procedure when developing the resistance factor for load rating by assuming $\alpha_R = 0.55$, $b_R = 1.10$, $V_R = 0.12$, $\beta = 2.5$, and lognormally distributed resistance. Later in Chapter 5, the current project uses the same method for calibrating live load factors for RC box culverts.

CHAPTER 3

UNCERTAINTY QUANTIFICATION OF LOAD DISTRIBUTION MODEL

3.1 INTRODUCTION

To determine the load demands in culverts, the LRFD Specifications provide a practical method to estimate the distribution of wheel load through backfill soil. This method adopts a load spreading angle consistent with many geotechnical applications and applicable to any culverts with a backfill greater than 2 ft and less than the threshold for ignoring vehicular live loads altogether. However, the resulting load effects may be considerably overestimated, causing conservative designs or additional load postings (McGrath et al., 2005; Ulger et al., 2020).

Recognizing this, various studies have been conducted for shallow culverts with a backfill around 2 ft (Acharya et al., 2016b, 2016a; Ramadan and Naggar, 2022; Sun et al., 2011). Katona (2019) revealed that the high conservatism for shallow culverts may stem from (a) the continued load attenuation along the height of a culvert (McGrath et al., 2005; Seo et al., 2017; Wood et al., 2016) and (b) the so-called "3D stiffness effect" due to localized wheel loads not well captured by 2D models. Hence, the ultimate goal of these previous studies is to provide a revised load distribution model for shallow culverts that can yield better transition from the equivalent strip model, used for no-fill or low-fill culverts, to the live load distribution model, used for moderately buried culverts (Katona, 2019; Okeil and Jafari, 2024). Herein, a moderate backfill should yield consistent uncertainties of the live load distribution model regardless of the backfill depth. For RC box culverts, results presented later in this chapter suggest a moderate backfill depth ranging from 4 ft to 8 ft.

Besides shallow and moderate backfill described above, there have also been studies on deep culverts. Based on the LRFD Specifications, if a culvert has a deep backfill, the live load effect in the culvert can be neglected. Consequently, the studies on deep culverts deal primarily with the permanent load effects, especially focusing on the effects of soil-structure interaction (Abuhajar et al., 2015). Since the live load effect is negligible, deep culverts are not included in the analysis herein.

By focusing on shallow and deep culverts for their respective challenges, previous studies fall short in the understanding and analysis of the live load distribution model in moderately buried culverts. Specifically, although the AASHTO model is considered to behave better in moderately buried culverts than shallow counterparts, there is a lack of quantitative models to characterize the model uncertainties. This chapter aims to model and quantify the uncertainties in the estimated load demands in moderately buried RC box culverts. The developed uncertainty model can be converted to the uncertainty model of λ_{LDS} in Equation 2.9, laying the foundation for reliability analysis and calibration.

In the following sections, the AASHTO load distribution model and the methods for 2D frame and FE analyses are first described. Based on these methods, the model biases are analyzed for the typical RC box culverts described in Chapter 1. Focusing on the midspan bending moment in the top slab, the uncertainty in the model bias is quantified using Bayesian regression. The UQ results

are then used to (a) demonstrate the necessity of regression analysis for UQ and (b) compare the quantified uncertainty with those used in girder bridges.

3.2 LIVE LOAD EFFECT WITH LRFD SPECIFICATIONS

3.2.1 LRFD Specifications for Live Load Distribution

Based on the LRFD Specifications (AASHTO 2020), the vehicular live loads are localized patches of wheel loads on the road surface. These surface loads distribute through the backfill and reach the top slab of a culvert. This live load distribution model is illustrated in Figure 3.1(a), where the tire patch is distributed in both the longitudinal and transverse directions before reaching the top slab. In both directions, the distribution assumes an approximately 60-degree spreading angle, which gives rise to the live load distribution factor (LLDF) equal to 1.15. In the transverse direction, the backfill depth to the outer surface of the top slab is used to determine the length of the distributed load. In the longitudinal direction, an extra term related to the clear cell span is added to the backfill depth to obtain the width of the distributed load (Petersen et al. 2010). Specifically, the distribution of one wheel load in both directions can be expressed as

$$l_w = l_t + LLDF \cdot (D)$$

Equation 3.1 Length of the distributed load (single wheel)

$$w_w = w_t + LLDF \cdot (D) + 0.06S$$

Equation 3.2 Width of the distributed load (single wheel)

where l_w and w_w = length (transverse direction in Figure 3.1) and width (longitudinal direction in Figure 3.1) of the distributed load on the top slab, respectively; l_t and w_t = tire patch length (10 in = 0.833 ft) and width (20 in = 1.667 ft), respectively; $LLDF$ = 1.15; D and S = backfill depth and clear span of a culvert in ft, respectively. It should be noted that as the backfill depth increases, the distributed load on the top slab may overlap under multiple wheel loads as illustrated in Figure 3.1(b) and (c). In this case, the length and width of the distributed load should be adjusted to reflect the overlapping load. For a special case of two interacting wheels, the length and width of the distributed load on the top slab can be expressed as:

$$l_a = l_t + s_a + LLDF \cdot (D)$$

Equation 3.3 Length of the distributed load (axle group)

$$w_a = w_t + s_w + LLDF \cdot (D) + 0.06S$$

Equation 3.4 Width of the distributed load (axle group)

where l_a and w_a = length and width of the distributed load under multiple wheels in an axle group; s_a = spacing between two axles (4 ft); s_w = spacing between two wheels in one axle (6 ft). To obtain load demands in a culvert, the distributed load on the top slab is treated as a uniformly distributed load and applied to a 2D frame model as described subsequently.

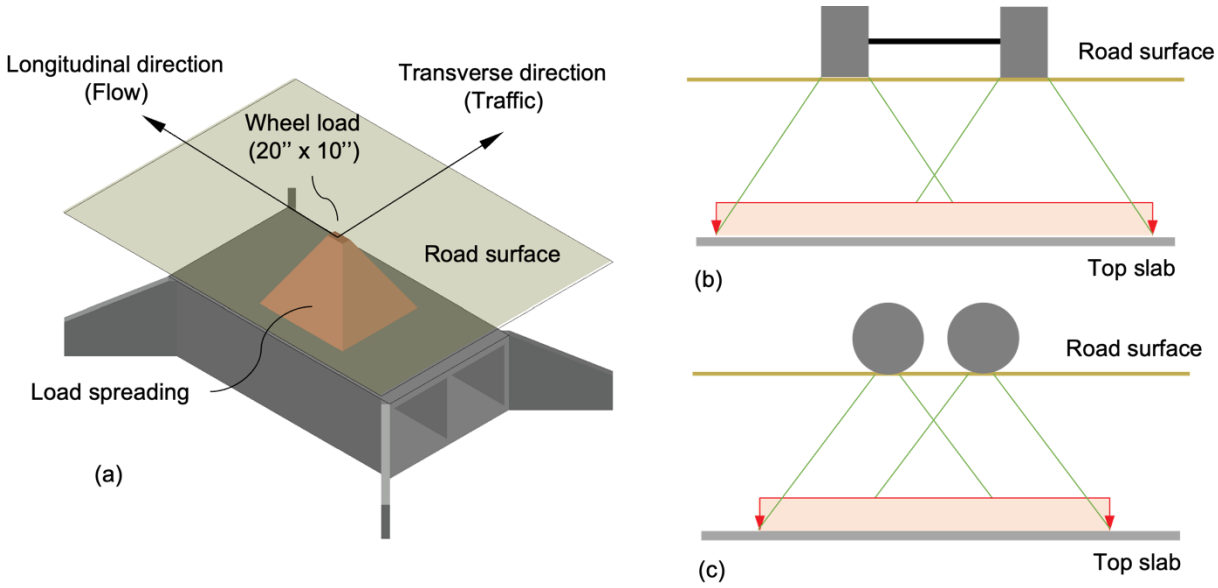

Figure 3.1 AASHTO LRFD Specifications for live load distribution: (a) load spreading under one wheel load, (b) overlapping spreading in the longitudinal direction (to obtain the width of the distributed load), and (c) overlapping spreading in the transverse direction (to obtain the length of the distributed load).

3.2.2 Frame Model for RC Box Culverts

Live load demands in RC box culverts are commonly evaluated using 2D frame models (Peiris et al., 2024). Such models are especially popular in system-wide load rating and screening, during which a large number of culverts are analyzed in batch (Wood et al., 2015). Figure 3.2 shows the frame model of a double-cell culvert. The 2D model uses the plane strain assumption to extract a thin slice of a culvert in the longitudinal direction (usually 1 ft in thickness). The slice is then restrained at the bottom slab by a pinned support on the leftmost joint and a roller support on the rightmost joint, as shown in Figure 3.2(b). To determine load demands, the frame members representing the culvert slabs and walls are assumed to behave in a linear elastic fashion, with parameters determined by the culvert dimensions and material properties. It should be noted that while there may be haunches at slab-wall joints, which can reduce the load effects in culverts (Ulger et al., 2020), they are not considered in this study because (a) many CIP culverts do not have haunches, (b) the size of haunches brings in additional uncertainty, and (c) the load demands estimated without haunches provide conservative results.

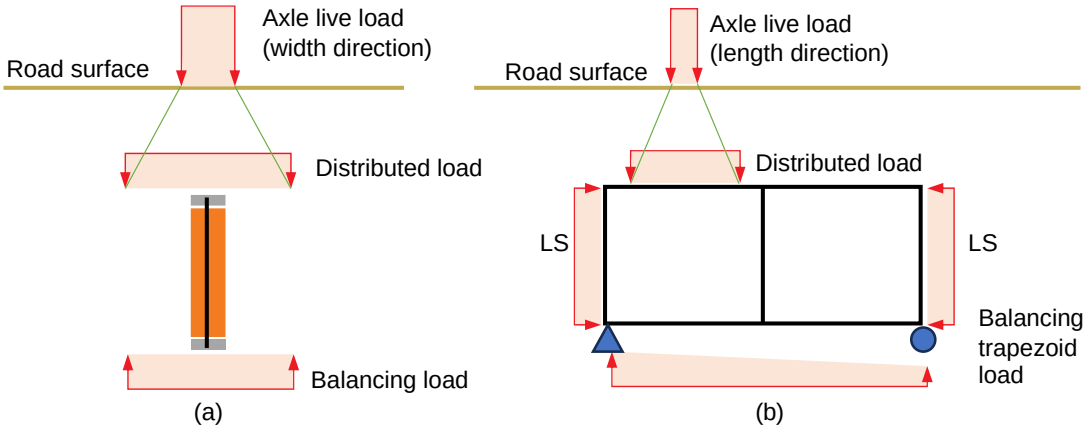

Figure 3.2 Frame analysis of a double-cell culvert: (a) slice of culvert in longitudianl direction and (b) 2D frame model for structural analysis

In this project, a Python script is developed using OpenSeesPy[1] (Zhu et al., 2018) to automatically generate the frame models described above given the number of cells (N), clear span (S) and height (H) of a cell, slab (T) and wall thickness (U), as well as the elastic modulus of reinforced concrete. Note that the modulus associated with the gross cross section is used herein as suggested in previous studies (Mlynarski et al., 2019; Petersen et al., 2010). This treatment assumes no cracking or equal extent of cracking in culvert members (Mlynarski et al., 2019) and renders a more conservative estimation of load demands in the top slab. In practice, the elastic modulus of cracked sections can also be used to match the field observations of cracked members (Wood et al., 2017).

To determine the load demands in a culvert, the uniformly distributed load on the top slab is first determined using the LRFD model described previously and then applied to the frame model in Figure 3.2(b) for structural analysis. The load on the top slab continues to attenuate along the height of a culvert and is eventually balanced by the soil pressure exerted upon the bottom slab. In frame analysis, the MBE and LRFD Specifications indicate that the vertical load on the bottom slab should balance the load on the top slab so that no support reactions are generated. This project uses a trapezoidal balancing load that is determined by solving the equations of equilibrium in vertical and rotational directions. Since soil pressure cannot be in tension, the balancing soil pressure may evolve to a triangular shape partially loaded on the bottom slab. This balancing pressure is referred to in Figure 3.2(b) as the "trapezoid" load and has been adopted by software packages for culvert design and analysis (McGrath et al., 1989). Note that some studies and agencies (MnDOT, 2013; Wood et al., 2016) simply use an equal and opposite load on the bottom slab based on the load on the top slab. The trapezoid load typically results in higher bending moments at the external wall-slab joints, while the midspan bending moment is not affected by the choice of balancing soil pressure models.

To better represent the soil pressure, the LRFD specifications also allow for the use of soil springs to support the bottom slab in lieu of the pin and roller supports. This modeling technique is not considered herein for the following reasons: (a) the inclusion of soil springs introduces additional

[1] The U.S. Government does not endorse products or manufacturers. They are included for informational purposes only and are not intended to reflect a preference, approval, or endorsement of any one product or entity.

uncertainty related to subgrade stiffness, (b) the increased model complexity hinders its practical use in the batch analysis of large numbers of culverts. Moreover, previous analysis indicates that the critical load effect decreases as more stiff soil springs are used (Mlynarski et al., 2019). Therefore, using soil pressure instead of soil springs provides a conservative bound for the load effects in culverts regardless of subgrade properties.

3.3 FINITE ELEMENT MODEL FOR SOIL-CULVERT SYSTEMS

The bias caused by the load distribution model and 2D frame analysis is analyzed herein using the ratio between the result from the frame analysis and the FE analysis of the entire soil-culvert system. This ratio is the inverse of the random variable, λ_{LDS}, defined in Equation 2.9. The reason of not directly using λ_{LDS} is that the load ratio of frame to FE results has been shown to correlate better with culvert properties such as cell span and backfill depth (Petersen et al., 2010).

The FE model for a soil-culvert system is created following the same procedures presented and validated in Petersen et al. (2010). 3D modeling is used to capture (a) load distribution in both transverse and longitudinal directions and (b) the 3D stiffness effect related to the limited width of the distributed load compared to the overall longitudinal dimension (i.e. lay length) of a culvert (Katona, 2019). For RC box culverts, previous studies (Petersen et al., 2010; Wood et al., 2016) indicate that linear elastic materials can be used for both the culvert and the surrounding soil without losing accuracy in the estimated bending moments in the top slab. A multi-layered soil model is considered to reflect the effect of soil stress on the increasing moduli of elasticity in the depth direction (Selig, 1990). Specifically, the properties for well graded or gravelly sand at 85% standard compaction are used. Table 3.1 summarizes the RC and soil properties used in the analysis. The Poisson's ratio for RC material is assumed to be zero following the simplification made by Petersen et al. (2010). This is deemed reasonable due to the large discrepancy between the elastic moduli of soil and RC materials. Also note that less compacted soil was also investigated by Petersen et al. (2010), but the bending moments in RC box culverts were shown to be insensitive to the two sets of soil properties due to the much higher stiffness of RC than soil.

Table 3.1 Material properties used in FE analysis

Material	Elastic modulus, E (ksi)	Poisson's Ratio
RC	4,030	0
Soil (depth: 0-1 ft)	1.3	0.26
Soil (depth: 1-6 ft)	2.1	0.21
Soil (depth: 6-11 ft)	2.6	0.19
Soil (depth: 11-18 ft)	3.3	0.19

To mitigate the effects of soil boundary conditions on the analysis results, the dimensions of the soil mass are sufficiently large in all directions. To this end, the typical culverts analyzed in this project all use a sufficiently large soil mass, with 30 ft in the backfill depth direction, 60 ft in the transverse direction, and 36 ft in the longitudinal direction (Petersen et al., 2010). A culvert is assumed to have a lay length of 36 ft, indicating that the culvert penetrates through the entire soil mass in the longitudinal direction. The soil-culvert system is loaded on the road surface based on the tire patch shown in Figure 3.1(a). The midpoint between the two wheels of an axle lies in the culvert mid-plane that is perpendicular to the longitudinal direction. Consequently, only a half-

space with a length of 18 ft is considered because of the symmetry of the geometric and loading conditions.

Figure 3.3 shows the FE models of single- and double-cell culverts, respectively. These models are created using Abaqus (2010a)[1]. For soil mass, eight-node solid elements with reduced integration and hourglass control are used (Abaqus, 2010a). Four-node doubly curved shell elements with reduced integration and hourglass control (Abaqus, 2010a) are used for the slabs and walls of a culvert. It should be noted that different reference surfaces can be used to define nodal degrees of freedom (DOFs) of shell elements. For external walls and slabs, the reference surface is selected as the outer surface of the members so that the contact with the surrounding soil can be precisely modeled by tying the DOFs of contacting shell and solid elements. For the internal wall of a multi-cell culvert, the mid-surface is used as the reference surface of the shell elements.

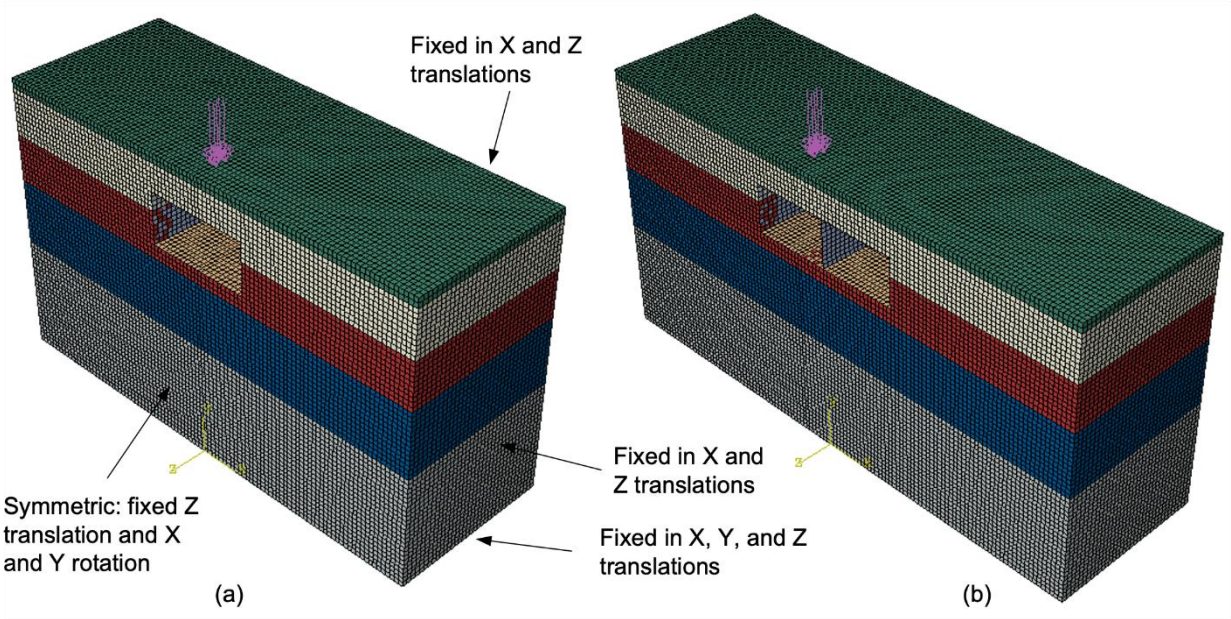

Figure 3.3 FE models of (a) a single-cell culvert and (b) a double-cell culvert

On the peripheries of the soil mass, roller supports are provided to restrain the displacement perpendicular to the peripheries. On the symmetric plane (the XY plane in Figure 3.3), both translational displacement in the Z direction and the rotational displacement around the X and Y directions are restrained. The FE modeling techniques are validated with the results of single-cell culverts reported in Petersen et al. (2010). To facilitate the analysis of all typical culverts, the creation of FE models and the analyses for load effects are automated using the Abaqus Scripting Interface[2] (Abaqus, 2010b).

[1] The U.S. Government does not endorse products or manufacturers. They are included for informational purposes only and are not intended to reflect a preference, approval, or endorsement of any one product or entity.

[2] The U.S. Government does not endorse products or manufacturers. They are included for informational purposes only and are not intended to reflect a preference, approval, or endorsement of any one product or entity.

3.4 BIAS OF LRFD LIVE LOAD DISTRIBUTION MODEL

For all the typical culverts described in Chapter 1, the bending moments at the three critical sections shown in Figure 1.1 are analyzed using the LRFD load distribution model and 2D frame analysis as well as the FE models for the entire soil-culvert systems. The results are presented in Appendix B. The maximum bending moment at each section is determined with a moving load analysis. Specifically, an axle group is moved on the road surface from outside the leftmost wall to beyond the rightmost wall of a culvert. The start and the end points of the moving load are so selected that the distributed load on the top slab, as determined with the LRFD load distribution model, starts to enter and completely exits the span of a culvert, respectively. The critical location causing the maximum load effect is then determined using the 2D frame analysis described previously. Due to the relatively short span of culverts, the load demands in culverts are generally controlled by the weight and configurations of axle groups instead of the entire vehicle. Therefore, single and tandem axle groups are analyzed herein. Although tri- and quad-axle groups also exist, they generally do not control the bending moments in culverts and have usually been ignored in previous studies (Elshimi et al., 2014; Katona, 2019, 2017; Peiris et al., 2024). In each axle group, a single axle is represented by a total of 1 kip uniformly applied on the two tire patches (each having a dimension of 20 inches by 10 inches). Tandem loads are modeled by two unit axle loads spaced 4 ft apart. The use of unit loads can be justified by the linear elastic properties of both the culvert and the surrounding soil. Due to the principle of superposition, the model bias defined previously is not dependent on the magnitude of axle weight. Additionally, the frame analysis results under unit loads can be later used as scalers to efficiently generate large numbers of load effect samples for constructing load spectra without conducting additional frame analysis.

Moving load analysis as described previously is implemented to obtain the maximum values and their corresponding axle locations for Sections S1, S2, and S3, respectively. Based on the LRFD Specifications, the maximum moment at Sections S1 and S3 also considers the potential addition of a live load surcharge equal to 0.00375 klf on external walls. Note that the surcharge height used to obtain the maximum moments is scaled from the original value of 2 ft (Mlynarski et al., 2019) by a factor of 1/32 to account for the difference between the HL93 axle load (32 kips) and the unit load analyzed herein.

The model bias, i.e., load ratio between results from frame and FE analyses, is calculated for all typical culverts and critical sections. Using a selective set of culverts, the frame analysis is shown to be able to reasonably predict the axle location that results in the maximum load effect. Therefore, the moving load analysis is only implemented with the frame model (instead of the FE model). This implies that the uncertainty quantified later is exclusively due to the live load distribution model and does not include the uncertainty in placing the axle group. For implementation, the axle locations are determined using the frame model. Once the critical axle locations are determined, the FE model is created, and the axle load is placed at the same location to compute the model bias. It should be noted that the placement of the axle load is generally different for different sections. This results in more than 300 FE runs using the automated script mentioned previously. Before the quantitative calibration of model uncertainty, the following discussion provides a qualitative investigation of the obtained model biases with respect to several potential explanatory variables.

3.4.1 Model Bias versus Backfill Depth

Figure 3.4 shows the model biases with respect to different backfill depths for the typical culverts. All four backfill depths are considered, ranging from 2 to 8 ft. Figure 3.4 indicates that the LRFD load distribution model, paired with the 2D frame analysis, overestimates the load demands in culverts, which is consistent with the findings in previous studies (Awwad et al., 2008; Katona, 2022; Sharifi et al., 2023). In rare cases, the bending moment at S1 may be slightly underestimated. In practice, this underestimation may not be a concern due to the excessive reinforcement at the corner used to satisfy other design requirements (e.g., cracking) (Mlynarski et al., 2019). In terms of variability, it can be observed that the model biases for moments at Sections S1 (external wall-slab joint) and S3 (internal wall-slab joint) exhibit much greater uncertainty than Section S2 (midspan). This is understandable due to the focus on calibrating the moment at Section S2 during the development and refinement of the live load distribution model (Okeil et al., 2018; Peiris et al., 2024). To reconcile the different levels of model conservatism, a recent study (Okeil and Jafari, 2024) suggests that the live load distribution model should be modified based on the load effect and the cross section of interest.

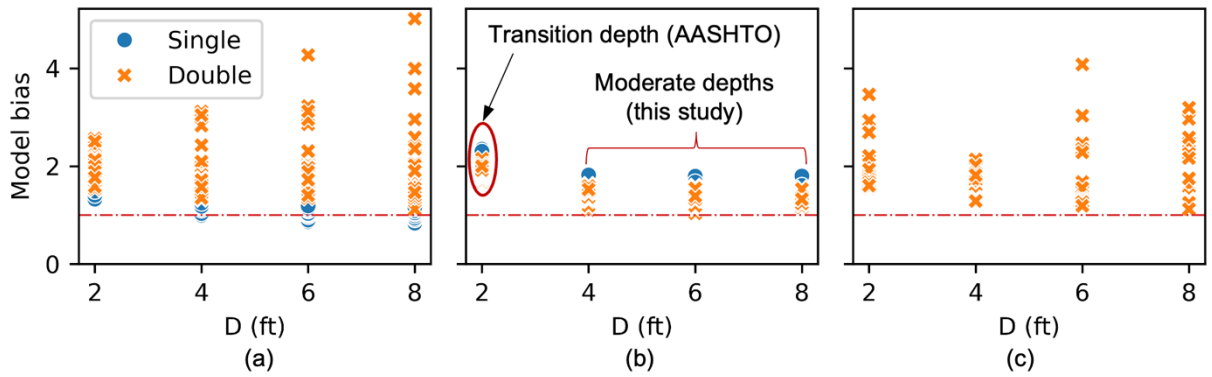

Figure 3.4 Model bias with respect to backfill depth, D (ft), at Sections (a) S1 (external wall-slab joint), (b) S2 (midspan), and (c) S3 (internal wall-slab joint)

Figure 3.4 verifies that the model bias is indeed insensitive to backfill depth between 4 and 8 ft of backfill. Table 3.2 summarizes the computed coefficients of determination (R^2) between the model bias and the backfill depth in the range of moderate backfill. The R^2 scores are also calculated by including the biases associated with 2 ft of backfill. For Sections S1 and S3, the variability of model biases is so large that the R^2 scores are relatively low regardless of whether the 2 ft of backfill is considered. By contrast, both Figure 3.4(b) and Table 3.2 suggest that the extent of overestimation is much more pronounced for 2 ft of backfill than that with the moderate backfill. This high conservatism at 2 ft of backfill has also been reported in recent studies (Katona, 2019; Okeil and Jafari, 2024). Katona (2019) attributed this overestimation to the limited size of the distributed load on the top slab compared to the overall lay length of a culvert, resulting in a more severe 3D stiffness effect that makes the 2D frame model much more conservative. These previous studies and the results presented herein all note the desire for a better transition model from shallow culverts to moderately buried culverts. Due to the scope of this project, the later UQ process focuses only on the 4-8ft backfill. The obtained uncertainty model can still be used for culverts with 2 ft of backfill for reliability analysis and calibration at Section S2. However, it should be recognized that the reliability indices obtained for culverts with 2 ft of backfill represent a lower

bound for how reliable these culverts actually are because of the higher model bias for 2-fit backfill, as shown in Figure 3.4(b).

Table 3.2 Relationship between model bias and backfill depth

Data	Coefficients of determination (R^2) for the following sections		
	S1	S2	S3
Without 2 ft backfill	0.0060	–0.0594	0.0234
With 2 ft backfill	–0.0017	–0.4496	–0.0103

3.4.2 Model Bias versus Cell Span

Besides backfill, cell span has also been shown to influence the live load distribution (Peiris et al., 2024). Therefore, Petersen (2010) introduced an extra term related to the clear cell span for the load spreading in the longitudinal direction, as shown in Equation 3.2 and Equation 3.4. Figure 3.5 shows the relationship between the model bias and the clear cell span. The R^2 scores are directly provided in the figure using only data associated with moderate backfill (4-8 ft). Compared to backfill depth, the cell span can more effectively explain the variance of model biases. Among all three sections, the midspan moment (Section S2) is most clearly correlated to the cell span. Specifically, the conservatism of the estimated load demand at Section S2 increases with respect to the cell span. This trend is again in line with existing results of single-cell culverts (Petersen et al., 2010). The opposite trend is observed in Sections S1 and S3 albeit with noticeably lower R^2 scores. Figure 3.4 and Figure 3.5 indicate that the cell span is a more suitable explanatory variable to quantify the uncertainty of the model bias.

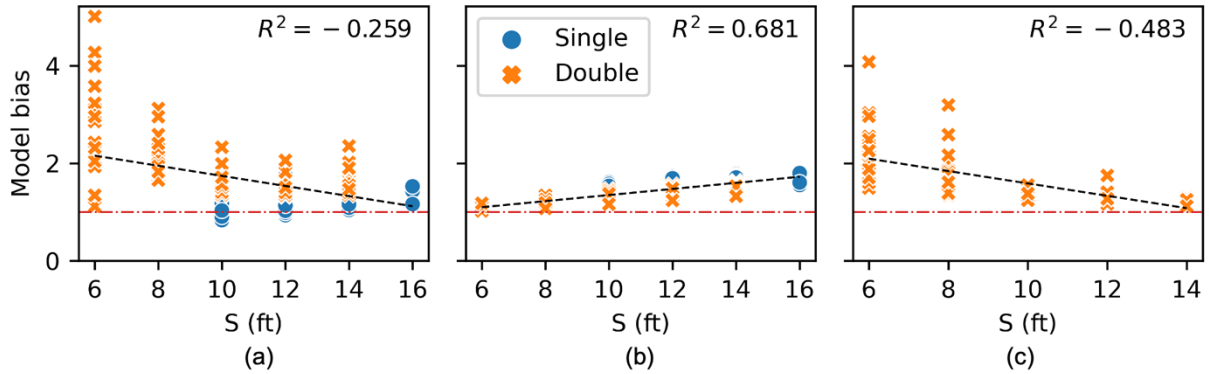

Figure 3.5 Model bias with respect to clear cell span, S (ft), at Sections (a) S1, (b) S2, and (c) S3

3.4.3 Other Explanatory Variables

Apart from the two variables examined above, other potential variables are also considered, including the cell height, cell aspect ratio (i.e., span to height ratio), wall thickness to cell span, total span of the culvert, and a flexural stiffness ratio defined below

$$\rho_{stiff} = \left(\frac{H}{S}\right) \cdot \left(\frac{T}{U}\right)^3 \propto \frac{K_{slab}}{K_{wall}}$$

Equation 3.5 Flexural stiffness ratio factor

where K_{slab} and K_{wall} = flexural stiffness coefficients of the slab and the wall, respectively. Table 3.3 presents the R^2 scores associated with all these variables as well as the backfill depth and cell span considered previously. Table 3.3 indicates that the cell span is the most predictive variable to explain the variance of model biases except for the moment at Section S1, where the ratio of wall thickness to cell span shows slightly higher correlation. It can also be seen that only the midspan moment (S2) has a variance explained by more than 50% using a single variable. In particular, the cell span can account for 68.13% of the variance in the model bias. Another important observation from this investigation is that the total span of a culvert is not a useful explanatory variable. This observation further justifies the typical culvert designs analyzed in this project, i.e., considering only single- and double-cell culverts with a maximum total span of 30.17 ft.

Table 3.3 Relationship between model biases and potential explanatory variables (highest scores in terms of absolute values are bolded)

Variable	Coefficients of determination (R^2) for the following sections		
	S1	**S2**	**S3**
Backfill depth	0.0060	–0.0594	0.0234
Cell span	–0.2585	**0.6813**	**–0.4830**
Cell height	–0.0713	0.3078	–0.2709
Aspect ratio	–0.0000	–0.0096	0.0348
Wall thickness to cell span	**0.2851**	−0.3350	0.3187
Total span	0.0056	0.0000	–0.4782
Stiffness ratio	–0.0718	–0.1037	0.1978

It should also be noted that the investigation herein does not consider combinations of multiple explanatory variables, although the coupling of variables can be somewhat reflected with the introduced compound variables such as the aspect ratio, total span, and stiffness ratio. The R^2 score may be further improved by combining different variables. However, unless supported by a clear understanding of the mechanisms, more complicated designs of explanatory variables risk overfitting the model biases to only match the typical culverts analyzed in this project. It is also worth mentioning that the goal of the present study is to quantify the uncertainty instead of eliminating the model bias.

Based on the previous discussion, the subsequent UQ effort focuses on the midspan bending moment at Section S2 using the cell span as the explanatory variable. Model biases for moments at Sections S1 and S3 do not undergo the UQ process because of the following reasons:

- The much higher uncertainties of their model biases, as evidenced in Figure 3.4 and Figure 3.5, warrant the refinement of the live load distribution model rather than attempt to quantify the uncertainties currently in existence. By using the moment at S2 as an example of UQ, the same procedures can be implemented to any refined models once they become available.

- For moderately buried culverts, upper reinforcement in the top slab is commonly controlled by other criteria (e.g., cracking) or detailing requirement (Cristelo et al., 2019; Freeseman, 2022; Mlynarski et al., 2019) instead of the flexural load demands. As a result, the upper layer of the top slab may have greater amount of reinforcement than the lower layer even though the flexural demands at Sections S1 and S3 are mostly smaller than that at Section S2. Hence, Sections S1 and S3 are most likely to have adequate flexural capacities.

3.5 QUANTIFIED UNCERTAINTY OF MODEL BIAS

For the UQ of load demand at Section S2, Bayesian linear regression is conducted using the clear cell span as the explanatory variable and the model bias as the outcome variable. Compared to existing studies that consider the model bias as a single random variable (Wood et al., 2016), regression analysis can characterize the total uncertainty into an "explained" part using the cell span and an "unexplained" part, which is then modeled as a random variable. As a result, the epistemic uncertainty related to the LRFD load distribution model can be reduced to only the "unexplained" part. Specifically, the model bias is expressed by the following equation:

$$y \equiv \frac{S_{frame}}{S_{FEM}} = w_0 + w_1 S + \epsilon$$

Equation 3.6 Model bias expressed by cell span and model error

where y = outcome variable, i.e., the model bias; S_{frame} and S_{FEM} = load effects obtained from the frame and FE analyses, respectively; w_0 and w_1 = intercept and slope of the linear function; ϵ = normally distributed random variable to reflect the unexplained variance.

In contrast to conventional regression analysis, Bayesian linear regression can directly provide the probability distribution of the outcome variable y, also known as the predictive distribution, based on the cell spans of analyzed culverts and their model biases (i.e., the training data). The mean and the STD of this predictive distribution can be converted to the distribution parameters of λ_{LDS} by the following equation:

$$\bar{\lambda}_{LDS} = \frac{1}{\mu_y}\left[\frac{\sigma_y^2}{\mu_y^2} + 1\right] \approx \frac{1}{\mu_y}$$
$$V_{LDS} = \frac{\sigma_y}{\mu_y}$$

Equation 3.7 Mean and COV of LDS factor given the mean and STD of model bias

where μ_y = mean model bias given a specific cell span, i.e., $\mu_y = w_0 + w_1 S$; σ_y = STD of the model bias given the cell span. The expression of σ_y and more details about Bayesian linear regression can be found in Appendix C.

Based on the cell span of the typical culverts and their corresponding model biases, Table 3.4 presents the results of the Bayesian linear regression. Note that the parameters α^* and λ^* in Table 3.4 are used to compute σ_y based on Equation C.3. Using the parameters in Table 3.4, Figure 3.6 shows the quantified uncertainty for culverts with different clear cell spans. For each cell span, the

Bayesian regression model can yield both the model bias as well as its uncertainty, shown in the figure by areas enclosed by one and three STDs from the mean values.

Table 3.4 Results of Bayesian regression for UQ

Model bias	**Regression parameters and score**				
	w_0	w_1	α^*	λ^*	R^2
Moment at S2	0.7250	0.0623	66.6888	256.9978	0.6813

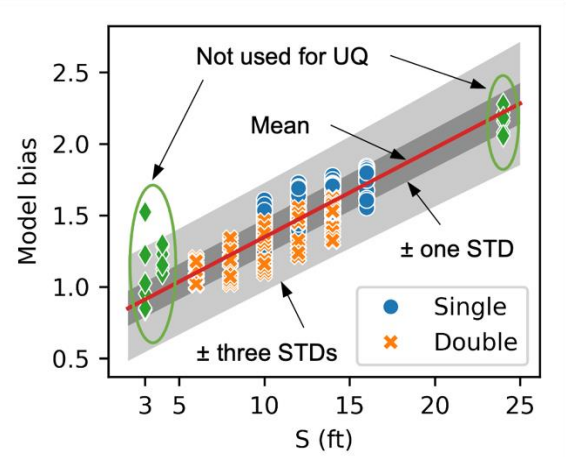

Figure 3.6 Quantified uncertainty with respect to clear cell span

Figure 3.6 also presents the model biases for three culverts not considered in the UQ process. Details of these culverts are shown in Table 3.5. They have either more than two cells and/or clear cell spans outside the range of the training data. In particular, Culverts 101 and 102 have three and four cells respectively, with a clear span less than 6 ft. These designs are adapted from the standard designs provided by Caltrans and TxDOT. Culvert 103 is a 24-ft long-span single-cell culvert analyzed in McGrath et al. (2005). Figure 3.6 indicates that the developed uncertainty model is able to capture the model bias for longer-span culverts at least up to 25 ft. This agreement, in conjunction with the insensitivity of model bias to cell height and total span, indicates that the quantified uncertainty can be applied to a wide range of moderately buried culverts used in practice. However, caution should be taken when extrapolating the model bias to culverts with span shorter than 6 ft. In these culverts, the model bias rarely drops below the predicted mean value from the Bayesian regression model. In these shorter cell spans, the LRFD load distribution model still yields mostly conservative estimations of load effects.

Table 3.5 Additional culvert design for UQ validation

Culvert	*N*	*S* (ft)	*H* (ft)	*T* (in)	*U* (in)
101	3	4	3	6.25	6
102	4	3	2	8	7
103	1	24	8	16	12

Note: N = number of cells; S = clear cell span; H = clear cell height; T = slab thickness; U = wall thickness

3.6 COMPARISON WITH MODEL UNCERTAINTIES OF BRIDGES

The UQ results above indicate that the model bias varies significantly with the clear cell span. Therefore, modeling model bias as one single random variable can introduce considerable error. This finding is demonstrated via the comparison of model bias uncertainties shown in Table 3.6, where the uncertainties are compared for (a) the statistics drawn from all model biases used for UQ, (b) the model bias for a double-cell culvert with a 6 ft clear cell span (the smallest cell span used for UQ), (c) the model bias for a single-cell culvert with a 16 ft clear cell span (the largest cell span used for UQ), and (d) the model bias associated with the moment GDF used for girder bridges. The statistics of GDFs, obtained from NCHRP Project 12-26 (Zokaie et al., 1991 Table F.4), are associated with the moments in interior girders obtained from refined analysis and analytical equations. The inclusion of GDF statistics is because the GDF functions similarly to the live load distribution model of culverts, both of which serve as a link to convert vehicle loads to load effects at critical sections. The following observations can be drawn from this comparison:

- When analyzed as a whole, the load distribution model for culverts is more conservative on average and contains more uncertainty when compared to girder bridges. This is consistent with previous studies on culverts (Bednarcyk, 2012).
- However, the conservatism is not uniform among all culverts. Specifically, the LRFD load distribution model can result in much more conservative load demands in culverts with longer cell spans.

These observations have important implications on the analysis and load rating of RC box culverts. Currently, the load factors for design and evaluation of culverts originate from analyses on girder bridges based on GDF statistics similar to those presented in Table 3.6. As a result, the safety margin of culverts with different cell spans may differ drastically using the current set of live load factors. This situation can be rectified by either developing variable load factors (e.g., related to cell span) or refining load distribution models. The Bayesian model developed herein can facilitate efforts in both directions, and this project opts for the first option for reliability calibration. It should be noted that the findings described herein are based on results for the midspan moment in the top slab. However, the general methodology can be extended to other locations and limit states.

Table 3.6 Comparison of model bias uncertainties

Statistics	All culverts[a]	Double-cell culvert (S=6ft)	Single-cell culvert (S=16ft)	GDF for flexural effect
Mean	1.4468	1.1119	1.7292	1.029
STD	0.2169	0.0628	0.0887	0.034
COV	0.1499	0.0565	0.0513	0.033

Note: (a) Not including 2-ft backfill, culverts with clear cell span shorter than 6 ft, or culverts with clear cell span longer than 16 ft.

CHAPTER 4

UNCERTAINTY QUANTIFICATION OF VEHICULAR LOAD

4.1 INTRODUCTION

Apart from load distribution through backfill soil, another major difference of culverts compared to bridges is the load spectrum. Due to the relatively short span of culverts, the load effects in culverts are primarily controlled by axle groups. This contrasts with bridges where the entire vehicle weight and configuration control the load effects. Additionally, given the absence of girders in the traffic direction, the design and evaluation of RC box culvert are based on a slice (usually 1 ft in length) in the lay length direction of a culvert. As a result, during structural analysis, the increase in the load effect due to side-by-side loading (two-lane loading), if present at all, is not as pronounced as that in bridge girders. This chapter aims to investigate the following research problems related to the culvert load spectrum and the resulting maximum load effect:

- What are the load spectra and the resulting maximum load effect of a culvert under random axle groups?
- What is the site-to-site variation for the maximum load effect derived from different sites?
- Given the single-lane load spectrum and side-by-side frequency, is two-lane loading still the dominant load pattern as in bridges?

In this project, rather than collect and process raw WIM data, the statistics of axle weights and configurations reported in NCHRP Report 683 (Sivakumar et al., 2011) are utilized to generate synthetic samples of loading events. These statistics were obtained from the WIM data in Florida (FL), including FL sites 9919, 9926, 9927, and 9936. The data were originally used for the reliability analysis of bridge decks, which, like culverts, are more affected by the axle groups than the entire vehicles. The statistics at these sites are adopted herein because of the following reasons:

- Compared to raw WIM data, the statistics in NCHRP Report 683 are drawn from data that have already received rigorous screening and processing.
- The sites include typical truck traffic on the interstate and state highway systems. Compared to other states studied in NCHRP Project 12-76 (Sivakumar et al., 2011), the FL sites exhibit greater site-to-site variation. As a result, the uncertainty quantified can be viewed as a conservative estimation suitable for other states.
- Among all FL sites, FL site 9916 has WIM data in only one direction. Moreover, the average daily truck traffic (ADTT) is much lower than the other sites. Hence, it is not used in the analysis.

As mentioned previously, a load spectrum is represented by a normal probability plot of the load effects. In this chapter, only the top-slab midspan moment (i.e., bending moment at Section S2 in Figure 1.1) is considered herein to match the discussion in Chapter 3. As stated in Chapter 3, rather than quantify uncertainties at other cross sections, it is more advisable to refine load distribution models.

4.2 LOAD SPECTRA UNDER RANDOM AXLE GROUPS

4.2.1 Influence of Data Distribution on Load Spectrum

In addition to statistics such as means and STDs of axle weight, it is also important to know the distribution type of the axle group weight. For FL WIM Site 9926, Figure 4.1 shows the histograms of axle group weight of different configurations. Following NCHRP Report 368 (Nowak, 1999) and the MBE, only the statistics of the top 20% heaviest axle groups are used to derive the load spectrum. The histogram in Figure 4.1 is useful to determining the most appropriate distribution type for the top 20% heaviest weight of axle groups. Two distribution types are considered and compared: a normal distribution and a shifted exponential distribution. Although a normal distribution might be a common assumption, the histogram in Figure 4.1 indicates that a shifted exponential distribution is more appropriate to describe the top 20% data for different axle configurations.

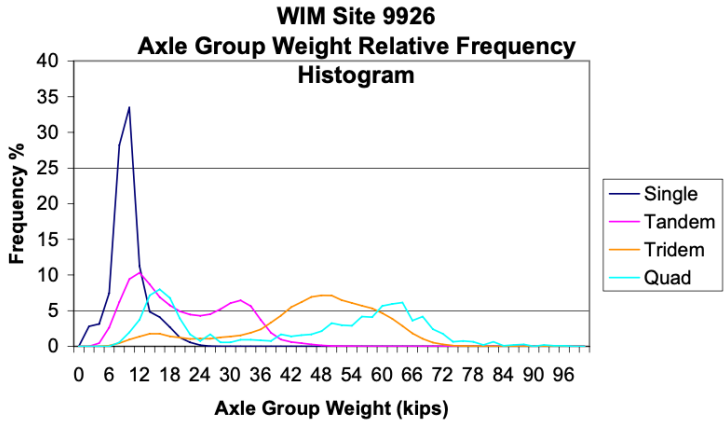

Figure 4.1 Histogram of axle group weight (reprinted from NCHRP Report 683)

The effect of different distribution types on the constructed load spectrum is demonstrated using Culvert 16 with 8 ft backfill. It also serves as an example to derive the load spectrum using the statistics from one specific WIM site. In particular, the load spectrum is constructed based on the statistics of FL site 9926, as shown in Table 4.1. It should be noted that the top 20% mean values for tridem and quad-dem configurations are considerably higher than the legal limits. This is due to the heavy axle weights potentially of permit vehicles with lower GVW. As a result, they were not entirely screened out based on GVW. Similarly heavy tridem and quad-dem axle groups also appeared for another FL site (Site 9936) used in this study. Therefore, for all sites, tridem and quad-dem configurations are not considered by setting their frequencies to zero. Due to their relatively low frequencies, comparison not shown herein indicates that including or excluding these configurations does not vary the projected 5-year and 75-years extremes.

The top 20% means and STDs shown in Table 4.1 can be assumed to follow different probability distributions to generate samples of loading events. To obtain the load spectrum, Monte Carlo simulation (MCS) with 1,000,000 samples is conducted. For each sample, an axle configuration is first randomly selected based on the frequencies of different configurations shown in Table 4.1. Given the selected configuration, its axle weight is then randomly generated based on the assumed distribution and the distribution parameters corresponding to the mean and the STD in Table 4.1.

The generated axle weight is then multiplied by the maximum load effect under unit axle weights, as obtained from Chapter 3, to determine the load effect under the generated axle group.

Table 4.1 Statistics of axle groups based on WIM data

Statistic	Axle configuration and weight (in kips)			
	Single	**Tandem**	**Tridem**	**Quad-dem**
Frequency	2,986,536	3,293,111	94,115	1,077
Mean (top 20%)	16.039	36.285	63.111	70.777
STD (top 20%)	2.932	3.763	3.976	6.282

Note: The mean and STD values for tandem, tridem, and quad-dem axle groups refer to the total weight of all axles in the group. For load spectra, tridem and quad-dem frequencies are ignored (by setting them to zero).

Using the procedure described above, Figure 4.2 shows the two load spectra for Culvert 16 with 8 ft backfill, obtained assuming normal and shifted exponential distributions, respectively. As described in Chapter 2, the upper tail region (95% percentile and above) is used to quantify the uncertainty of the maximum load effect in a given reference period. Considering a 5-year reference period and the number of trucks in 5 years equal to 1,500,000 (Nowak, 1999), the corresponding theoretical quantile is plotted in Figure 4.2. Note that for each truck record, it is assumed that there are two axle group records based on the ratio between truck and axle group numbers for FL site 9926 (Sivakumar et al., 2011). The intersection between the 5-year theoretical quantile and the load spectrum indicates the expected maximum load effect in 5 years. Figure 4.2 indicates that a normal distribution results in an underestimated extreme load effect compared to the shifted exponential distribution. Analyses not presented here indicate that the similar conclusion can be drawn for other culverts, backfill depths, and WIM sites. Therefore, the load spectrum of a culvert is constructed using shifted exponential distributions.

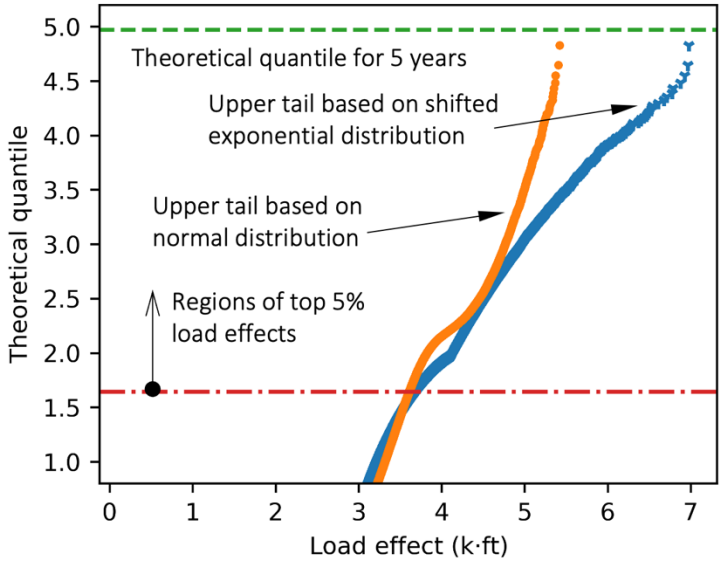

Figure 4.2 Load spectra obtained with axle statistics

4.2.2 Site-to-Site Variation of Maximum Live Load Effects

A load spectrum is constructed similarly for each of the four FL sites considered in this project. The load spectrum is leveraged to project extreme load effects in a given reference period. For each site, the mean and the COV of the maximum live load effect are estimated following the steps in Section 2.2.3.2. For the UQ of the projected live load effect, the average among the four sites is used to represent the mean value of LL_{FR} in Equation 2.9. The COV of LL_{FR} is determined using the average value of COVs associated with the projected value at each site. Appendix D provides the statistics of LL_{FR} for all typical culverts.

The COV of the four mean extreme values at different sites is used to represent the site-to-site variation (Sivakumar et al., 2011). Based on results in Table D.1, the site-to-site variation is 0.168 based on the site-to-site COVs among all culverts. It should be noted that this COV is considerably higher than the bridge data reported in NCHRP Report 683, which ranges from 0.05 to 0.10 for bridges between 40 ft and 200 ft (Table 38 of NCHRP Report 683). However, it is similar to bridges with a 20 ft span. By further considering the variation related to data availability, the overall COV of λ_{NET} in Equation 2.9 can be calculated by the following equation:

$$V_{NET} = \sqrt{V_{site}^2 + V_{data}^2} = \sqrt{0.168^2 + 0.02^2} \approx 0.17$$

Equation 4.1 COV due to site-to-site variation and data availability

where V_{site} = COV due to site-to-site variation; V_{data} = COV due to collection duration of WIM data; $V_{data} = 0.02$ (Sivakumar et al., 2011). It is considered that the mean value of λ_{NET} is 1.0 (Sivakumar et al., 2011).

4.2.3 Bias of Rating Loads to Represent Extreme Load Effect

The extreme load effect obtained from statistical projection and site comparison can differ significantly from the nominal load effect under rating loads. The bias of the loads described in Section 1.2.3 is quantified by the bias factor defined as the ratio of the expected maximum load effect to the nominal load effect under the design or legal loads. If a bias factor is greater than one, it indicates that the maximum live load effect in the reference period is higher than that estimated using the rating vehicle. For the nominal load effect, the dynamic effect is not considered. Therefore, the bias factor can be expressed as follows:

$$b_{FR} = \frac{\overline{LL}_{FR}}{LL_{n,static}}$$

Equation 4.2 Bias factor for static nominal loads

where $\overline{LL}_{FR}$ = mean live load effect obtained with the statistical projection and site-to-site comparison; $LL_{n,static}$ = load effect without dynamic allowance or MPF, and it is estimated with the LRFD load distribution model and the 2D frame analysis. Focusing on the midspan moment, the statistics of the bias factors are summarized in Table 4.2 for different types of rating loads. It should be noted that the FAST Act emergency vehicles were only recently introduced to represent vehicles to support mitigation of hazardous situations, so sufficient samples of these vehicles may

not have been taken before their introduction. Herein, the FAST Act emergency vehicles considered in this study should thus be regarded as surrogate loads rather than actual vehicles made legal on Interstate System by the FAST Act enacted in 2015.

Table 4.2 Statistics of bias factors between the projected and nominal load effects

Load	Mean	STD	Min.	25 percentile	75 percentile	Max.
Design	1.421	0.0213	1.300	1.423	1.424	1.441
Legal	2.071	0.0851	1.793	2.085	2.099	2.309
Emergency	1.156	0.0193	1.129	1.149	1.156	1.262

Figure 4.3 shows the bias factor associated with the design loads grouped by different backfill depths and clear ce ll spans. A reference period of 5 years is considered to determine the expected maximum load effect. Figure 4.3 indicates that the design tandem controls the nominal load effect in single-cell culverts for all the backfill depths considered. For double-cell culverts, when the backfill is low (2 ft and 4 ft), the controlling load switches from the design tandem for longer-span cells to the design truck for shorter-span cells (more specifically the 32 kips axle). When the backfill is deeper than 4 ft, the design tandem again controls regardless of the cell span. Similar plots are presented in Figure 4.4 for the AASHTO legal loads. Among the various AASHTO legal loads considered herein, the T3 load is most likely to control the nominal load effect with the exceptions of culverts with a 2 ft backfill. For the 2 ft backfill, the single-cell culverts are controlled by the NRL, while the SU4 load closely matches the controlling load effect in double-cell culverts. The dominance of the T3 load contrasts with the baseline legal load for bridges, T3S2, used for the reliability analysis and calibration in NCHRP Report 454 (Moses, 2001). For the FAST Act emergency vehicles, Figure 4.5 indicates that the EV3 load, with its heavy rear tandem, dominates the nominal load effects in culverts. The only exception is for 6 ft double-cell culverts under 2 ft backfill. In this case, the heavy rear single axle of the EV2 load yields the maximum midspan bending moment. Comparing the bias factor among all rating vehicles also indicates the FAST Act emergency loads yield the highest nominal load effects, followed by the design loads. The AASHTO legal loads, on the other hand, give the lowest nominal load effects in culverts.

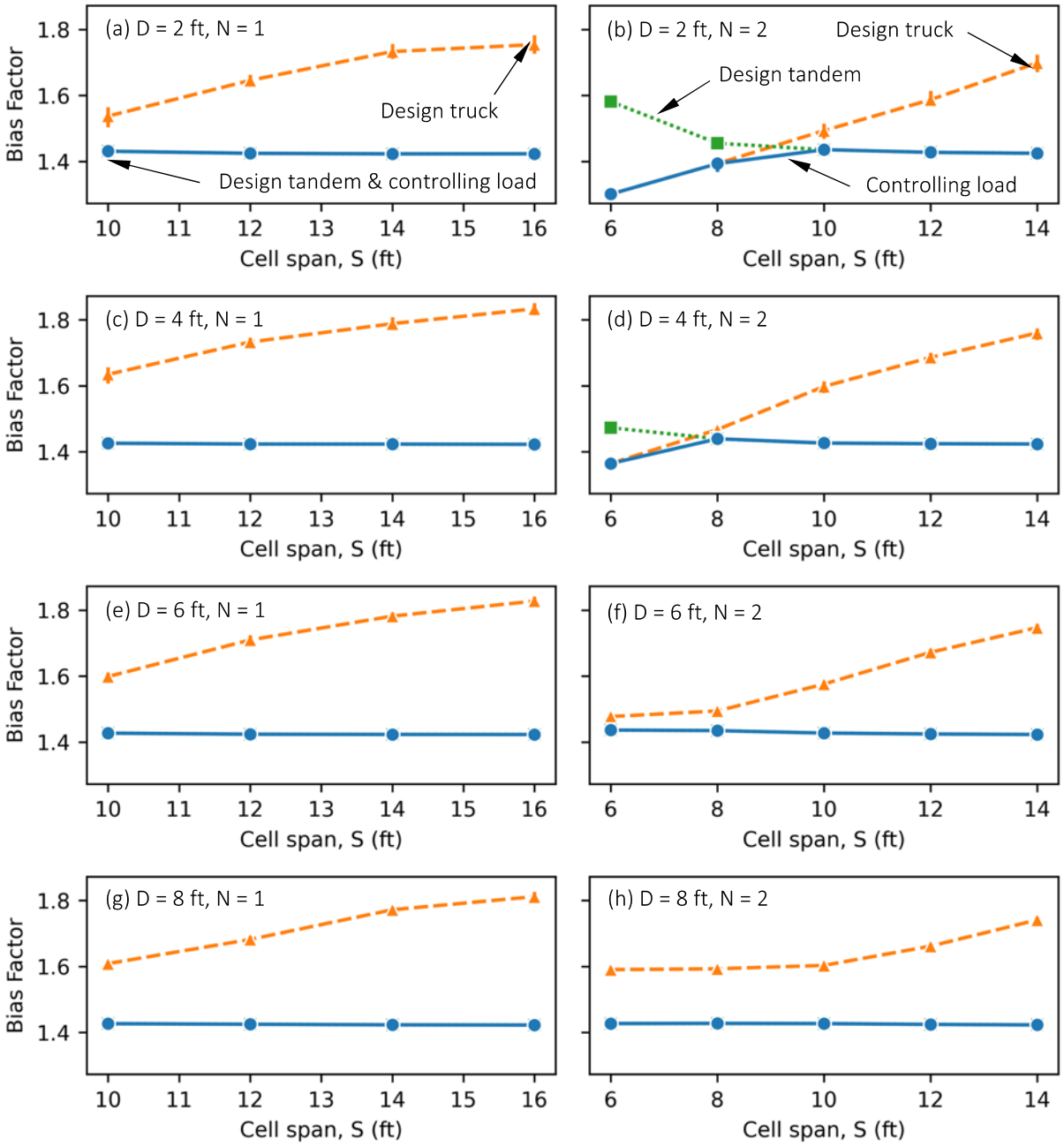

Figure 4.3 Bias factor under static design loads with different backfill depths, *D*, and numbers of cells, *N*

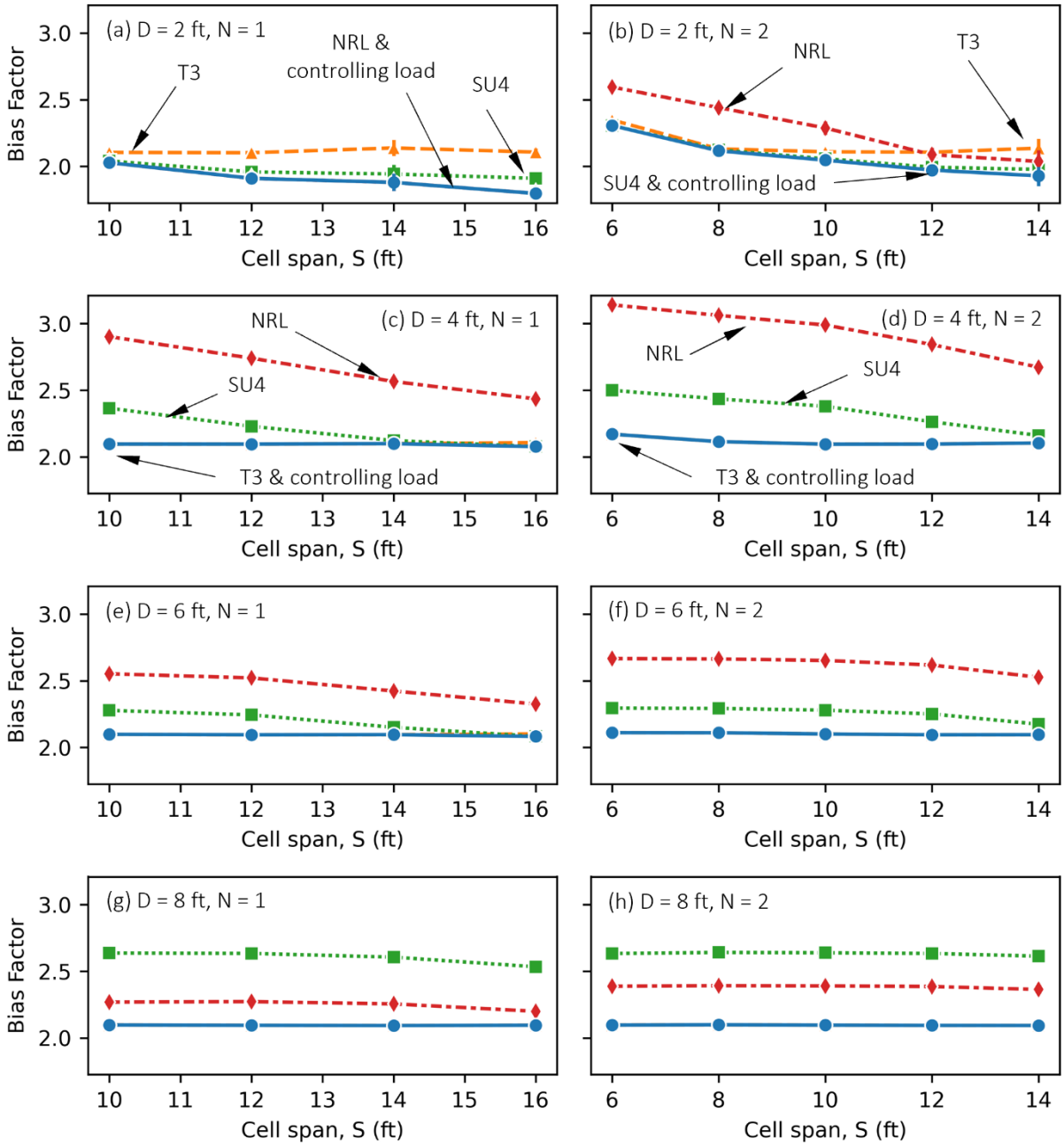

Figure 4.4 Bias factor under static AASHTO legal loads with different backfill depths, *D*, and numbers of cells, *N*

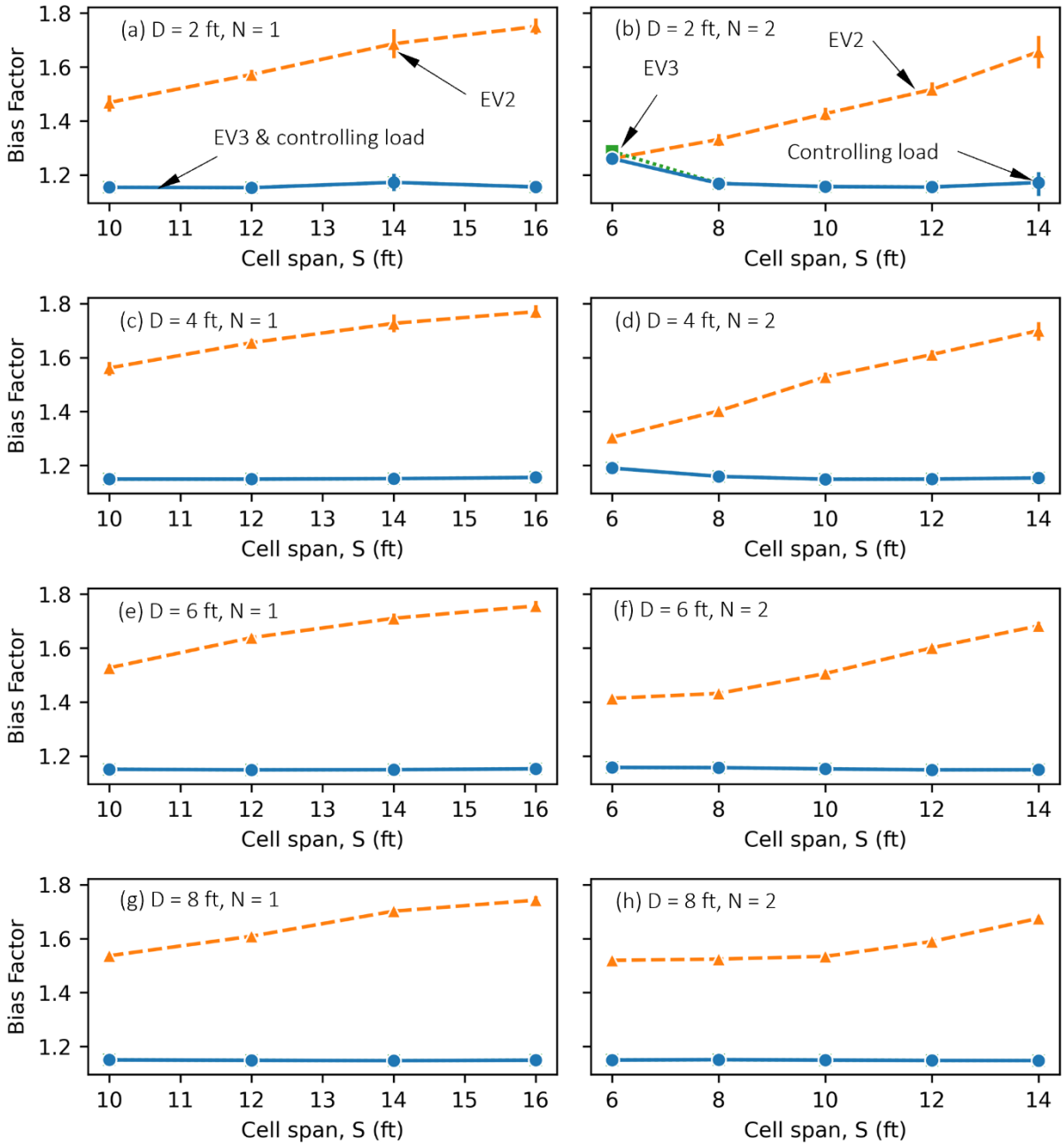

Figure 4.5 Bias factor under static FAST Act emergency vehicle as surrogate loads with different backfill depths, *D*, and numbers of cells, *N*

4.3 MULTIPLE PRESENCE EFFECT UNDER TWO-LANE LOADING

The statistics presented in Table D.1 are associated with axle groups on one lane. Hence, the load spectrum obtained above represents the load effect caused by single-lane traffic. The maximum load effect in a structure may also be caused by side-by-side traffic in two adjacent traffic lanes. The potential influence of side-by-side traffic on the maximum load effect is referred to herein as

the multiple presence effect. For the design and rating of conventional girder bridges, two competing considerations should be examined to determine the most critical loading pattern:

- **Structural behavior:** given the same single-lane load, the load effect in a girder under two-lane loading is always greater than that under one-lane loading.
- **Load spectrum:** given a specific reference period, the GVW that results in the maximum load effect under one-lane loading is greater than that under two-lane loading.

According to NCHRP Report 368 (Nowak, 1999), the two-lane loading pattern should be used as the baseline because in girder bridges, the first consideration affects the maximum load effect more than the second consideration. Therefore, the extreme load effect and the design loads were calibrated with the load spectrum under two-lane loading (Nowak, 1999). Culverts differ from girder bridges from both the perspectives of structural behavior and load spectra, as elaborated in the following subsections. As a result, it is investigated herein whether the UQ of live load effects should still be based on the two-lane loading.

4.3.1 Structural Behavior under Two-lane Loading

Given the absence of girders in the traffic direction, the analysis of RC box culverts is based on a 2D frame model. As a result, the increase in the load effect due to two-lane loading, if present at all, is not as pronounced as that in bridge girders. To illustrate the difference in structural behavior, we first consider the increase in load effect due to two-lane loading in girder bridges. Herein, we focus on the load effects in RC girders. Given the same vehicle load under one- and two-lane loading cases, the ratio of bending moments under two- and one-lane loading can be expressed using GDFs as follows:

$$r_{2/1,girder} = \frac{\left[0.075 + \left(\frac{S_g}{9.5}\right)^{0.6} \cdot \left(\frac{S_g}{L}\right)^{0.2} \cdot 1.05\right]}{\left[0.06 + \left(\frac{S_g}{14}\right)^{0.4} \cdot \left(\frac{S_g}{L}\right)^{0.3} \cdot 1.05\right]/1.2}$$

Equation 4.3 Ratio of girder bending moment under two- and one-lane loading

where $r_{2/1,girder}$ = ratio of bending moment in a girder; S_g = girder spacing in ft; L = girder span in ft. The GDF expressions in the ratio are based on the LRFD Specifications for typical section type (e). Additionally, the simplified value, i.e., 1.05 per Table 4.6.2.2.1-3 of the LRFD Specifications, is used to replace the term related to the longitudinal stiffness. The factor 1.2 in the denominator is applied to remove the multiple presence factor (MPF) embedded in the expression of one-lane GDFs. Therefore, the load ratio considers the bending moment under identical load in each lane in one and two-lane loading cases.

For RC box culverts, two-lane loading may or may not increase the load effect due to the strip model used for structure analysis. Figure 4.6 illustrates both possibilities. For culverts with shallow or moderate backfill, the pressure on the frame is controlled by the distributed width under one wheel load regardless of whether the culvert is loaded on one or two lanes. In this case, two-lane loading does not change the predicted load effect in the culvert. For deeper backfill, on the other hand, the two-lane loading corresponds to a distributed width that is slightly less than twice the

distributed width under one-lane loading. As a result, the pressure on the strip under two-lane loading becomes greater than that under one-lane loading. Using the LRFD load distribution model, the ratio of load effects (including bending moment) under two- and one-lane loading can be expressed as follows for culverts:

$$r_{2/1,culvert} = \begin{cases} 1.0 & D \le D_1 \\ \dfrac{2 \cdot (w_t + LLDF \cdot D + 0.06S)}{w_t + 4 + LLDF \cdot D + 0.06S} & D_1 < D \le D_2 \\ \dfrac{2 \cdot (w_t + s_a + LLDF \cdot D + 0.06S)}{w_t + s_w + LLDF \cdot D + 0.06S} & D > D_2 \end{cases}$$

Equation 4.4 Ratio of bending moment under two- and one-lane loading

where $r_{2/1,culvert}$ = ratio of load effects in a culvert; D = backfill depth in ft; D_1 = first overlapping depth between axle loads in adjacent lanes; D_2 = second overlapping depth between wheel loads in one lane; w_t = width of tire patch in ft (1.667 ft = 20 in); s_a = spacing between two axles (4 ft); s_w = spacing between two wheels in one axle (6 ft); $LLDF$ = live load distribution factor equal to 1.15; S = clear cell span in ft.

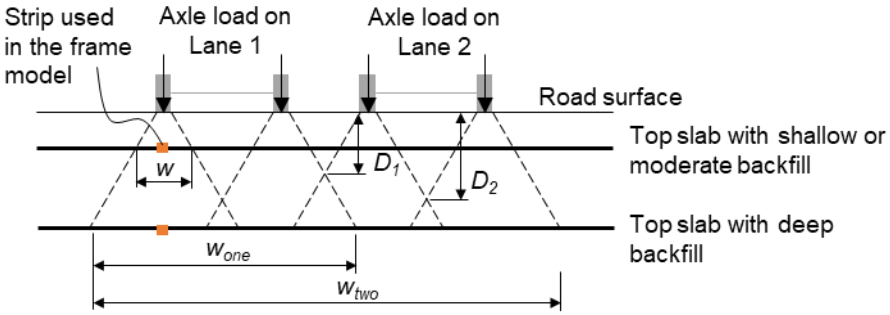

Figure 4.6 One- and two-lane loading cases for culverts

Based on Equation 4.3 and Equation 4.4, the ratios between two- and one-lane loading patterns are calculated for both girder bridges and culverts. For girder bridges, two girder spans, 60 ft and 200 ft are considered, and for each girder span, seven girder spacings ranging from 4 ft to 16 ft are examined. These lower and upper bounds for span and spacing values are determined based on the applicable scope of the GDF equations. For culverts, two clear cell spans, 6 ft and 14 ft, are considered. For each cell span, seven backfill depths evenly spaced between 2 ft and 14 ft are used to calculate the ratio. Figure 4.7 presents the load ratios calculated for both girders and culverts.

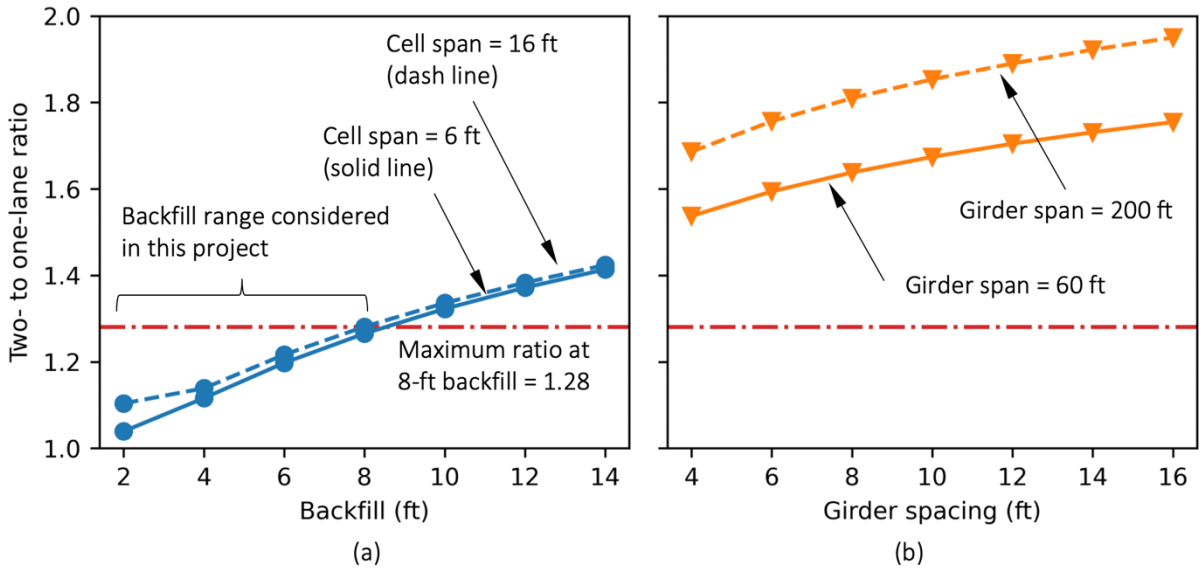

Figure 4.7 Ratio of load effect between two- and one-lane loading patterns: (a) culverts and (b) girder bridges

Figure 4.7 indicates that the ratio between two- and one-lane loading for girder bridges is considerably higher than that in culverts. For culverts with a backfill less than 8 ft, the load effect due to two-lane loading is only slightly increased by up to 28% in contrast to an at least 53% increase in the girder bridges. Therefore, although the load effect may still be increased due to two-lane loading, the increase for culverts is much less pronounced than that for girder bridges.

4.3.2 Load Spectrum under Two-lane Loading

The lack of clear dominance for two-lane loading can affect the shape of the two-lane load spectrum of culverts. Consider again Culvert 16 and the statistics at FL WIM Site 9926. The bending moment spectrum under two-lane loading can be determined in a similar fashion to that for bridges. The site data indicate that among all 6,374,839 records of one-lane events, 60,966 of them are side-by-side events with various axle configurations on the two adjacent lanes. Assuming conservatively that all side-by-side events include two fully correlated axle groups, the statistics yield a frequency of two-lane loading equal to 60,966/6,374,839 = 0.00956, i.e., on average every 104th axle group passage is accompanied by an identical axle group passage in the adjacent lane. It should be noted that to derive two-lane load spectrum for bridges, the NCHRP Report 368 (Nowak, 1999) assumed a two-lane frequency of 0.00222[1]. Although each event of side-by-side truck may include several events of side-by-side axle groups, the adopted two-lane frequency associated with culverts is still considered a reasonable overestimation.

Similar to the one-lane spectrum shown in Figure 4.2, the two-lane spectrum can be obtained using Monte Carlo simulation and the adopted two-lane frequency. To ensure sufficient samples of two-

[1] It is assumed that every 15th truck is accompanied by another truck on the adjacent lane, and two fully correlated trucks occurs every 30 side-by-side events. Hence, the two-lane loading frequency is 1/15/30=0.00222.

lane loading, 10,000,000 one-lane samples are first generated. Subsequently, one sample on the two-lane spectrum is generated by (a) randomly selecting a one-lane sample with a probability equal to the two-lane frequency (i.e., 0.00956 for culverts) and (b) multiplying the selected one-lane load effect by the ratio in Equation 4.4. Figure 4.8(a)-(d) shows both the one- and two-lane spectra of Culvert 16 under different backfill depths from 2 ft to 8 ft. For comparison, the one- and two-lane load spectra of a typical girder bridge with a 60 ft span and a 4 ft girder spacing are also generated and presented in Figure 4.8(e). To better showcase the difference, the samples in each culvert or bridge are nominalized by the mean value of one-lane load effects.

For each load spectrum in Figure 4.8, the upper tail (the top 5% samples) is fitted to a normal distribution. According to Section 2.2.3.2, the intersection between the fitted tail and the theoretical quantile represents the expected maximum load effect within the given reference period. Figure 4.8 highlights these points considering a reference period of 5 years. The expected maxima for both 5- and 75-year reference periods are provided in Table 4.3.

The ratios in Table 4.3 indicate that for the majority of the analyzed backfill depths (i.e., 2-6ft), one-lane loading either controls the maximum load effect or closely matches that under two-lane loading. Even for the 8 ft backfill when two-lane loading does control, the difference in the maximum load effect between two- and one-lane loading is noticeably lower than that in bridges. It should be noted that since the analyzed culvert has a relatively long cell span of 16 ft, Figure 4.7(a) indicates that the potential dominance of two-lane loading is likely to be the most extreme scenario among all typical culverts, i.e., other culverts are even more likely to be controlled by one-lane loading. By contrast, due to the girder span and spacing for the analyzed bridge, it is least affected by two-lane loading as demonstrated by the lowest ratio shown in Figure 4.7(b). Hence, the difference in the controlling loading pattern between culverts and bridges is likely to be much more salient than the results presented herein.

As one-lane loading typically controls, the uncertainty in the estimated live load effect in culverts, i.e., LL_{FR} in Equation 2.9, should be quantified using the load spectrum under one-lane loading. This is different from bridges, where two-lane loading typically controls (Nowak, 1999). Additionally, the culvert load spectrum differs from the bridge load spectrum. Most notably, the COV associated with the upper tail fitting is larger for culverts than bridges. Among all culverts under consideration, the COV averages at 45%, while for bridges under one heavy truck, the average COV is around 35% (inferred from Fig. B-12 of NCHRP Report 368). Both the one-lane loading and the distinct shape of a culvert load spectrum affect the quantified uncertainty of LL_{FR}, which can be found for all typical culverts in Table D.1. The total uncertainty of the live load effect, considering both load spectra and the model uncertainty analyzed in Chapter 3, is presented in Table D.2.

Table 4.3 Comparison of nominalized load effects under one- and two-lane loading patterns

Culvert or bridge	Expected maximum (75 years)			Expected maximum (5 years)		
	One-lane	Two-lane	Ratio	One-lane	Two-lane	Ratio
D=2 ft	3.254	3.179	0.977	3.055	2.916	0.955
D=4 ft	3.240	3.305	1.020	3.043	3.027	0.995
D=6 ft	3.232	3.485	1.078	3.035	3.198	1.054
D=8 ft	3.251	3.674	1.130	3.053	3.370	1.104
Bridge	2.558	3.269	1.278	2.414	3.005	1.245

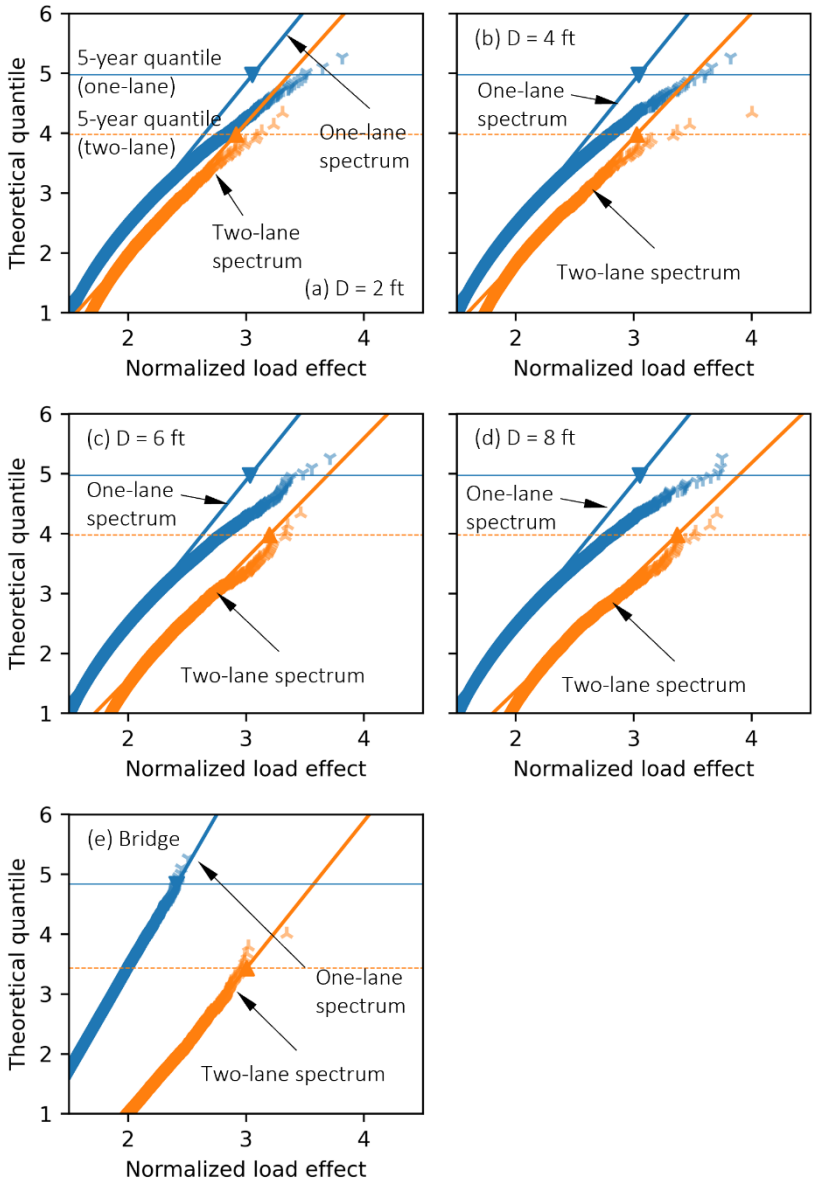

Figure 4.8 One- and two-land load spectra: (a) Culvert 16 with 2 ft backfill, (b) Culvert 16 with 4 ft backfill, (c) Culvert 16 with 6 ft backfill, (d) Culvert 16 with 8 ft backfill, and (e) a bridge girder (Note: The two-lane theoretical quantile corresponds to the frequency of axle group weight on one of the two-loaded lanes)

CHAPTER 5

RELIABILITY ANALYSIS AND LOAD FACTOR CALIBRATION

5.1 INTRODUCTION

Based on the uncertainty quantification results, the reliability indices of all typical culverts are analyzed using the first order reliability method (FORM) presented in Section 2.3. A novel approach to reliability-based calibration is developed to adjust the live load factor for load rating. The scope in this chapter is limited to the midspan bending moment in the top slab of a culvert, primarily due to its well-defined uncertainty compared to other cross sections and limit states (see Chapter 3 for justification and more details).

In this chapter, the reliability indices of all typical culverts presented in Chapter 1 are computed using the existing load and resistance factors for load rating at the inventory and operating levels of the design load rating as well as legal load rating. For the calibration of live load factors, three types of rating vehicles are considered herein, including design load HL-93 for operating rating, AASHTO legal vehicles, and FAST Act emergency vehicles as surrogate loads, as summarized in Section 1.2.3. For all the rating levels and rating vehicles, the target reliability index and the reference period as well as the existing load factors can be found in Table 2.1 and Table 2.2, respectively. Using the proposed calibration approach, the live load factor is adjusted based on the bias of the nominal live load effects and the variations quantified in the previous chapters. A step-by-step procedure is laid out in Section 5.6 to facilitate application.

5.2 APPROACH TO CALIBRATING LIVE LOAD FACTORS

Based on the discussion in Section 2.3, the factored live load effect can be determined using the sensitivity factor associated with the live load effect and the target reliability index. Since the live load effect follows a Gumbel distribution, the live load factor can be expressed as follows:

$$\gamma_{LL} = \frac{LL_d}{LL_n} = \frac{u_{LL} - \frac{1}{a_{LL}} ln\{-ln[\Phi(-\alpha_{LL}\beta_T)]\}}{LL_n}$$

Equation 5.1 Live load factor based on the uncertainty characteristics of live load effect

where γ_{LL} = live load factor determined with the sensitivity factor; LL_d and LL_n = design (i.e., factored) and nominal live load effects, respectively; the latter is obtained using the LRFD load distribution model and the 2D frame analysis; α_{LL} = sensitivity factor of the live load effect described in Section 2.3 and hereafter referred to as the live load sensitivity for brevity; u_{LL} and a_{LL} = parameters of a Gumbel distribution, and they can be obtained from the mean and the COV of the live load effect. For operating and legal rating investigated in this project, the target reliability index β_T is 2.5. The expression in Equation 5.1 can be further simplified by using the following approximations (Yerukala and Boiroju, 2015):

$$\Phi(z) \approx \frac{exp(1.5958z)}{1 + exp(1.5958z)}$$
$$ln(1 + x) \approx x \quad for\ x \to 0$$

Equation 5.2 Approximations for simplifying the expression of live load factor

The simplified live load factor can then be written as:

$$\gamma_{LL} = \frac{u_{LL} + 1.5958/a_{LL}}{LL_n} = b_{LL} \cdot (1 - 0.4499V_{LL} + 1.2442\alpha_{LL}\beta_T V_{LL})$$

Equation 5.3 Simplified expression of live load factor

where b_{LL} = bias factor of the live load effect defined as the ratio of the mean to the nominal load effect, determined based on the rating loads; V_{LL} = total COV of the live load effect (referred hereafter as the live load COV for short). Note that different rating loads give rise to different nominal values and, thereby, bias factors. In particular, the bias factor can be expressed as follows:

$$b_{LL} = \frac{b_{FR}}{MPF \cdot (1 + IM)} \cdot \bar{\lambda}_{NET} \cdot \bar{\lambda}_{LDS} \cdot \bar{\lambda}_{BF} \cdot \bar{\lambda}_{DYN}$$

Equation 5.4 Bias factor of live load effects

where b_{FR} = bias factor of the projected load effect, the statistics of which are presented in Table 4.2; MPF = 1.2 for the design loads and 1.0 for legal loads; IM = nominal value of the dynamic allowance, evaluated following the LRFD Specifications. The mean values, $\bar{\lambda}_{NET}$ and $\bar{\lambda}_{BF}$, are equal to 1.0 based on the discussions in Chapter 2. The mean value, $\bar{\lambda}_{LDS}$, is obtained from the Bayesian regression in Chapter 3. The mean value, $\bar{\lambda}_{DYN}$, is calculated based on the backfill depth using Equation 2.12.

Since the target reliability is given, and b_{LL} and V_{LL} can be obtained from UQ, the live load factor can be calibrated once the live load sensitivity, α_{LL}, is evaluated. For the performance function in Equation 2.1, the live load sensitivity is related to the means and COVs of resistance, permanent, and live load effects. In this project, the resistance is back-calculated from the factored permanent and live load effects, and the COVs of resistance and permanent load effects do not vary significantly among analyzed culverts. Therefore, the key factors influencing the live load sensitivity include the ratio of the mean permanent load effect to the mean live load effect (referred to hereafter as the load ratio), the live load COV, and the adopted live load factor (since the permanent load factors are not calibrated).

Considering the typical load ratio and the live load COV in bridges and buildings, several sensitivity factors for the live load effects have been proposed (e.g., CEN 1990, 2002). However, these existing factors are not suitable for culverts due to the wide range of load ratios dependent on the backfill depth. Therefore, a new approach is proposed to determine the live load sensitivity and, thereby, the live load factor appropriate for culverts. The proposed approach relates the live load sensitivity to culvert characteristics that can reflect the aforementioned influencing factors, specifically the load ratio.

Given a culvert with a specific backfill depth, the load ratio should be determined with UQ results. Since these results are typically not available during load rating, a proxy for the load ratio is developed. One natural choice is the ratio of the nominal permanent to live load effects. However, load rating includes several different rating loads that can significantly change the nominal live load effect and thereby the nominal load ratio, although the load ratio between the mean values does not change. In this project, a simplified beam analog shown in Figure 5.1 is used to derive the geometries affecting the load ratio. The beam in the figure represents the top slab of one cell. For the permanent load effect, the distributed load has a magnitude of $\gamma_s D$, where γ_s is the soil density and D is backfill depth. For the live load effect, a simplified point load proportional to W/D is considered, where W is the weight of an axle group, and the denominator D is used to reflect the load distribution perpendicular to the beam plane. As a result, the ratio of the midspan moments is proportional to $D^2 S$, where S is the clear cell span. Therefore, the proxy variable below is used to replace the load ratio:

$$X_{LL} = D^2 S$$

Equation 5.5 Explanatory variable to predict the live load sensitivity

where X_{LL} = proxy for the load ratio; D and S = backfill depth and clear cell span in ft, respectively. Since the proxy variable is only related to the culvert and backfill dimensions, the value does not change with the rating loads, thus better representing the load ratio between mean values. To reflect the wide range of the load ratio, all typical culverts with different backfill depths are considered.

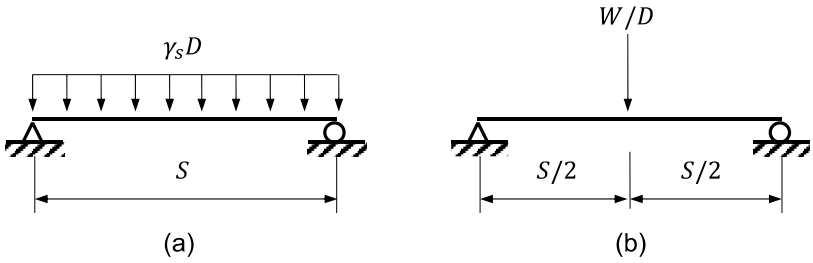

Figure 5.1 Beam simplifications for estimating midspan moments: (a) under permanent load and (b) under vehicular live load.

In addition to the load ratio, several live load COVs and live load factors are also considered, including

- live load COVs ranging from 0.05 to 0.30 with a 0.05 interval, and
- live load factors for the design loads ranging from 1.0 to 2.2 with a 0.2 interval.

For each unique combination of the culvert, backfill depth, live load COV, and live load factor, the reliability index and the live load sensitivity are determined using the iHLRF algorithm. For reliability indices between 2.0 and 4.0, the live load sensitivities are plotted in Figure 5.2 with respect to the live load factor, the proxy variable defined in Equation 5.5, and the live load COV. Among these three influencing factors, Figure 5.2 indicates that the live load sensitivity is least affected by the live load factor. This observation can simplify the calibration of live load factors, because the live load sensitivity and the use of Equation 5.3 for calibration are not predicated on an initial guess on the appropriate live load factor, thus avoiding iteration. The live load sensitivity

does vary significantly with both the proxy variable and the live load COV. As expected, the live load sensitivity increases with the live load COV and decreases with the load ratio approximated by the proxy variable.

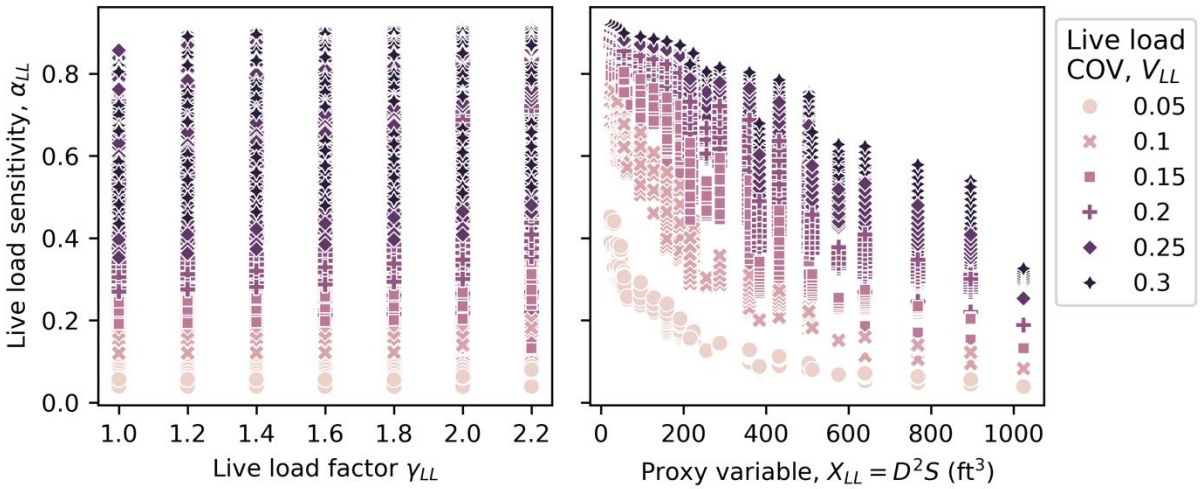

Figure 5.2 Live load sensitivity with respect to (a) live load factor and (b) proxy variable for load ratio

Using the results in Figure 5.2 (b), a series of regression analyses are conducted to allow the prediction of the live load sensitivity based on the proxy variable. Specifically, for each live load COV, the following function is adopted to predict the live load sensitivity:

$$\hat{\alpha}_{LL} = exp(kX_{LL} + b)$$

Equation 5.6 Regression model for live load sensitivity

where k and b = model parameters obtained from regression using maximum likelihood estimation. Table 5.1 provides the model parameters for different live load COVs and the accuracy of the model in terms of R^2 scores. The R^2 scores are also calculated when the load ratio is used in lieu of the proxy variable for regression analysis. The similarity between the two sets of R^2 scores demonstrates the effectiveness of the proxy variable. Based on the model parameters, Figure 5.3 shows the fitted model versus the data.

Table 5.1 Parameters of the regression model to estimate live load sensitivity

Live load	**Model parameters**		**R^2 value based on**	
COV V_{LL}	k ($\times 10^{-3}$)	b	Proxy	Load ratio
0.05	–2.130	–1.319	0.823	0.826
0.10	–2.208	–0.488	0.910	0.916
0.15	–1.965	–0.164	0.956	0.976
0.20	–1.618	–0.0500	0.946	0.977
0.25	–1.289	–0.0148	0.922	0.963
0.30	–1.018	–0.00795	0.902	0.935

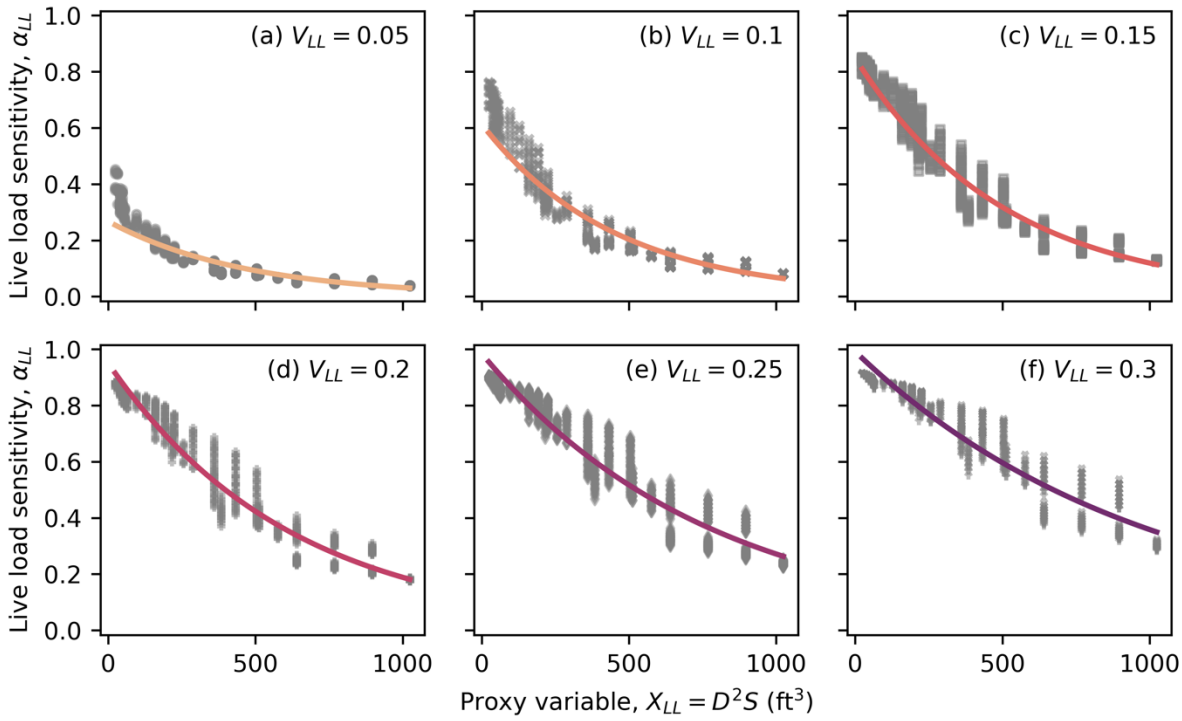

Figure 5.3 Regression results for live load sensitivity with different live load COVs, V_{LL}

As an existing structure, the live load COV may vary within the considered range based on the availability of site- and structure-specific information. For a specific COV within 0.05 and 0.30, interpolation can be conducted to estimate the corresponding live load sensitivity. For instance, if a culvert renders a proxy variable equal to 96 ft^3 and a live load COV equal to 0.125, the live load sensitivity is 0.6 based on the interpolation between $\alpha_{LL} = 0.497$ at $V_{LL} = 0.10$ and $\alpha_{LL} = 0.703$ at $V_{LL} = 0.15$.

Once the live load sensitivity is obtained, the live load factor can be calibrated based on Equation 5.3. We refer to this calibrated factor as the "sensitivity-based" live load factor. Similarly, using the expressions in Table 2.5, the sensitivity-based resistance and permanent load factors can be similarly calculated as follows.

$$\phi_{sens} = b_R \cdot exp(\alpha_R \cdot \beta_T \cdot V_R)$$
$$\gamma_{DL,sens} = b_{DL} \cdot (1 + \alpha_{DL} \cdot \beta_T \cdot V_{DL})$$

Equation 5.7 Sensitivity-based resistance factor

where b_R and b_{DL} = bias factors of the resistance and permanent load effect, respectively, defined as the ratio of the mean to the nominal values; α_R and α_{DL} = sensitivity factors for the resistance and permanent load effect, respectively. These sensitivity-based resistance and permanent load factors are not necessarily the same as or close to the factors used in the MBE. Table 5.2 summarizes statistics of these sensitivity-based factors obtained from Equation 5.7. The bias factors and the COVs of the resistance and permanent load effect are taken from the UQ results (Section 2.2.1 and Table A.1, respectively). The sensitivity factors are obtained from the previous

reliability analyses conducted for the regression analysis of live load sensitivity. In particular, among all the live load COVs and live load factors considered previously, the statistics in Table 5.2 are drawn from data corresponding to the live load COV equal to 0.25 and the live load factors resulting in a reliability index close to 3.5. This is to stay consistent with the UQ results for culverts and the target reliability index used to derive the resistance and permanent load factors in the MBE.

Table 5.2 Sensitivity-based resistance and permanent load factors

Factor	Mean	STD	Min.	25% percentile	75% percentile	Max.
Resistance	0.85	0.05	0.77	0.80	0.90	0.93
Permanent load	1.10	0.06	1.02	1.05	1.15	1.24

Table 5.2 indicates that while the sensitivity-based resistance factor is close to the MBE factor of 0.9, the sensitivity-based permanent-load factor is consistently lower than that specified in the MBE, which ranges from 1.25 to 1.35 for different sources of the permanent load effect. When the sensitivity factor is used to adjust only the live load factor, the reliability index would be overestimated. The implications on reliability are investigated in the following sections.

5.3 RELIABILITY UNDER DESIGN LOADS

The reliability indices associated with RF = 1 are calculated for all typical culverts using the iHLRF algorithm. For the design loads, both inventory and operating levels are considered using single-lane loading and MPF=1.2. The two levels have the following key differences:

- The reference periods for inventory and operating levels are 75 years and 5 years, respectively. As a result, the uncertainties of the maximum load effect are different.
- The target reliability index at the inventory level is 3.5, which is consistent with design. By contrast, the target reliability index at the operating level is 2.5.

The reliability indices of all culverts are provided in Table E.1 of Appendix E. Table 5.3 shows the statistics of the reliability indices at both levels. As expected, the reliability for the inventory level is higher than that for the operating level. The average reliability index for inventory rating is slightly higher than the target reliability index of 3.5, while the average reliability index for operating rating is considerably higher than the target reliability index of 2.5.

Table 5.3 Results of reliability analysis under design loads

Rating level	Mean	STD	Min.	25th percentile	75th percentile	Max.
Inventory (γ_{LL} = 1.75)	3.75	0.35	3.02	3.50	4.01	4.45
Operating (γ_{LL} = 1.35)	3.29	0.34	2.44	3.12	3.51	3.96

Given the average indices in Table 5.3 and the necessary match between the inventory rating and the LRFD Specifications, this project focuses on the calibration of the live load factor for the operating level. Equation 5.3 is used to calibrate the live load factor for operating rating based on the following assumptions:

- The bias factor of the live load effect, b_{LL}, is computed using Equation 5.4 with $b_{FR} = 1.421$ according to the mean value for design loads shown in Table 4.2.
- The live load COV, V_{LL}, is equal to 0.25, which is the average COV of all culverts based on results in Table D.2.
- The live load sensitivity, α_{LL}, is approximated by Equation 5.6 and parameters in Table 5.1.

Figure 5.4 shows the calibrated live load factor for culverts grouped by different backfill depths and clear cell spans. Note that the number of cells does not influence the calibration procedure. Figure 5.4 indicates that the calibrated live load factor is considerably higher than the current live load factor of 1.35. This is attributed to (a) the high live load COV compared to that of bridges and (b) the compensation for the low sensitivity-based permanent load factor, as shown in Table 5.2. Instead of a constant value, the calibrated live load factor decreases with increasing backfill depth and clear cell span. The former (relation with backfill depth) is due to the increased permanent load effect, while the latter (relation with clear cell span) is due to the rising conservatism of the load distribution model with respect to the cell span.

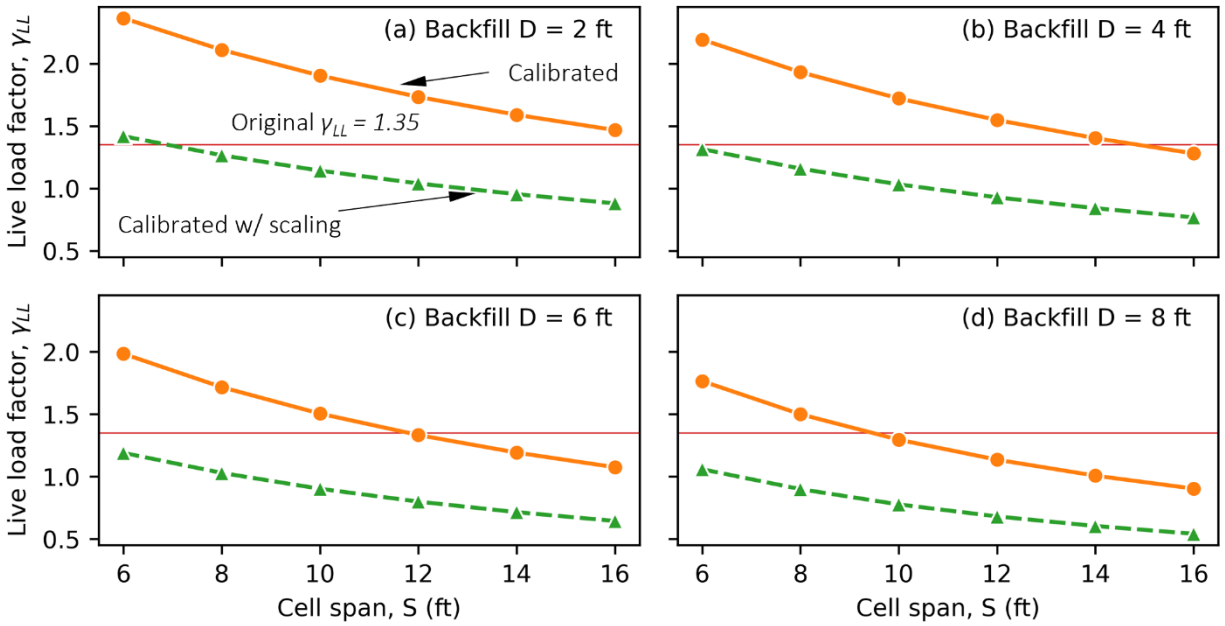

Figure 5.4 Calibrated live load factors for operating rating

Since the permanent load factors used in the MBE are higher than the sensitivity-based counterpart, the calibrated live load factor shown in Figure 5.4 leads to higher reliability indices than the 2.5 target, as illustrated in Figure 5.5. Nonetheless, the calibration yields more consistent reliability levels across all culvert dimensions and backfill depths. To compensate for the high reliability while preserving the consistent reliability level, the calibrated load factors can be further scaled. If the calibrated live load factors are multiplied by 0.6, as shown in Figure 5.4, the resulting reliability indices closely match the 2.5 target, as illustrated in Figure 5.5. Table 5.4 summarizes all the reliability indices with original and calibrated load factors as well as calibrated load factors with scaling. Note that the scaling operation herein only serves as a demonstration of feasibility. The scaling is not optimized in this project to match the target reliability. Future studies can be

conducted using this methodology. Several calibrated live load factors are smaller than 1.0, which suggests that the MPF can be potentially removed from operating rating.

Table 5.4 Reliability with calibrated load factors for operating rating

Calibration	Mean	STD	Min.	25th percentile	75th percentile	Max.
Original (γ_{LL} = 1.35)	3.29	0.34	2.44	3.12	3.51	3.96
Calibrated	3.58	0.34	2.86	3.32	3.88	4.13
With scaling	2.56	0.09	2.35	2.50	2.63	2.80

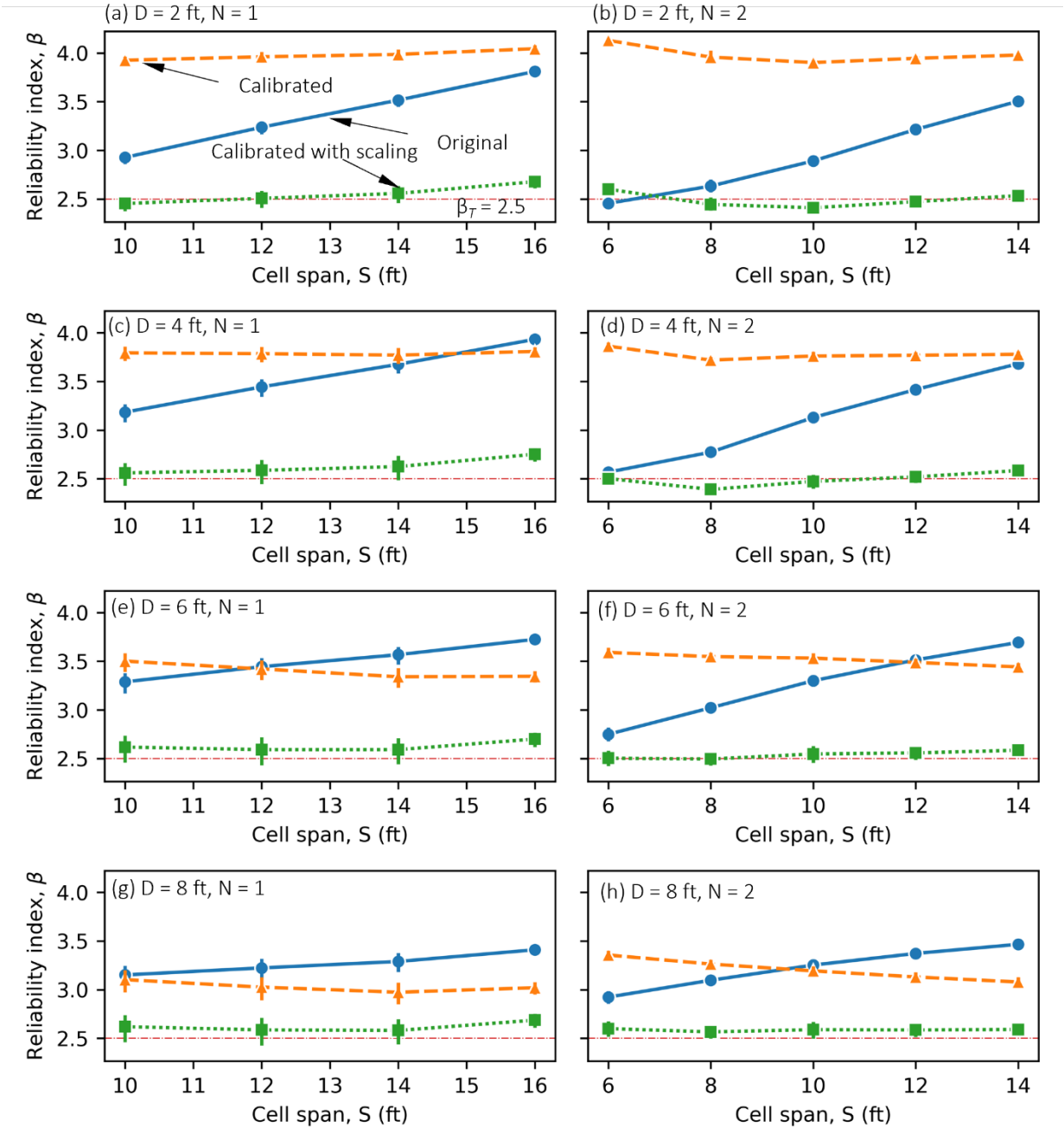

Figure 5.5 Reliability index of culverts with different backfill depths, *D* and numbers of cells, *N*, using original and calibrated load factors (operating rating)

5.4 RELIABILITY UNDER AASHTO LEGAL LOADS

For legal load rating, the reference period is 5 years, and the target reliability index is 2.5 (Moses, 2001). These are identical to those considered previously for operating rating. The same reference period indicates that the mean and the COV of the live load effect are the same as those used in the previous analysis of operating rating. The nominal load effect and the corresponding legal vehicle are provided in Table D.3. The live load factor is 2.0, and the MPF is not considered based on the MBE. Similar calibration is carried out for culverts under the AASHTO legal loads. Table 5.5 presents the statistics of the reliability indices with and without calibration. Results for individual culverts are provided in Table E.2.

Table 5.5 Reliability with calibrated load factors for AASHTO legal loads

Calibration	Mean	STD	Min.	25th percentile	75th percentile	Max.
Original (γ_{LL} = 2.0)	2.95	0.44	1.35	2.76	3.24	3.76
Calibrated	3.21	0.28	2.69	3.00	3.37	3.76
With scaling	2.53	0.17	1.92	2.44	2.62	3.00

Similar to the previous results for design loads, the calibrated live load factors result in a higher but more consistent reliability level. Figure 5.6 and Figure 5.7 present the calibrated live load factor and the resulting reliability indices for culverts with different backfill depths and cell spans. It is found that the average reliability index with the existing live load factor of 2.0 yields an average reliability index higher than the 2.5 target. Moreover, the variation of the reliability level is very high, primarily due to several culverts with very low reliability. The minimum or low reliability appears in small double-cell culverts with 6 and 8 ft cell spans. This observation coincides well with the high bias factors shown in Figure 4.4(b), which indicates that the legal loads underestimate the projected live load effects in these culverts. The high bias is further compounded by the low conservatism of the load distribution model when the cell span is small. Both factors contribute to the much lower reliability. The calibration process can account for the uneven distribution of reliability. However, the resulting reliability level is again over the target level due to (a) the higher live load COV compared to bridges and (b) the pairing of the larger permanent load factors instead of the sensitivity-based factors with the calibrated live load factor. The high reliability level can be similarly adjusted by scaling down the calibrated factor. Table 5.5, Figure 5.6, and Figure 5.7 also provide the results after scaling down the calibrated factor by 30% (multiplied by 0.7). The calibrated live load factors after scaling deliver more consistent reliability indices around the 2.5 target.

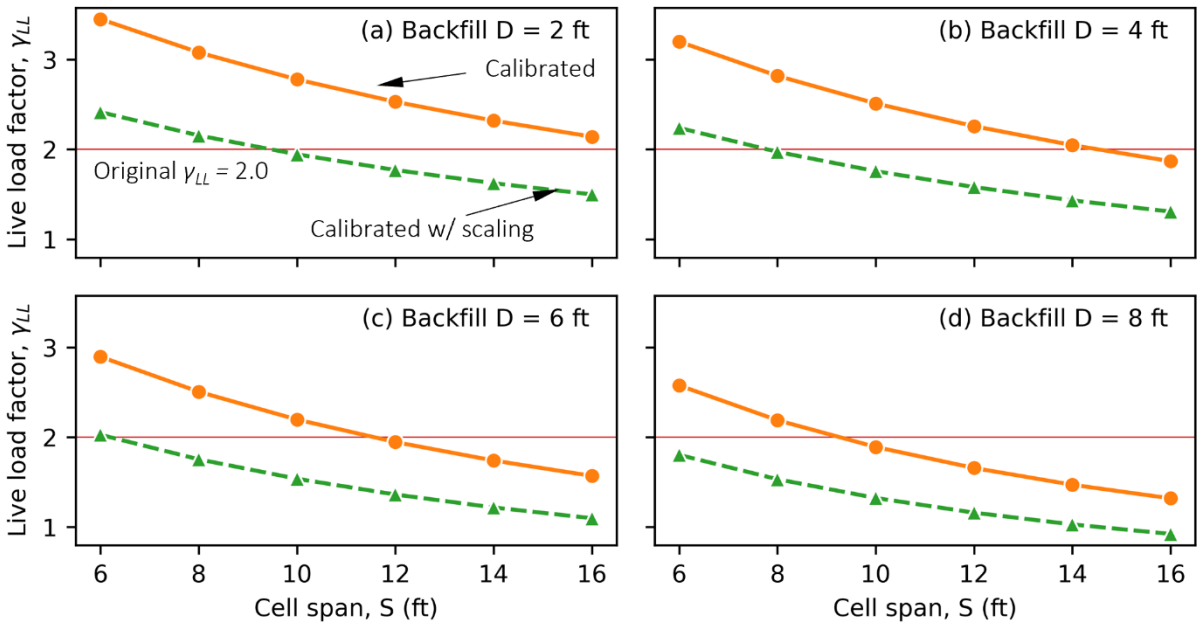

Figure 5.6 Calibrated live load factors for AASHTO legal loads

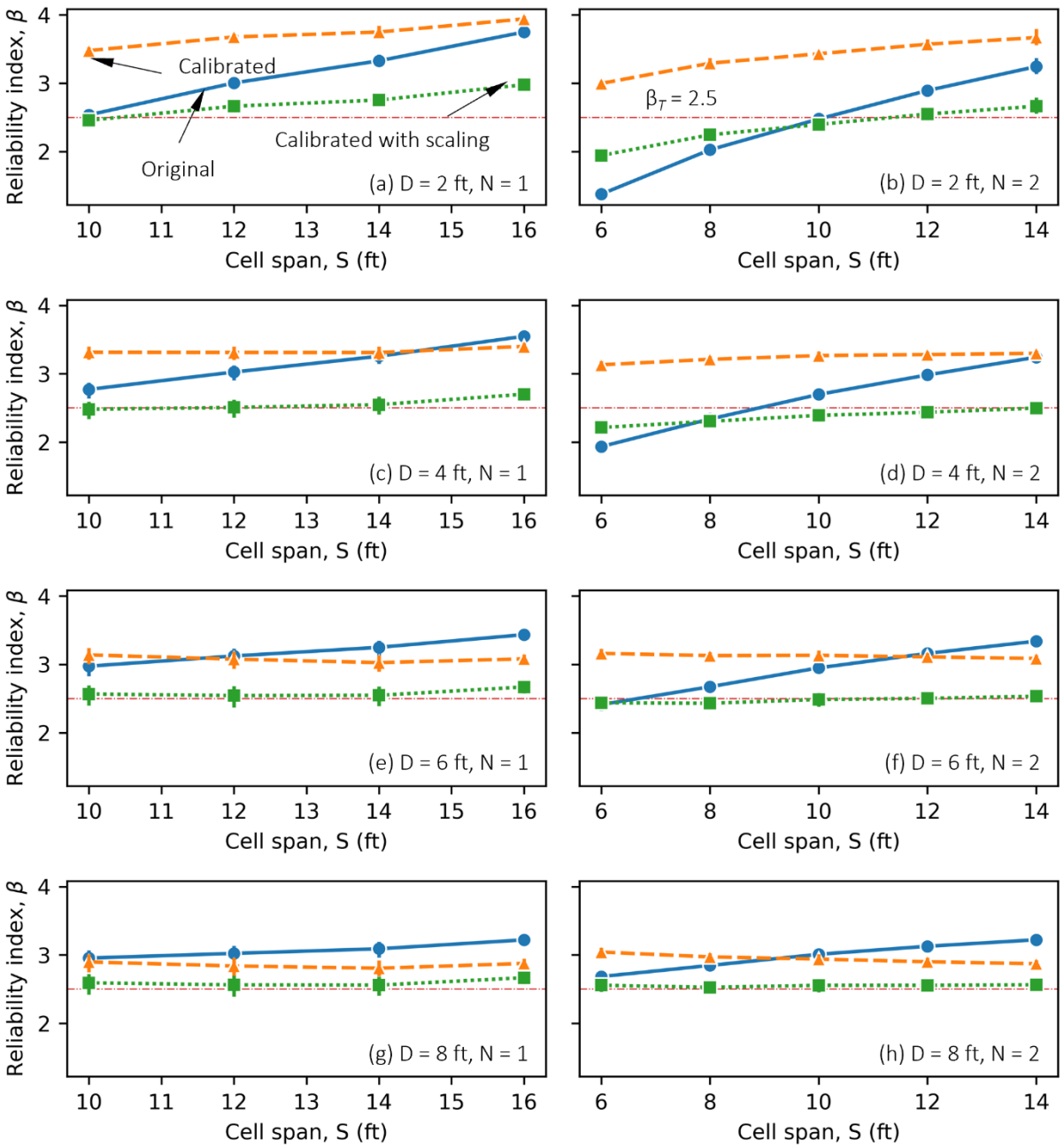

Figure 5.7 Reliability index of culverts with different backfill depths, *D* and numbers of cells, *N*, using original and calibrated load factors (AASHTO legal loads)

5.5 RELIABILITY UNDER FAST ACT EMERGENCY LOADS

Similar to the AASHTO legal loads, the target reliability for FAST Act emergency vehicles as surrogate loads is 2.5, and the reference period is 5 years (HNTB Corporation and Ghosn, 2019). Furthermore, the MPF is not used. The current MBE does not specify the live load factor for the FAST Act emergency loads. A live load factor of 2.0 was mentioned for culvert rating in the NCHRP Project 20-07 Task 410 (HNTB Corporation and Ghosn, 2019) in order to be consistent

with other legal loads, though the focus of that project was on girder bridges. Hence, the factor of 2.0 is studied for its implications on the reliability of rated culverts. The results from the reliability analysis are presented in Table E.3. Table 5.6 summarizes the statistics of reliability indices with and without calibration. Figure 5.8 and Figure 5.9 present the calibrated live load factors and the resulting reliability indices for culverts with different backfill depths and cell spans. These results indicate that a single load factor of 2.0 yields both considerably higher reliability than the 2.5 target and a wide range of reliability levels among culverts. Again, although the reliability level after calibration is still high, the variation of the reliability level is significantly reduced. Table 5.6 also provides the statistics of reliability indices if the calibrated live load factors are further scaled down. Similar to the AASHTO legal loads, a scaler of 0.7 results in an average reliability index close to the target. The corresponding live load factors and reliability indices are plotted in Figure 5.8 and Figure 5.9. Due to the higher nominal load effects under the surrogate loads, some culverts with 4 ft or deeper backfill can use a live load factor smaller than 1.0. In practice, a minimum value of 1.0 can be assigned for those culverts.

Table 5.6 Reliability with calibrated load factors for FAST Act emergency vehicles as surrogate loads

Calibration	Mean	STD	Min.	25% percentile	75% percentile	Max.
Original (2.0)	4.27	0.42	3.16	3.97	4.56	5.05
Calibrated	3.19	0.20	2.71	3.04	3.38	3.57
With scaling	2.51	0.14	1.99	2.44	2.61	2.76

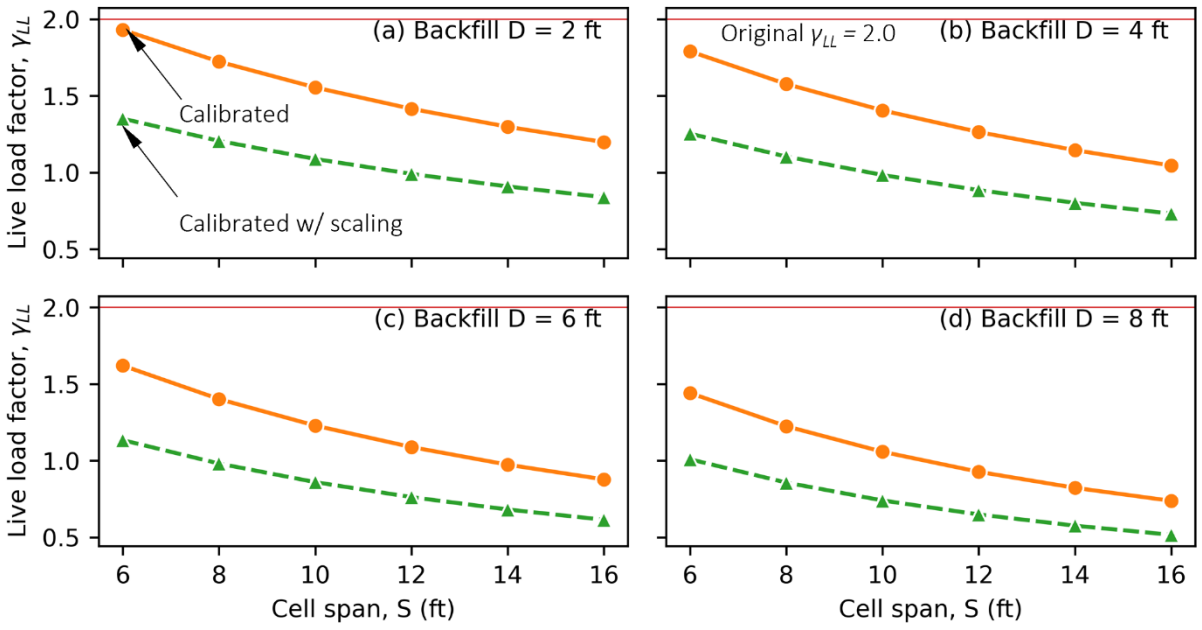

Figure 5.8 Calibrated live load factors for FAST Act emergency vehicles as surrogate loads

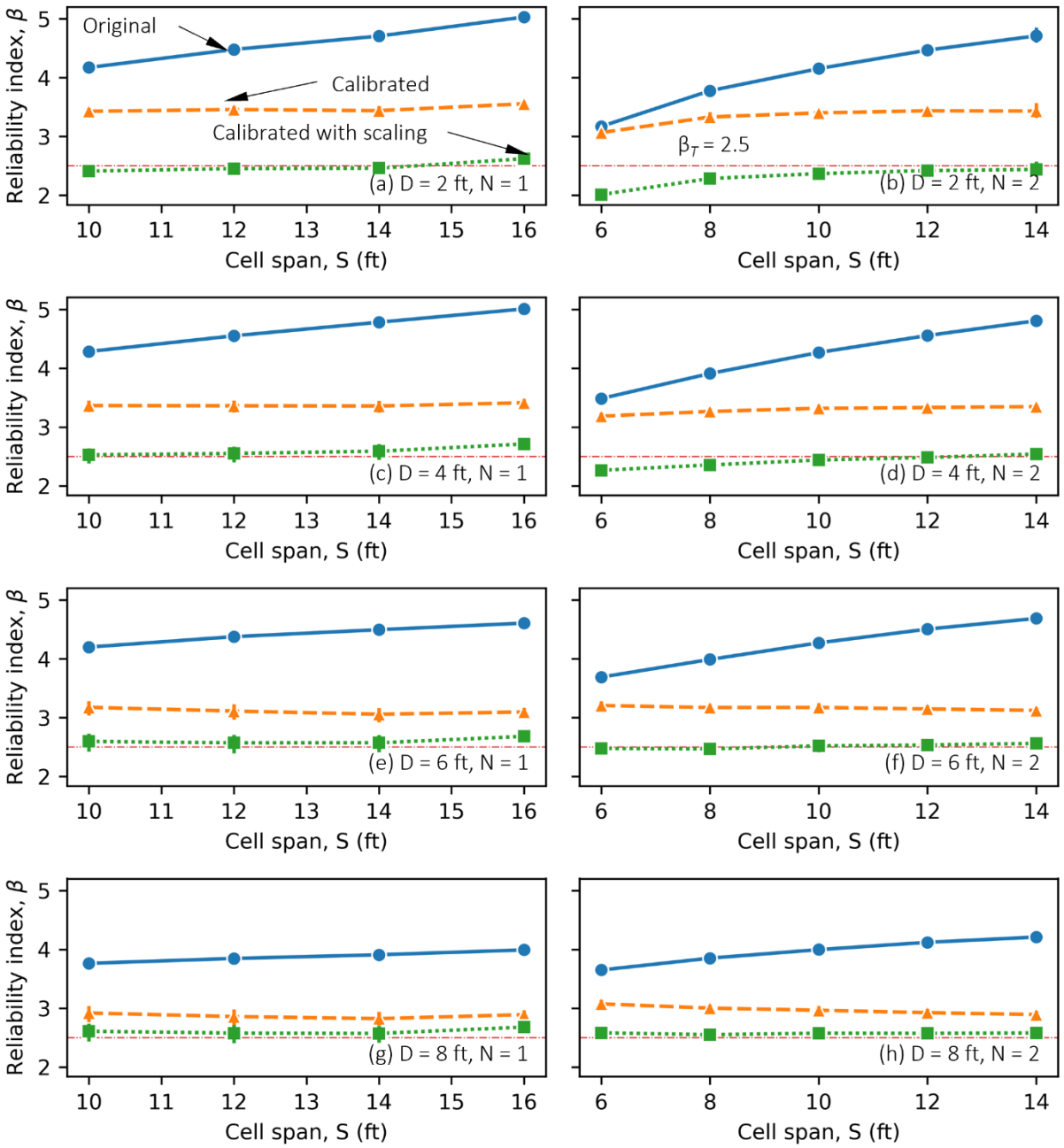

Figure 5.9 Reliability index of culverts with different backfill depths, *D* and numbers of cells, *N*, using original and calibrated load factors (FAST Act emergency vehicles as surroaget loads)

5.6 STEPS OF CALIBRATING LOAD FACTORS

The previous results indicate that calibration with scaling can result in reliability levels more aligned with the target reliability index. This section summarizes the detailed steps to calibrate and scale the live load factors:

Step 1. Follow the common load rating procedure to calculate the nominal permanent and live load effects. For the live load effects, use the LRFD load distribution model and the 2D frame model to estimate the load effects.

Step 2. Estimate the mean values for factors λ_{NET}, λ_{LDS}, λ_{BF}, and λ_{DYN}:

- Assume that factors considering site-to-site variability, WIM data availability, and backfill depth and properties have no bias:
  - $\bar{\lambda}_{NET} = \bar{\lambda}_{BF} = 1.0$
- Factor considering live load distribution through backfill soil (λ_{LDS}):
  - Given the clear cell span S in ft ($S < 24$),

$$\bar{\lambda}_{LDS} = \frac{1}{0.725 + 0.0623S}$$

- Factor considering dynamic effect of vehicular load (λ_{DYN})
  - Given the backfill depth D in ft,

$$\bar{\lambda}_{DYN} = 1 + 0.15 \times (1 - 0.125D) \geq 1.0$$

Step 3. Use Equation 5.4 (also shown below) to compute the bias of the live load effect.

$$b_{LL} = \frac{b_{FR}}{MPF \cdot (1 + IM)} \cdot \bar{\lambda}_{NET} \cdot \bar{\lambda}_{LDS} \cdot \bar{\lambda}_{BF} \cdot \bar{\lambda}_{DYN}$$

Based on Table 4.2, use $b_{FR} = 1.421$ for operating rating, $b_{FR} = 2.071$ for the AASHTO legal loads, and $b_{FR} = 1.156$ for the FAST Act emergency vehicles as surrogate loads. Note that $MPF = 1.2$ for operating rating, but $MPF = 1.0$ for legal rating.

Step 4. Determine the scaled and calibrated live load factor using the following equation with model parameters, k and b, in Table 5.1 and $\beta_T = 2.5$:

$$\hat{\alpha}_{LL} = exp\,(-1.289 \times 10^{-3} D^2 S - 0.0148)$$
$$\gamma_{LL} = c \cdot b_{LL} \cdot (1 - 0.4499 V_{LL} + 1.2442 \hat{\alpha}_{LL} \beta_T V_{LL})$$

where $\beta_T = 2.5$; $c = 0.6$ for operating rating, and $c = 0.7$ for legal rating; $V_{LL} = 0.25$ based on the following composition: $V_{FR} \approx 0.10$, $V_{NET} \approx 0.17$, $V_{LDS} \approx 0.10$, $V_{BF} \approx 0.11$, and $V_{DYN} = 0.12 \times (1 - 0.125D)/\bar{\lambda}_{DYN}$.

Using these steps, calibrated live load factors can be obtained, as presented previously in Section 5.3 to Section 5.5. Table 5.7 to Table 5.9 summarize the averaged live load factors for culverts grouped by different clear cell spans and backfill depths. All three types of rating loads are considered in the three tables respectively. For operating rating, the live load factors in Table 5.7 can be further capped between 1/1.2 = 0.83 and 1.35, the former of which is equivalent to fully negating the effect of the MPF. For AASHTO legal loads (Table 5.8), the calibrated live load factors can be similarly capped between 1.0 and 2.0. For FAST Act emergency vehicles as surrogate loads (Table 5.9), a factor lower than 1.0 can be justified due to the heavier axle weights than the design axles. Based on the weight ratio between the design tandem and the EV3 tandem, a lower bound of the live load factor can be set as 50 kips/62 kips = 0.81.

Table 5.7 Average calibrated live load factor (operating rating with design loads)

Backfill depth (ft)	**Clear cell span (ft)**					
	6	8	10	12	14	16
2	1.418	1.266	1.142	1.040	0.954	0.880
4	1.315	1.159	1.033	0.929	0.842	0.768
6	1.191	1.030	0.903	0.800	0.716	0.645
8	1.059	0.900	0.778	0.682	0.605	0.543

Table 5.8 Average calibrated live load factor (AASHTO legal loads)

Backfill depth (ft)	**Clear cell span (ft)**					
	6	8	10	12	14	16
2	2.416	2.156	1.945	1.771	1.624	1.499
4	2.240	1.973	1.758	1.581	1.433	1.308
6	2.028	1.754	1.538	1.363	1.219	1.099
8	1.804	1.533	1.324	1.161	1.030	0.924

Table 5.9 Average calibrated live load factor (FAST Act emergency vehicles as surrogate loads)

Backfill depth (ft)	**Clear cell span (ft)**					
	6	8	10	12	14	16
2	1.351	1.206	1.088	0.991	0.909	0.839
4	1.253	1.104	0.984	0.885	0.802	0.732
6	1.134	0.981	0.860	0.762	0.682	0.615
8	1.009	0.857	0.741	0.649	0.576	0.517

It should be noted that the live load factors presented in Table 5.7 to Table 5.9 are obtained based on an ADTT equal to 5000. Analysis based on ADTT equal to 1000 has also been conducted. The results indicate that the live load factors in the tables can be further discounted by multiplying a scaling factor equal to 0.96. This factor is used to account for the reduction in the bias factor, b_{FR}, due to the decreased ADTT value. It is also worth mentioning that the live factors are derived based on the target reliability index of 2.5, which is consistent with the reliability target for bridges. If a lower target is acceptable (e.g., 2.0 or 1.75), the live load factor can be further reduced using the equation in Step 4.

5.7 INCORPORATION OF SITE- AND STRUCTURE-SPECIFIC INFORMATION

The calibration steps described above use an estimated live load COV based on the UQ results. Existing structures may also have site- or structure-specific information, including for example

- WIM data at or near a culvert;
- Refined estimation of live load effects, e.g., via a FE model of the soil-culvert system and/or field measurement.

The calibration steps can be modified to reflect such information.

5.7.1 WIM Data at or near a Culvert

In general, the quality of the WIM data is more important than the quantity. The collection and processing of raw WIM data should follow the protocol developed in NCHRP Project 12-76 (Sivakumar et al., 2011). For the culvert load spectrum, both the weight and configuration of axle groups should be used to update the live load effect. Therefore, Step 9 of the NCHRP protocol should be followed to either directly obtain axle group events or axle statistics similar to that in Table 4.1. If the latter is used, the statistics from the heaviest 20% axle weight for each axle group configuration should be used considering a shifted exponential distribution (see Section 4.2.1 for more details). Reliable WIM data at or near a culvert can affect the calibration process through the following mechanisms:

- The statistics for the projected maximum load effect can be updated, resulting in new b_{FR} and V_{FR} used in the steps in Section 5.6;
- The site-to-site variation can be eliminated, yielding $V_{NET} = 0.02$;
- The total live load COV, as a result, can be adjusted based on Equation 2.10 and the COV composition listed in Section 5.6

5.7.2 Refined Load Distribution Analysis

Calibrated FE models or direct field measurements can also provide more accurate estimation of the live load effect, thereby reducing the bias and variation related to the LRFD load distribution model. When such refined analysis is available, the following steps can be implemented to modify the calibration process:

- Run the FE model with different axle configurations and weights to determine the load effect of interest (e.g., midspan positive moment in the scope of this report); in case of field measurements, gather the measured load effects under the different axle configurations and weights. Note that the axle configurations should at least include single-axle and tandem loads considered in the design loads.
- Conduct 2D frame analysis using the LRFD load distribution model for the same culvert under the same set of axle loads; record the load effects of interest from the frame analysis.
- Compute the ratio of the FE (or field) to frame results for all analyzed loads; use the mean and the COV of this ratio to replace $\bar{\lambda}_{LDS}$ and V_{LDS}, respectively.
- Use the new values of $\bar{\lambda}_{LDS}$ and V_{LDS} in the calibration steps.

The aforementioned steps assume that sufficient ratios between FE (or field) and frame results are available to derive a reliable COV. If this is not the case, $V_{LDS} = 0.1$ should be kept unchanged, and only the mean value, $\bar{\lambda}_{LDS}$, should be updated.

CHAPTER 6

SUMMARY, CONCLUSIONS, AND FUTURE RESEARCH

6.1 SUMMARY AND CONCLUSIONS

This project systematically investigated the uncertainty and reliability of typical RC box culverts. For uncertainty quantification, this project clearly identified the various sources and quantitatively assessed the characteristics of uncertainties in the live load effects of culverts. Compared to bridges, culverts have (a) distinct models to estimate the load effects and model uncertainties, (b) unique load spectra and behavior under side-by-side loading, and (c) different dynamic response under moving vehicles. This project focused primarily on the first two aspects.

For model uncertainties, the bias of the LRFD load distribution model was analyzed, focusing on culverts with 2- to 8-ft backfill. The model bias was characterized by the ratio of the load effects obtained from the frame and FE analyses. Focusing on the midspan bending moment in the top slab, the epistemic uncertainty related to the use of the LRFD load distribution model was quantified via Bayesian regression analysis.

For load spectrum uncertainty, the project considered the effects of the unique characteristics of culverts, including the dominance of axle groups, load spectrum from axle group data, elevated site-to-site variation, and less severe overloading under side-by-side axle groups.

The conclusions drawn from the uncertainty quantification efforts are summarized as follows:

- The LRFD load distribution model can overestimate the bending moments at critical cross sections in the top slab, including the external wall-slab joint, midspan of the first cell, and internal wall-slab joint. Among the three locations, the model bias associated with the midspan bending moment exhibits the lowest amount of variance. Different variables were explored to explain the observed variance at the midspan, including the backfill depth, cell span, cell height, cell aspect ratio, total span, and stiffness ratio between slab and wall. It is shown that the model bias (i.e., conservatism) for the estimated moment at the midspan increases considerably with the cell span, which can account for about 68% of the total variance observed. For the other cross sections, none of the considered variables can explain more than 50% of the total variance.
- The model uncertainty obtained for the midspan moment was compared (a) among culverts with different cell spans and (b) with the model bias of girder distribution factors used for bridges. The comparison indicates that the mean value of the model bias increases with the cell span, and so does the variance, albeit to a much less extent. Depending on the cell span, the mean model bias can be considerably higher (i.e., by more than 20%) than that associated with the use of girder distribution factors. Hence, the results provide the basis for reassessment of structural reliability for RC box culverts.
- Due to the relatively short span of culverts, the weight and configuration of axle groups play a crucial role in the uncertainty quantification of the live load effects. Similar to bridges, the top 20% heaviest axle groups with different configurations can be used to develop the culvert load spectrum. It is important to know the relative frequency of different axle configurations, i.e., single-axle, tandem, tridem, etc. For each configuration, if the mean and the COV of the top 20% weight are provided, the shifted exponential distribution is more appropriate than the

normal distribution to develop the load spectrum. Due to the use of axle groups, analysis from this project also found that the site-to-site variation is considerably higher for culverts than that for bridges.

- Based on the load spectrum and the statistical projection, the maximum live load effect was compared with the nominal live load effect obtained with different rating loads, including the design loads at the operating level, the AASHTO legal loads, and the FAST Act emergency vehicles as surrogate loads. It is found that the design loads give the most consistent ratio of mean to nominal load effects across all culverts and backfill depths under consideration. The AASHTO legal loads render the lowest nominal load effects and the highest amount of variation among culverts and backfill depths considered. Due to the heavy axle groups, the nominal load effects under FAST Act emergency vehicles as surrogate loads differ considerably from the AASHTO legal loads. They consistently give the highest nominal load effects, and the ratio of mean to nominal effects shows a similar amount of variation to that for the design loads.
- When identical axle groups are side-by-side on two adjacent lanes, the increase in the midspan moment from two-lane loading, compared to one-lane loading, is much lower in culverts than the increase associated with bridge girders. This difference in structural response is further compounded by the difference in single-lane load spectrum and the unique side-by-side statistics for axle groups. The result is a less dominant two-lane spectrum. The maximum load effect in most culverts should be controlled by the one-lane loading case. Therefore, the uncertainty quantification of maximum live load effects was also based on one-lane loading in contrast to the two-lane loading used for bridges.

Based on the results of uncertainty quantification, reliability of typical culverts was assessed considering the design loads at the operating level, the AASHTO legal loads, and the FAST Act emergency vehicles as surrogate loads. Practical calibration steps were proposed to adjust the live load factors used for load rating in order to meet the target reliability index. These steps were provided in Section 5.6. This approach is better suited for existing structures with site- and structure-specific statistics of the live load effect, e.g. from WIM data at or near a culvert, field measurements, and refined structural models. The following conclusions can be drawn from the reliability analyses and calibration:

- The proposed calibration approach is based on the sensitivity factor of the live load effect to structural reliability. A higher sensitivity suggests a larger load factor. In general, the live load sensitivity is affected by backfill depth, clear cell span, and the COV of the live load effect. Specifically, the sensitivity factor decreases with backfill depth due to the reduced load effect from live loads compared to the permanent load effect. It also decreases with the clear cell span, which can be partially attributed to the increasing conservatism of the LRFD load distribution model. The live load sensitivity increases with the live load COV to account for the higher uncertainty.
- The results from the reliability analysis under design loads indicate that the existing live load factor for operating rating (1.35) results in an average reliability index of 3.29, which is higher than the target reliability index of 2.5. With calibration, the average reliability index can drop to 2.56, with most of the calibrated live load factors lower than the current value of 1.35. Calibration also results in a much narrower range of reliability indices among all culverts, which indicates a more uniform safety margin. This is achieved by using different live load

factors for different backfill depths and cell spans. This benefit is especially salient for culverts with longer cell spans, which had high safety margins when rated with the existing live load factor.

- Compared to operating rating, culverts rated with the AASHTO legal loads and the 2.0 live load factor have both an average reliability index (2.95) higher than the 2.5 target and a wider range of reliability indices. Although the average reliability index is above the target reliability, culverts with smaller cell spans and shallow backfill (e.g., 2 and 4 ft) may have a low reliability index around 1.35. This is primarily due to the axle configurations of legal loads that result in lower nominal live load effects in some culverts compared to the mean load effects obtained from uncertainty quantification. The proposed calibration approach can similarly account for the situation, resulting in an average reliability index of 2.53, with most of the calibrated live load factors below 2.0 and in the range of 1.0 to 2.0. The variation of reliability is also much lower than that from using the original factor of 2.0. Similar to the operating rating, the uniform reliability level is achieved by varying load factors with the backfill depth and cell span.
- The FAST Act emergency vehicles as surrogate loads and a constant live load factor of 2.0 yield an average reliability index equal to 4.27, which is greater than the 2.5 target. Similar to the reliability analysis of other loads, calibrated live load factors can result in an average reliability index equal to 2.51 and a narrow range of reliability indices among culverts. The calibrated live load factors are always lower than the factor of 2.0, with most of the calibrated factors below 1.30. The calibrated live load factor again varies with the cell span and the backfill depth.
- The calibrated live load factors can be considered when the midspan bending moment controls the rating. This is especially relevant when rating factor is lower than 1, yet either the field inspection suggests little distress and/or the rating factor only dipped below one due to the change in the live load distribution model in the LRFD Specifications.

6.2 SUGGESTED FUTURE RESEARCH

The scope of this project is limited to RC box culverts and the positive bending moment in the top slab. Although the proposed methodology is generalizable, the following future research activities are suggested to implement the proposed methodology beyond the scope of this project:

- The uncertainty quantification for the LRFD load distribution model indicates that the model can overestimate the load effects in culverts. More importantly, this conservatism is not uniformly distributed among culverts of different cell spans. The conservatism can vary for other cross sections and load effects not further investigated in this project. It is, therefore, suggested that refined load distribution models, especially those individually fine-tuned for different cross sections and load effects, should be developed to better estimate the load effects in culverts.
- Another important difference between culverts and bridges is the dynamic effect of moving vehicles. Future research should be conducted on the uncertainty quantification of the dynamic allowance model currently used in the LRFD Specifications for culverts. If deemed necessary (e.g., high bias and inconsistent uncertainty across culvert dimensions and backfill depths), improved models should be developed.
- With revised load distribution model and better quantified dynamic effect, the calibration process proposed in this project can be extended to other cross sections and load effects,

including the bending moments and shear forces in slabs and walls. The same methodology, ranging from the collection of typical culverts to the calibration of load factors, can be extended to other types of culverts such as concrete arches, concrete pipes, and corrugated metal culverts.

- The current project investigated the design loads and AASHTO legal loads, while the FAST Act emergency vehicles are regarded as surrogate loads due to the absence or rare occurrences of such vehicles in the WIM data used in the study. New WIM data can be utilized in the future to fully consider the impacts of these emergency vehicles. Additionally, the methodology can be extended to permit loads and the corresponding loading rating.

ACKNOWLEDGMENTS

The authors would like to acknowledge the financial and technical support from Federal Highway Administration (FHWA), especially from the FHWA Technical Manager, Lubin Gao, Ph.D., P.E., FHWA Contracting Officer Representative (COR), Tuonglinh (Linh) Warren, P.E., and the Technical Advisory Panel made up of officials and engineers from FHWA, State DOTs, and the industry, including Jason Hastings, DelDOT; Yihong Gao, MnDOT; Ruben Boehler, Illinois DOT; Biniam Aregawi, TxDOT; Josh Beakley, ACPA; Tony Zhang, Caltrans; Matt Farrar, Idaho Transportation Department (retired); Murugesu Vinayagamoorthy, Caltrans (retired); David Garber, FHWA; Thomas Saad, USDOT. We are also grateful for the insightful discussion with Dr. Timothy McGrath regarding results and data in NCHRP Report 647 and FE modeling of RC culverts in general. Finally, the assistance with the FE modeling of soil-culvert systems from Mr. Mohd Firoj, a former graduate student of the PI, is acknowledged.

REFERENCES

AASHTO, 2020. AASHTO LRFD Bridge Design Specifications. American Association of State Highway and Transportation Officials (AASHTO), Washington, D.C.

AASHTO, 2018. The Manual for Bridge Evaluation. American Association of State Highway and Transportation Officials (AASHTO), Washington, D.C.

Abaqus, 2010a. Abaqus Analysis User's Manual. Dassault Systèmes Simulia Corp., Providence, RI.

Abaqus, 2010b. Abaqus Scripting User's Manual. Dassault Systèmes Simulia Corp., Providence, RI.

Abdel-Karim, A.M., Tadros, M.K., Benak, J.V., 1990. Live Load Distribution on Concrete Box Culverts. Transportation Research Record 1288, 136–151.

Abolmaali, A., Garg, A.K., 2008. Effect of Wheel Live Load on Shear Behavior of Precast Reinforced Concrete Box Culverts. Journal of Bridge Engineering 13, 93–99. https://doi.org/10.1061/(ASCE)1084-0702(2008)13:1(93)

Abuhajar, O., El Naggar, H., Newson, T., 2015. Static soil culvert interaction the effect of box culvert geometric configurations and soil properties. Computers and Geotechnics 69, 219–235. https://doi.org/10.1016/j.compgeo.2015.05.005

Abuhajar, O., Naggar, H.E., Newson, T., 2016. Numerical Modeling of Soil and Surface Foundation Pressure Effects on Buried Box Culvert Behavior. Journal of Geotechnical and Geoenvironmental Engineering 142. https://doi.org/10.1061/(ASCE)GT.1943-5606.0001567

Acharya, R., Han, J., Brennan, J.J., Parsons, R.L., Khatri, D.K., 2016a. Structural Response of a Low-Fill Box Culvert under Static and Traffic Loading. Journal of Performance of Constructed Facilities 30. https://doi.org/10.1061/(ASCE)CF.1943-5509.0000690

Acharya, R., Han, J., Parsons, R.L., 2016b. Numerical Analysis of Low-Fill Box Culvert under Rigid Pavement Subjected to Static Traffic Loading. International Journal of Geomechanics 16, 04016016. https://doi.org/10.1061/(ASCE)GM.1943-5622.0000652

Awwad, E., Mabsout, M., Sadek, S., Tarhini, K., 2008. Parametric study of load distribution in four-sided concrete box culverts. Bridge Structures 4, 99–107. https://doi.org/10.1080/15732480802180791

Bednarcyk, M.L., 2012. A Comparison of Load Factor Rating (LFR) and Load and Resistance Factor Rating (LRFR) in Reinforced Concrete Box and Slab Culverts.

Bugher, C.L., Manahiloh, K.N., Kaliakin, V.N., 2020. Dynamic amplification factor in culverts: A parametric study using three-dimensional finite element analysis. Transportation Infrastructure Geotechnology 7, 243–267. https://doi.org/10.1007/s40515-019-00097-4

Burati, J.L., Weed, R.M., Hughes, C.S., Hill, H.S., 2003. Optimal Procedures for Quality Assurance Specifications (FHWA-RD-02-095). Federal Highway Administration (FHWA), Washington, DC.

CEN 1990, 2002. Eurocode: Basis of Structural Design. European Committee for Standardization (CEN), Brussels, Belgium.

Chen, B., Sun, L., 2013. The impact of soil properties on the structural integrity of high-fill reinforced concrete culverts. Computers and Geotechnics 52, 46–53. https://doi.org/10.1016/j.compgeo.2013.03.006

Cristelo, N., Félix, C., Figueiras, J., 2019. Experimental behaviour of concrete box culverts — comparison with current codes of practice. Canadian Geotechnical Journal 56, 970–982. https://doi.org/10.1139/cgj-2018-0506

Der Kiureghian, A., 2022. Structural and System Reliability. Cambridge University Press, Cambridge, UK. https://doi.org/10.1017/9781108991889
Duncan, J.M., 2000. Factors of Safety and Reliability in Geotechnical Engineering. Journal of Geotechnical and Geoenvironmental Engineering 126, 307–316. https://doi.org/10.1061/(ASCE)1090-0241(2000)126:4(307)
Ellingwood, B.R., Galambos, T.V., MacGregor, J.G., Cornell, C.A., 1980. Development of a Probability Based Load Criterion for American National Standard A58: Building Code Requirements for Minimum Design Loads in Buildings and Other Structures. National Bureau of Standards, Washington, D.C.
Elshimi, T.M., Brachman, R.W.I., Moore, I.D., 2014. Effect of truck position and multiple truck loading on response of long-span metal culverts. Canadian Geotechnical Journal 51, 196–207. https://doi.org/10.1139/cgj-2013-0176
FHWA, 2016. Load Rating for the FAST Act's Emergency Vehicles [WWW Document]. Federal Highway Administration (FHWA). URL https://www.fhwa.dot.gov/bridge/loadrating/161103.cfm (accessed 3.19.25).
Freeseman, K., 2022. Concrete Box Culvert Earth Pressure Monitoring. Bridge Engineering Center, Iowa State University.
Ghahremannejad, M., Abolmaali, A., Mahdavi, M., 2019. Shear Strength of Top Slab of Reinforced Concrete Box Culverts. ACI Structural Journal 116. https://doi.org/10.14359/51716800
Han, J., Acharya, R., Parsons, R.L., Khatri, D., 2013. Improved Load Distribution for Load Rating of Low-Fill Box Structures. Kansas Department of Transportation, Topeka, KS.
HNTB Corporation, Ghosn, M., 2019. NCHRP Project 20-07/Task 410: Load Rating for the Fast Act Emergency Vehicles EV-2 and EV-3. National Cooperative Highway Research Program (NCHRP), Washington, DC.
Kadivar, M., Manahiloh, K.N., Kaliakin, V.N., Shenton, H.W., 2018. Assessment of Dynamic Load Allowance for Buried Culverts, in: IFCEE 2018. American Society of Civil Engineers, Reston, VA, pp. 179–188. https://doi.org/10.1061/9780784481608.018
Katona, M.G., 2022. Extension of AASHTO Load-Spreading Method to Include the Full Benefits of Pavements for Reliable Load Rating of Buried Culverts. Transportation Research Record: Journal of the Transportation Research Board 2676, 508–521. https://doi.org/10.1177/03611981221096121
Katona, M.G., 2019. Improved Methods for Simulating Live Loads for Two-Dimensional Structural Analysis of Buried Culverts. Transportation Research Record 2673, 449–462. https://doi.org/10.1177/0361198119846465
Katona, M.G., 2017. CANDE-2017 Culvert Analysis and Design User Manual and Guideline. Transportation Research Board (TRB), Washington, DC.
Lou, P., Nassif, H., Truban, P., 2018. Development of Live Load Model for Strength II Limit State in AASHTO LRFD Design Specifications. Transportation Research Record: Journal of the Transportation Research Board 2672, 11–23. https://doi.org/10.1177/0361198118756874
McGrath, T.J., Liepins, A.A., Beaver, J.L., 2005. Live Load Distribution Widths for Reinforced Concrete Box Sections. Transportation Research Record: Journal of the Transportation Research Board 99–108.

McGrath, T.J., Tigue, D.B., Rund, R.E., Heger, T.G., 1989. BOXCAR User and Programmer Manual (Version 1.0). Turner-Fairbank Highway Research Center (FHWA), McLean, VA.
Melchers, R.E., Beck, A.T., 2018. Structural Reliability Analysis and Prediction. John Wiley & Sons Ltd, Hoboken, NJ.
Miller, L.J., Durham, S.A., 2008. Comparison of Standard Load and Load and Resistance Factor Bridge Design Specifications for Buried Concrete Structures. Transportation Research Record: Journal of the Transportation Research Board 2050, 81–89. https://doi.org/10.3141/2050-08
Mlynarski, M., McGrath, T.J., Clancy, C., Katona, M.G., 2019. NCHRP Web-only Document 268 (Project 15-54): Proposed Modifications to AASHTO Culvert Load Rating Specifications. National Cooperative Highway Research Program (NCHRP), Washington, DC. https://doi.org/10.17226/25673
Mlynarski, M., Wassef, W.G., Andrzej, N.S., 2011. NCHRP Report 700: A Comparison of AASHTO Bridge Load Rating Methods. National Cooperative Highway Research Program (NCHRP), Washington, DC.
MnDOT, 2013. Buried Structures, in: LRFD Bridge Design. Minnesota Department of Transportation (MnDOT), St. Paul, MN.
Moses, F., 2001. NCHRP Report 454: Calibration of Load Factors for LRFR Bridge Evaluation. National Cooperative Highway Research Program (NCHRP), Washington, DC.
Moses, F., Verma, D., 1987. NCHRP Report 301 (Project 12-28): Load Capacity Evaluation of Existing Bridges. Transportation Research Board (TRB), Washington, DC.
Nowak, A.S., 1999. NCHRP Report 368: Calibration of LRFD Bridge Design Code. Transportation Research Board, Washington, DC.
Okeil, A.M., Jafari, N., 2024. Developing Load Distribution Formula for Louisiana Cast-in-place Reinforced Concrete Box Culverts (Report HWA/LA. 692). Louisiana Department of Transportation and Development, Baton Rouge, LA.
Okeil, A.M., Ulger, T., Elshoura, A., 2018. Live Load Rating of Cast-in-place Concrete Box Culverts (No. FHWA/LA. 17/593). Louisiana Transportation Research Center.
Orton, P., Vinogradov, S., Georgas, N., Blumberg, A., Lin, N., Gornitz, V., Little, C., Jacob, K., Horton, R., 2015. New york city panel on climate change 2015 report chapter 4: Dynamic coastal flood modeling. Annals of the New York Academy of Sciences 1336, 56–66. https://doi.org/10.1111/nyas.12589
Peiris, A., Cole, A., Russell, E., Hutchinson, C., Harik, I., 2024. Effect of live loads on top slab of cast-in-place reinforced concrete box culverts. Engineering Structures 318, 118709. https://doi.org/10.1016/j.engstruct.2024.118709
Petersen, D.L., Nelson, C.R., Li, G., McGrath, T.J., Kitane, Y., 2010. NCHRP Report 647 (Project 15-29): Recommended Design Specifications for Live Load Distribution to Buried Structures. National Cooperative Highway Research Program (NCHRP), Washington, DC.
Phoon, K.-K., Kulhawy, F.H., 1999. Characterization of geotechnical variability. Canadian Geotechnical Journal 36, 612–624. https://doi.org/10.1139/t99-038
Rackwitz, R., Fiessler, B., 1978. Structural reliability under combined random load sequences. Computers and Structures 9, 489–494. https://doi.org/10.1016/0045-7949(78)90046-9

Ramadan, S.H., Naggar, M.H.E., 2022. Design guidelines for reinforced concrete three-sided culverts. Tunnelling and Underground Space Technology 119, 104259. https://doi.org/10.1016/j.tust.2021.104259

SciPy Community, 2024. SciPy v1.15.1 Documentation [WWW Document]. URL https://docs.scipy.org/doc/scipy/reference/generated/scipy.stats.probplot.html (accessed 2.6.24).

Selig, E.T., 1990. Soil properties for plastic pipe installations, in: Buczala, G.S., Cassady, M.J. (Eds.), Buried Plastic Pipe Technology (STP 1093). American Society for Testing and Materials (ASTM), Philadelphia, PA, pp. 141–158.

Seo, H., Wood, T.A., Javid, A.H., Lawson, W.D., 2017. Simplified System-Level Pavement-Stiffness Model for Box Culvert Load-Rating Applications. Journal of Bridge Engineering 22, 04017066. https://doi.org/10.1061/(asce)be.1943-5592.0001098

Sharifi, H., Peiris, A., Harik, I., 2023. Triage method for load rating bridge size two-cell reinforced concrete box culverts for the AASHTO LRFD design load. Structure and Infrastructure Engineering 19, 1235–1248. https://doi.org/10.1080/15732479.2021.2015793

Sivakumar, B., Ghosn, M., Moses, F., TranSystems Corporation, 2011. NCHRP Report 683 (Project 12-76): Protocols for Collecting and Using Traffic Data in Bridge Design. National Cooperative Highway Research Program (NCHRP), Washington, DC.

Sun, L., Hopkins, T.C., Beckham, T.L., 2011. Long-Term Monitoring of Culvert Load Reduction Using an Imperfect Ditch Backfilled with Geofoam. Transportation Research Record: Journal of the Transportation Research Board 2212, 56–64. https://doi.org/10.3141/2212-06

Sykora, M., Diamantidis, D., Holicky, M., Jung, K., 2017. Target reliability for existing structures considering economic and societal aspects. Structure and Infrastructure Engineering 13, 181–194. https://doi.org/10.1080/15732479.2016.1198394

Ulger, T., Okeil, A.M., Elshoura, A., 2020. Load Testing and Rating of Cast-in-Place Concrete Box Culverts. Journal of Performance of Constructed Facilities 34, 04020008. https://doi.org/10.1061/(asce)cf.1943-5509.0001401

Wood, T.A., Lawson, W.D., Jayawickrama, P.W., Newhouse, C.D., 2015. Evaluation of production models for load rating reinforced concrete box culverts. Journal of Bridge Engineering, ASCE 20, 04014057. https://doi.org/10.1061/(ASCE)BE.1943-5592.0000638

Wood, T.A., Lawson, W.D., Surles, J.G., Jayawickrama, P.W., Seo, H., 2016. Improved load rating of reinforced-concrete box culverts using depth-calibrated live-load attenuation. Journal of Bridge Engineering, ASCE 21, 04016095. https://doi.org/10.1061/(ASCE)BE.1943-5592.0000967

Wood, T.A., Surles, J.G., Mousavi, S.M., Jayawickrama, P.W., Javid, A.H., Seo, H., Lawson, W.D., 2017. Modeling factors influencing culvert load ratings: A parametric analysis, in: Geotechnical Frontiers 2017. American Society of Civil Engineers, Reston, VA, pp. 243–252. https://doi.org/10.1061/9780784480441.026

Yerukala, R., Boiroju, N.K., 2015. Approximations to Standard Normal Distribution Function.

Zhang, Y., Der Kiureghian, A., 1995. Two Improved Algorithms for Reliability Analysis, in: Rackwitz, R., Augusti, G., Borri, A. (Eds.), Reliability and Optimization of Structural Systems. IFIP — The International Federation for Information Processing. Springer, Boston, MA, pp. 297–304. https://doi.org/10.1007/978-0-387-34866-7_32

Zhu, M., McKenna, F., Scott, M.H., 2018. OpenSeesPy: Python library for the OpenSees finite element framework. SoftwareX 7, 6–11. https://doi.org/10.1016/j.softx.2017.10.009
Zokaie, T., Osterkamp, T.A., Imbsen, R.A., 1991. Distribution of Wheel Loads on Highway Bridges. Transportation Research Board (TRB), Washington, DC.

APPENDIX A UNCERTAINTY OF PERMANENT LOAD EFFECTS

Based on the discussion in Section 2.2.2, Table A.1 presents the mean and the COV of the permanent bending moment at Section S2 (in kip-ft or k-ft for short) of all typical culverts analyzed in this project. The mean values are obtained from the bias factor and the nominal load effect calculated following the LRFD Specifications. These nominal values are also provided in Table A.1. In addition, the factored permanent load effects are computed using the load factors in the MBE and summarized in Table 2.2. The factored value is useful to back-calculate the nominal resistance.

Table A.1 Permanent load effects

Culvert	D (ft)	Factored DL(k-ft/ft)	Nominal DL (k-ft/ft)	Mean (k-ft/ft)	COV
1	2	3.7697	2.9400	2.9874	0.0852
2	2	3.8864	3.0408	3.0927	0.0912
3	2	3.6900	2.9060	2.9614	0.1056
4	2	3.1429	2.5092	2.5673	0.1408
5	2	6.0256	4.7128	4.7975	0.0870
6	2	5.9102	4.6430	4.7330	0.0958
7	2	5.1659	4.0855	4.1734	0.1110
8	2	4.3630	3.5012	3.5927	0.1486
9	2	8.4990	6.6708	6.8100	0.0877
10	2	8.1781	6.4516	6.5976	0.0978
11	2	6.9550	5.5175	5.6531	0.1103
12	2	5.9998	4.8234	4.9641	0.1432
13	2	10.5898	8.2823	8.4449	0.0814
14	2	10.8641	8.5150	8.6886	0.0850
15	2	9.6861	7.6092	7.7704	0.0892
16	2	9.3096	7.3500	7.5186	0.0994
1	4	6.6157	5.1309	5.1783	0.0955
2	4	6.9269	5.3838	5.4357	0.1003
3	4	6.8097	5.3138	5.3692	0.1102
4	4	6.2469	4.9100	4.9681	0.1307
5	4	10.4703	8.1364	8.2211	0.0965
6	4	10.5020	8.1838	8.2737	0.1030
7	4	9.5177	7.4453	7.5332	0.1128
8	4	8.6886	6.8470	6.9384	0.1337
9	4	14.4509	11.2572	11.3963	0.0960
10	4	14.2581	11.1416	11.2876	0.1032
11	4	12.4895	9.7899	9.9255	0.1109
12	4	11.5291	9.0984	9.2391	0.1294
13	4	17.6751	13.7365	13.8991	0.0910
14	4	18.3137	14.2530	14.4266	0.0939
15	4	16.5214	12.8762	13.0375	0.0969
16	4	16.2959	12.7382	12.9068	0.1038
1	6	9.6472	7.4645	7.5119	0.1007

Culvert	D (ft)	Factored DL(k-ft/ft)	Nominal DL (k-ft/ft)	Mean (k-ft/ft)	COV
2	6	10.1708	7.8832	7.9352	0.1049
3	6	10.1464	7.8884	7.9438	0.1131
4	6	9.5783	7.4857	7.5438	0.1286
5	6	15.1685	11.7551	11.8397	0.1018
6	6	15.3632	11.9318	12.0218	0.1072
7	6	14.1296	11.0050	11.0929	0.1149
8	6	13.2847	10.4008	10.4922	0.1303
9	6	20.6984	16.0709	16.2101	0.1013
10	6	20.6483	16.0702	16.2162	0.1073
11	6	18.3061	14.2793	14.4149	0.1132
12	6	17.3510	13.5984	13.7391	0.1267
13	6	25.0668	19.4263	19.5889	0.0968
14	6	26.0903	20.2425	20.4161	0.0994
15	6	23.6549	18.3727	18.5340	0.1019
16	6	23.5939	18.3661	18.5347	0.1074
1	8	12.8641	9.9407	9.9881	0.1038
2	8	13.6181	10.5391	10.5911	0.1076
3	8	13.7000	10.6298	10.6852	0.1148
4	8	13.1372	10.2364	10.2945	0.1277
5	8	20.1203	15.5688	15.6534	0.1048
6	8	20.4939	15.8872	15.9772	0.1097
7	8	19.0016	14.7648	14.8527	0.1163
8	8	18.1513	14.1627	14.2541	0.1289
9	8	27.2415	21.1120	21.2511	0.1046
10	8	27.3486	21.2373	21.3833	0.1098
11	8	24.4047	18.9856	19.1212	0.1148
12	8	23.4654	18.3234	18.4641	0.1259
13	8	32.7647	25.3517	25.5143	0.1004
14	8	34.1939	26.4835	26.6571	0.1028
15	8	31.0866	24.0985	24.2598	0.1050
16	8	31.2036	24.2338	24.4023	0.1098
17	2	1.0346	0.8053	0.8170	0.0850
18	2	1.0371	0.8089	0.8212	0.0888
19	2	0.9729	0.7623	0.7749	0.0983
20	2	1.8763	1.4634	1.4871	0.0849
21	2	1.8153	1.4191	1.4431	0.0892
22	2	1.7005	1.3354	1.3598	0.0985
23	2	2.7361	2.1323	2.1664	0.0835
24	2	2.7478	2.1445	2.1798	0.0860
25	2	2.6717	2.0906	2.1267	0.0909
26	2	2.5067	1.9702	2.0069	0.1003
27	2	4.1017	3.2023	3.2583	0.0834
28	2	3.9976	3.1259	3.1822	0.0861
29	2	3.8373	3.0076	3.0640	0.0905
30	2	3.6187	2.8482	2.9055	0.0993

Culvert	D (ft)	Factored DL(k-ft/ft)	Nominal DL (k-ft/ft)	Mean (k-ft/ft)	COV
31	2	5.9034	4.6202	4.7124	0.0823
32	2	5.7824	4.5347	4.6284	0.0857
33	2	5.5076	4.3286	4.4214	0.0898
34	2	5.4916	4.3138	4.4055	0.0888
17	4	1.8248	1.4133	1.4251	0.0953
18	4	1.8431	1.4297	1.4420	0.0987
19	4	1.7646	1.3731	1.3857	0.1063
20	4	3.2525	2.5229	2.5466	0.0951
21	4	3.1789	2.4697	2.4938	0.0986
22	4	3.0424	2.3706	2.3951	0.1057
23	4	4.7129	3.6535	3.6877	0.0937
24	4	4.7635	3.6965	3.7318	0.0958
25	4	4.6925	3.6476	3.6837	0.0997
26	4	4.5071	3.5131	3.5498	0.1063
27	4	6.9750	5.4140	5.4700	0.0933
28	4	6.8503	5.3228	5.3791	0.0955
29	4	6.6588	5.1815	5.2380	0.0987
30	4	6.4238	5.0113	5.0686	0.1047
31	4	9.7975	7.6183	7.7105	0.0915
32	4	9.6872	7.5425	7.6362	0.0942
33	4	9.3360	7.2787	7.3714	0.0971
34	4	9.2886	7.2392	7.3310	0.0963
17	6	2.6583	2.0548	2.0665	0.1004
18	6	2.6946	2.0855	2.0978	0.1036
19	6	2.6028	2.0197	2.0322	0.1103
20	6	4.6889	3.6286	3.6524	0.1004
21	6	4.6026	3.5666	3.5906	0.1036
22	6	4.4455	3.4529	3.4774	0.1097
23	6	6.7586	5.2277	5.2619	0.0989
24	6	6.8504	5.3032	5.3385	0.1009
25	6	6.7861	5.2607	5.2968	0.1043
26	6	6.5815	5.1129	5.1496	0.1098
27	6	9.9343	7.6920	7.7480	0.0987
28	6	9.7888	7.5856	7.6419	0.1006
29	6	9.5654	7.4210	7.4774	0.1034
30	6	9.3154	7.2408	7.2982	0.1083
31	6	13.7922	10.6938	10.7860	0.0972
32	6	13.6942	10.6290	10.7227	0.0996
33	6	13.2640	10.3054	10.3982	0.1019
34	6	13.0511	10.1453	10.2377	0.1032
17	8	3.5354	2.7296	2.7414	0.1033
18	8	3.5915	2.7762	2.7885	0.1063
19	8	3.4875	2.7020	2.7146	0.1125
20	8	6.1855	4.7807	4.8044	0.1034
21	8	6.0864	4.7096	4.7337	0.1064

Culvert	D (ft)	Factored DL(k-ft/ft)	Nominal DL (k-ft/ft)	Mean (k-ft/ft)	COV
22	8	5.9097	4.5823	4.6067	0.1120
23	8	8.8732	6.8550	6.8891	0.1020
24	8	9.0085	6.9647	7.0000	0.1039
25	8	8.9525	6.9297	6.9658	0.1070
26	8	8.7299	6.7697	6.8063	0.1119
27	8	12.9798	10.0361	10.0922	0.1020
28	8	12.8129	9.9143	9.9706	0.1037
29	8	12.5572	9.7258	9.7823	0.1062
30	8	12.2933	9.5369	9.5942	0.1105
31	8	17.8875	13.8467	13.9389	0.1007
32	8	17.8035	13.7942	13.8879	0.1029
33	8	17.2917	13.4087	13.5015	0.1050
34	8	16.8602	13.0901	13.1831	0.1081

APPENDIX B RESULTS OF FRAME AND FE ANALYSES

Table B.1 presents the load effects (bending moment) under unit axle loads discussed in Section 3.4. The results are obtained from the finite element models of the soil-culvert system. Only one- and two-axle configurations are modeled. Table B.2 presents the load effects estimated from the LRFD load distribution model and the 2D frame analysis. One- to four-axle configurations are modeled. The values in both tables are used to quantify the uncertainty related to the use of the LRFD load distribution, as discussed in Chapter 3. Values in Table B.2 are also used in Chapter 4 as multipliers to efficiently generate load effects under random axle groups.

Table B.1 Results from FE analysis of soil-culvert systems (1 kip each axle)

Cul-vert	D (ft)	No. of axles	S1 (k-ft/ft)	S2 (k-ft/ft)	S3 (k-ft/ft)	No. of axles	S1 (k-ft/ft)	S2 (k-ft/ft)	S3 (k-ft/ft)
1	2	1	0.0612	0.0851	0.0612	2	0.1007	0.1109	0.1007
2	2	1	0.0572	0.0892	0.0572	2	0.0942	0.1180	0.0942
3	2	1	0.0550	0.0912	0.0550	2	0.0905	0.1227	0.0905
4	2	1	0.0537	0.0924	0.0537	2	0.0887	0.1247	0.0887
5	2	1	0.0597	0.1045	0.0597	2	0.1054	0.1468	0.1054
6	2	1	0.0569	0.1068	0.0569	2	0.1009	0.1512	0.1009
7	2	1	0.0656	0.1046	0.0656	2	0.1161	0.1483	0.1161
8	2	1	0.0644	0.1054	0.0644	2	0.1148	0.1497	0.1148
9	2	1	0.0684	0.1168	0.0684	2	0.1256	0.1706	0.1256
10	2	1	0.0670	0.1183	0.0670	2	0.1242	0.1736	0.1242
11	2	1	0.0831	0.1140	0.0831	2	0.1522	0.1655	0.1522
12	2	1	0.0820	0.1138	0.0820	2	0.1519	0.1667	0.1519
13	2	1	0.0795	0.1213	0.0795	2	0.1474	0.1809	0.1474
14	2	1	0.0757	0.1240	0.0757	2	0.1428	0.1850	0.1428
15	2	1	0.0921	0.1203	0.0921	2	0.1722	0.1791	0.1722
16	2	1	0.0901	0.1213	0.0901	2	0.1712	0.1811	0.1712
1	4	1	0.0493	0.0639	0.0493	2	0.0867	0.0978	0.0867
2	4	1	0.0460	0.0671	0.0460	2	0.0809	0.1034	0.0809
3	4	1	0.0442	0.0688	0.0442	2	0.0777	0.1062	0.0777
4	4	1	0.0442	0.0696	0.0442	2	0.0757	0.1077	0.0757
5	4	1	0.0497	0.0808	0.0497	2	0.0885	0.1289	0.0885
6	4	1	0.0475	0.0827	0.0475	2	0.0845	0.1322	0.0845
7	4	1	0.0548	0.0809	0.0548	2	0.0975	0.1291	0.0975
8	4	1	0.0540	0.0814	0.0540	2	0.0963	0.1301	0.0963
9	4	1	0.0596	0.0932	0.0596	2	0.1105	0.1523	0.1105
10	4	1	0.0580	0.0945	0.0580	2	0.1076	0.1548	0.1076
11	4	1	0.0722	0.0908	0.0722	2	0.1337	0.1482	0.1337
12	4	1	0.0714	0.0912	0.0714	2	0.1327	0.1492	0.1327
13	4	1	0.0699	0.0972	0.0699	2	0.1306	0.1608	0.1306
14	4	1	0.0667	0.0995	0.0667	2	0.1255	0.1650	0.1255
15	4	1	0.0812	0.0963	0.0812	2	0.1527	0.1589	0.1527
16	4	1	0.0796	0.0971	0.0796	2	0.1505	0.1606	0.1505

Cul-vert	D (ft)	No. of axles	S1 (k-ft/ft)	S2 (k-ft/ft)	S3 (k-ft/ft)	No. of axles	S1 (k-ft/ft)	S2 (k-ft/ft)	S3 (k-ft/ft)
1	6	1	0.0384	0.0465	0.0384	2	0.0713	0.0770	0.0713
2	6	1	0.0359	0.0491	0.0359	2	0.0664	0.0811	0.0664
3	6	1	0.0345	0.0504	0.0345	2	0.0632	0.0853	0.0632
4	6	1	0.0337	0.0511	0.0337	2	0.0616	0.0852	0.0616
5	6	1	0.0392	0.0605	0.0392	2	0.0724	0.1040	0.0724
6	6	1	0.0375	0.0619	0.0375	2	0.0691	0.1068	0.0691
7	6	1	0.0432	0.0607	0.0432	2	0.0796	0.1045	0.0796
8	6	1	0.0432	0.0611	0.0432	2	0.0786	0.1053	0.0786
9	6	1	0.0491	0.0719	0.0491	2	0.0923	0.1255	0.0923
10	6	1	0.0473	0.0725	0.0473	2	0.0889	0.1276	0.0889
11	6	1	0.0593	0.0701	0.0593	2	0.1102	0.1223	0.1102
12	6	1	0.0589	0.0705	0.0589	2	0.1106	0.1231	0.1106
13	6	1	0.0581	0.0755	0.0581	2	0.1101	0.1328	0.1101
14	6	1	0.0555	0.0773	0.0555	2	0.1054	0.1364	0.1054
15	6	1	0.0676	0.0744	0.0676	2	0.1275	0.1316	0.1275
16	6	1	0.0671	0.0755	0.0671	2	0.1266	0.1330	0.1266
1	8	1	0.0295	0.0344	0.0295	2	0.0563	0.0569	0.0563
2	8	1	0.0276	0.0364	0.0276	2	0.0522	0.0604	0.0522
3	8	1	0.0265	0.0375	0.0265	2	0.0494	0.0622	0.0494
4	8	1	0.0260	0.0380	0.0260	2	0.0478	0.0631	0.0478
5	8	1	0.0306	0.0456	0.0306	2	0.0585	0.0810	0.0585
6	8	1	0.0293	0.0468	0.0293	2	0.0554	0.0832	0.0554
7	8	1	0.0339	0.0459	0.0339	2	0.0633	0.0816	0.0633
8	8	1	0.0334	0.0462	0.0334	2	0.0622	0.0823	0.0622
9	8	1	0.0394	0.0557	0.0394	2	0.0743	0.1012	0.0743
10	8	1	0.0384	0.0565	0.0384	2	0.0721	0.1028	0.0721
11	8	1	0.0479	0.0543	0.0479	2	0.0897	0.0986	0.0897
12	8	1	0.0475	0.0546	0.0475	2	0.0889	0.0993	0.0889
13	8	1	0.0472	0.0587	0.0472	2	0.0895	0.1069	0.0895
14	8	1	0.0451	0.0602	0.0451	2	0.0863	0.1099	0.0863
15	8	1	0.0551	0.0583	0.0551	2	0.1052	0.1062	0.1052
16	8	1	0.0542	0.0588	0.0542	2	0.1036	0.1073	0.1036
17	2	1	0.0188	0.0519	0.0276	2	0.0275	0.0517	0.0218
18	2	1	0.0160	0.0564	0.0275	2	0.0260	0.0571	0.0246
19	2	1	0.0167	0.0584	0.0255	2	0.0242	0.0598	0.0260
20	2	1	0.0226	0.0764	0.0409	2	0.0364	0.0931	0.0626
21	2	1	0.0294	0.0757	0.0435	2	0.0467	0.0921	0.0656
22	2	1	0.0288	0.0772	0.0420	2	0.0456	0.0942	0.0619
23	2	1	0.0528	0.0824	0.0662	2	0.0894	0.1077	0.1094
24	2	1	0.0509	0.0858	0.0635	2	0.0842	0.1136	0.1038
25	2	1	0.0496	0.0879	0.0611	2	0.0821	0.1170	0.0993
26	2	1	0.0490	0.0891	0.0611	2	0.0811	0.1189	0.1006
27	2	1	0.0523	0.1007	0.0741	2	0.0927	0.1411	0.1292
28	2	1	0.0603	0.0999	0.0764	2	0.1070	0.1400	0.1333

Cul-vert	D (ft)	No. of axles	S1 (k-ft/ft)	S2 (k-ft/ft)	S3 (k-ft/ft)	No. of axles	S1 (k-ft/ft)	S2 (k-ft/ft)	S3 (k-ft/ft)
29	2	1	0.0690	0.0990	0.0790	2	0.1208	0.1384	0.1374
30	2	1	0.0688	0.0999	0.0773	2	0.1220	0.1401	0.1341
31	2	1	0.0608	0.1099	0.0847	2	0.1136	0.1656	0.1509
32	2	1	0.0600	0.1113	0.0826	2	0.1112	0.1683	0.1468
33	2	1	0.0763	0.1082	0.0896	2	0.1411	0.1624	0.1597
34	2	1	0.0772	0.1109	0.0902	2	0.1370	0.1608	0.1646
17	4	1	0.0146	0.0364	0.0237	2	0.0113	0.0462	0.0213
18	4	1	0.0126	0.0398	0.0211	2	0.0110	0.0513	0.0229
19	4	1	0.0120	0.0413	0.0193	2	0.0108	0.0535	0.0237
20	4	1	0.0166	0.0564	0.0334	2	0.0247	0.0824	0.0338
21	4	1	0.0223	0.0560	0.0352	2	0.0336	0.0822	0.0372
22	4	1	0.0221	0.0571	0.0336	2	0.0335	0.0841	0.0373
23	4	1	0.0418	0.0620	0.0548	2	0.0734	0.0947	0.0960
24	4	1	0.0397	0.0647	0.0522	2	0.0697	0.0995	0.0934
25	4	1	0.0388	0.0662	0.0501	2	0.0688	0.1019	0.0890
26	4	1	0.0387	0.0671	0.0487	2	0.0684	0.1035	0.0859
27	4	1	0.0434	0.0779	0.0622	2	0.0780	0.1238	0.1113
28	4	1	0.0505	0.0773	0.0643	2	0.0905	0.1228	0.1145
29	4	1	0.0574	0.0765	0.0665	2	0.1026	0.1214	0.1180
30	4	1	0.0574	0.0772	0.0650	2	0.1023	0.1227	0.1151
31	4	1	0.0530	0.0904	0.0735	2	0.0973	0.1476	0.1323
32	4	1	0.0525	0.0916	0.0716	2	0.0977	0.1498	0.1286
33	4	1	0.0668	0.0889	0.0770	2	0.1237	0.1448	0.1398
34	4	1	0.0670	0.0880	0.0791	2	0.1136	0.1433	0.1439
17	6	1	0.0096	0.0248	0.0089	2	0.0051	0.0341	0.0173
18	6	1	0.0083	0.0274	0.0051	2	0.0062	0.0378	0.0187
19	6	1	0.0081	0.0285	0.0066	2	0.0078	0.0394	0.0194
20	6	1	0.0133	0.0401	0.0251	2	0.0112	0.0620	0.0299
21	6	1	0.0175	0.0399	0.0264	2	0.0254	0.0647	0.0321
22	6	1	0.0171	0.0408	0.0251	2	0.0259	0.0661	0.0297
23	6	1	0.0328	0.0450	0.0419	2	0.0573	0.0757	0.0589
24	6	1	0.0311	0.0471	0.0397	2	0.0544	0.0795	0.0488
25	6	1	0.0303	0.0483	0.0381	2	0.0532	0.0816	0.0497
26	6	1	0.0301	0.0490	0.0379	2	0.0531	0.0827	0.0469
27	6	1	0.0340	0.0580	0.0487	2	0.0633	0.0997	0.0900
28	6	1	0.0395	0.0577	0.0502	2	0.0730	0.0990	0.0927
29	6	1	0.0450	0.0571	0.0520	2	0.0824	0.0981	0.0955
30	6	1	0.0450	0.0577	0.0508	2	0.0820	0.0992	0.0932
31	6	1	0.0431	0.0695	0.0585	2	0.0810	0.1212	0.1110
32	6	1	0.0425	0.0704	0.0570	2	0.0793	0.1231	0.1080
33	6	1	0.0544	0.0676	0.0621	2	0.1009	0.1181	0.1155
34	6	1	0.0537	0.0677	0.0652	2	0.0875	0.1182	0.1208
17	8	1	0.0035	0.0157	0.0057	2	0.0147	0.0213	0.0168
18	8	1	0.0034	0.0175	0.0067	2	0.0143	0.0237	0.0171

Cul-vert	D (ft)	No. of axles	S1 (k-ft/ft)	S2 (k-ft/ft)	S3 (k-ft/ft)	No. of axles	S1 (k-ft/ft)	S2 (k-ft/ft)	S3 (k-ft/ft)
19	8	1	0.0037	0.0183	0.0068	2	0.0147	0.0247	0.0171
20	8	1	0.0081	0.0284	0.0091	2	0.0142	0.0425	0.0265
21	8	1	0.0113	0.0285	0.0075	2	0.0183	0.0455	0.0283
22	8	1	0.0114	0.0292	0.0109	2	0.0197	0.0462	0.0288
23	8	1	0.0242	0.0332	0.0340	2	0.0384	0.0564	0.0409
24	8	1	0.0229	0.0348	0.0322	2	0.0372	0.0593	0.0413
25	8	1	0.0224	0.0357	0.0308	2	0.0374	0.0609	0.0416
26	8	1	0.0224	0.0362	0.0299	2	0.0379	0.0617	0.0397
27	8	1	0.0258	0.0437	0.0390	2	0.0479	0.0782	0.0442
28	8	1	0.0302	0.0435	0.0402	2	0.0560	0.0779	0.0591
29	8	1	0.0351	0.0432	0.0414	2	0.0655	0.0773	0.0571
30	8	1	0.0352	0.0435	0.0405	2	0.0655	0.0781	0.0622
31	8	1	0.0340	0.0538	0.0485	2	0.0656	0.0974	0.0917
32	8	1	0.0339	0.0545	0.0472	2	0.0647	0.0988	0.0892
33	8	1	0.0435	0.0528	0.0513	2	0.0820	0.0959	0.0966
34	8	1	0.0398	0.0523	0.0530	2	0.0706	0.0950	0.0985

Table B.2 Results from 2D frame analysis (1 kip per axle)

Cul-vert	D (ft)	No. of axles	S1 (k-ft/ft)	S2 (k-ft/ft)	S3 (k-ft/ft)	No. of axles	S1 (k-ft/ft)	S2 (k-ft/ft)	S3 (k-ft/ft)
1	2	1	0.0917	0.1585	0.0918	2	0.1432	0.2135	0.1427
2	2	1	0.0787	0.1701	0.0786	2	0.1224	0.2332	0.1218
3	2	1	0.0689	0.1791	0.0688	2	0.1068	0.2482	0.1063
4	2	1	0.0612	0.1862	0.0612	2	0.0945	0.2600	0.0941
5	2	1	0.0845	0.2087	0.0844	2	0.1425	0.3079	0.1424
6	2	1	0.0732	0.2190	0.0732	2	0.1233	0.3262	0.1233
7	2	1	0.0811	0.2152	0.0810	2	0.1346	0.3166	0.1341
8	2	1	0.0736	0.2221	0.0736	2	0.1220	0.3286	0.1216
9	2	1	0.1007	0.2498	0.1007	2	0.1789	0.3909	0.1789
10	2	1	0.0903	0.2592	0.0903	2	0.1603	0.4084	0.1603
11	2	1	0.1074	0.2370	0.1072	2	0.1908	0.3659	0.1906
12	2	1	0.1001	0.2435	0.0999	2	0.1778	0.3779	0.1776
13	2	1	0.1311	0.2581	0.1310	2	0.2390	0.4100	0.2389
14	2	1	0.1169	0.2706	0.1168	2	0.2131	0.4336	0.2129
15	2	1	0.1394	0.2578	0.1393	2	0.2481	0.4019	0.2475
16	2	1	0.1300	0.2661	0.1299	2	0.2312	0.4171	0.2306
1	4	1	0.0585	0.0936	0.0584	2	0.0870	0.1355	0.0869
2	4	1	0.0501	0.1013	0.0500	2	0.0741	0.1484	0.0740
3	4	1	0.0438	0.1073	0.0437	2	0.0643	0.1582	0.0643
4	4	1	0.0388	0.1119	0.0387	2	0.0567	0.1659	0.0566
5	4	1	0.0569	0.1314	0.0568	2	0.0922	0.2044	0.0921

Cul-vert	D (ft)	No. of axles	S1 (k-ft/ft)	S2 (k-ft/ft)	S3 (k-ft/ft)	No. of axles	S1 (k-ft/ft)	S2 (k-ft/ft)	S3 (k-ft/ft)
6	4	1	0.0493	0.1385	0.0492	2	0.0796	0.2169	0.0794
7	4	1	0.0546	0.1359	0.0545	2	0.0878	0.2110	0.0876
8	4	1	0.0495	0.1406	0.0495	2	0.0794	0.2192	0.0792
9	4	1	0.0684	0.1605	0.0683	2	0.1170	0.2590	0.1165
10	4	1	0.0613	0.1670	0.0612	2	0.1047	0.2709	0.1040
11	4	1	0.0769	0.1575	0.0769	2	0.1304	0.2514	0.1300
12	4	1	0.0717	0.1622	0.0717	2	0.1214	0.2599	0.1211
13	4	1	0.0947	0.1741	0.0947	2	0.1673	0.2851	0.1673
14	4	1	0.0845	0.1833	0.0844	2	0.1491	0.3022	0.1491
15	4	1	0.0978	0.1699	0.0977	2	0.1759	0.2809	0.1758
16	4	1	0.0911	0.1759	0.0910	2	0.1639	0.2920	0.1638
1	6	1	0.0429	0.0662	0.0428	2	0.0595	0.0944	0.0595
2	6	1	0.0366	0.0722	0.0366	2	0.0506	0.1035	0.0506
3	6	1	0.0320	0.0768	0.0319	2	0.0438	0.1104	0.0438
4	6	1	0.0283	0.0804	0.0282	2	0.0385	0.1158	0.0385
5	6	1	0.0439	0.0974	0.0438	2	0.0651	0.1488	0.0650
6	6	1	0.0380	0.1031	0.0379	2	0.0558	0.1581	0.0557
7	6	1	0.0416	0.1002	0.0415	2	0.0623	0.1544	0.0623
8	6	1	0.0377	0.1039	0.0376	2	0.0561	0.1606	0.0561
9	6	1	0.0542	0.1215	0.0542	2	0.0875	0.1941	0.0875
10	6	1	0.0485	0.1268	0.0485	2	0.0781	0.2035	0.0781
11	6	1	0.0600	0.1177	0.0600	2	0.0983	0.1885	0.0981
12	6	1	0.0559	0.1215	0.0559	2	0.0914	0.1953	0.0913
13	6	1	0.0746	0.1311	0.0745	2	0.1282	0.2154	0.1280
14	6	1	0.0665	0.1386	0.0664	2	0.1140	0.2290	0.1139
15	6	1	0.0795	0.1305	0.0794	2	0.1366	0.2137	0.1366
16	6	1	0.0741	0.1354	0.0740	2	0.1272	0.2227	0.1272
1	8	1	0.0302	0.0475	0.0302	2	0.0432	0.0685	0.0431
2	8	1	0.0257	0.0521	0.0257	2	0.0367	0.0752	0.0366
3	8	1	0.0222	0.0556	0.0222	2	0.0318	0.0802	0.0317
4	8	1	0.0196	0.0583	0.0196	2	0.0280	0.0841	0.0279
5	8	1	0.0326	0.0727	0.0326	2	0.0473	0.1095	0.0471
6	8	1	0.0281	0.0771	0.0281	2	0.0405	0.1164	0.0404
7	8	1	0.0311	0.0751	0.0311	2	0.0452	0.1137	0.0452
8	8	1	0.0281	0.0781	0.0281	2	0.0407	0.1183	0.0407
9	8	1	0.0420	0.0926	0.0419	2	0.0645	0.1476	0.0644
10	8	1	0.0375	0.0969	0.0375	2	0.0573	0.1549	0.0572
11	8	1	0.0469	0.0901	0.0468	2	0.0730	0.1436	0.0729

Cul-vert	D (ft)	No. of axles	S1 (k-ft/ft)	S2 (k-ft/ft)	S3 (k-ft/ft)	No. of axles	S1 (k-ft/ft)	S2 (k-ft/ft)	S3 (k-ft/ft)
12	8	1	0.0436	0.0932	0.0436	2	0.0677	0.1489	0.0676
13	8	1	0.0602	0.1023	0.0601	2	0.0989	0.1669	0.0989
14	8	1	0.0537	0.1085	0.0536	2	0.0879	0.1779	0.0878
15	8	1	0.0642	0.1016	0.0642	2	0.1047	0.1650	0.1051
16	8	1	0.0598	0.1057	0.0598	2	0.0975	0.1722	0.0977
17	2	1	0.0454	0.0863	0.0617	2	0.0645	0.0908	0.0755
18	2	1	0.0359	0.0938	0.0584	2	0.0505	0.0988	0.0721
19	2	1	0.0303	0.0983	0.0563	2	0.0423	0.1036	0.0701
20	2	1	0.0436	0.1285	0.0763	2	0.0695	0.1587	0.1198
21	2	1	0.0475	0.1317	0.0781	2	0.0789	0.1619	0.1209
22	2	1	0.0421	0.1361	0.0760	2	0.0698	0.1689	0.1185
23	2	1	0.0889	0.1478	0.1063	2	0.1477	0.1941	0.1797
24	2	1	0.0773	0.1555	0.1026	2	0.1306	0.2068	0.1746
25	2	1	0.0692	0.1614	0.0998	2	0.1181	0.2162	0.1708
26	2	1	0.0633	0.1660	0.0975	2	0.1084	0.2239	0.1678
27	2	1	0.0827	0.1895	0.1180	2	0.1499	0.2739	0.2099
28	2	1	0.0881	0.1892	0.1200	2	0.1530	0.2682	0.2147
29	2	1	0.0943	0.1884	0.1223	2	0.1631	0.2662	0.2179
30	2	1	0.0878	0.1929	0.1201	2	0.1529	0.2739	0.2144
31	2	1	0.1010	0.2280	0.1356	2	0.1880	0.3507	0.2497
32	2	1	0.0925	0.2342	0.1326	2	0.1735	0.3620	0.2446
33	2	1	0.1030	0.2179	0.1394	2	0.1902	0.3310	0.2563
34	2	1	0.1156	0.2129	0.1437	2	0.2123	0.3209	0.2636
17	4	1	0.0267	0.0431	0.0353	2	0.0337	0.0512	0.0456
18	4	1	0.0211	0.0473	0.0338	2	0.0260	0.0562	0.0453
19	4	1	0.0178	0.0498	0.0329	2	0.0216	0.0591	0.0447
20	4	1	0.0281	0.0737	0.0488	2	0.0437	0.0963	0.0685
21	4	1	0.0307	0.0739	0.0496	2	0.0472	0.0965	0.0703
22	4	1	0.0271	0.0766	0.0484	2	0.0417	0.1002	0.0689
23	4	1	0.0570	0.0862	0.0709	2	0.0979	0.1226	0.1132
24	4	1	0.0498	0.0913	0.0687	2	0.0865	0.1309	0.1102
25	4	1	0.0449	0.0951	0.0670	2	0.0781	0.1371	0.1081
26	4	1	0.0412	0.0981	0.0656	2	0.0716	0.1418	0.1064
27	4	1	0.0566	0.1179	0.0819	2	0.1023	0.1798	0.1412
28	4	1	0.0602	0.1176	0.0832	2	0.1060	0.1780	0.1445
29	4	1	0.0644	0.1169	0.0847	2	0.1130	0.1767	0.1466
30	4	1	0.0602	0.1200	0.0832	2	0.1061	0.1820	0.1445
31	4	1	0.0679	0.1446	0.0966	2	0.1238	0.2294	0.1742

Cul-vert	D (ft)	No. of axles	S1 (k-ft/ft)	S2 (k-ft/ft)	S3 (k-ft/ft)	No. of axles	S1 (k-ft/ft)	S2 (k-ft/ft)	S3 (k-ft/ft)
32	4	1	0.0623	0.1489	0.0947	2	0.1142	0.2370	0.1711
33	4	1	0.0760	0.1438	0.0996	2	0.1337	0.2254	0.1802
34	4	1	0.0851	0.1400	0.1027	2	0.1486	0.2184	0.1849
17	6	1	0.0181	0.0264	0.0219	2	0.0204	0.0348	0.0426
18	6	1	0.0141	0.0289	0.0210	2	0.0147	0.0382	0.0439
19	6	1	0.0118	0.0304	0.0204	2	0.0116	0.0402	0.0442
20	6	1	0.0210	0.0492	0.0352	2	0.0293	0.0658	0.0495
21	6	1	0.0230	0.0494	0.0355	2	0.0317	0.0658	0.0503
22	6	1	0.0204	0.0513	0.0348	2	0.0278	0.0683	0.0497
23	6	1	0.0446	0.0603	0.0537	2	0.0735	0.0850	0.0791
24	6	1	0.0395	0.0643	0.0522	2	0.0649	0.0909	0.0771
25	6	1	0.0357	0.0672	0.0511	2	0.0585	0.0952	0.0756
26	6	1	0.0328	0.0695	0.0502	2	0.0535	0.0986	0.0744
27	6	1	0.0465	0.0865	0.0642	2	0.0793	0.1294	0.1057
28	6	1	0.0479	0.0854	0.0658	2	0.0843	0.1288	0.1066
29	6	1	0.0511	0.0848	0.0668	2	0.0883	0.1274	0.1095
30	6	1	0.0479	0.0873	0.0658	2	0.0828	0.1314	0.1082
31	6	1	0.0559	0.1085	0.0778	2	0.0999	0.1704	0.1347
32	6	1	0.0513	0.1120	0.0763	2	0.0922	0.1763	0.1325
33	6	1	0.0601	0.1064	0.0805	2	0.1087	0.1678	0.1393
34	6	1	0.0653	0.1046	0.0822	2	0.1149	0.1636	0.1435
17	8	1	0.0111	0.0176	0.0169	2	0.0147	0.0252	0.0364
18	8	1	0.0084	0.0194	0.0170	2	0.0106	0.0277	0.0378
19	8	1	0.0070	0.0204	0.0169	2	0.0083	0.0291	0.0385
20	8	1	0.0154	0.0334	0.0232	2	0.0175	0.0477	0.0463
21	8	1	0.0165	0.0334	0.0243	2	0.0194	0.0478	0.0463
22	8	1	0.0145	0.0346	0.0238	2	0.0168	0.0496	0.0463
23	8	1	0.0353	0.0429	0.0395	2	0.0540	0.0617	0.0570
24	8	1	0.0311	0.0459	0.0385	2	0.0472	0.0660	0.0556
25	8	1	0.0281	0.0480	0.0377	2	0.0422	0.0691	0.0552
26	8	1	0.0258	0.0497	0.0371	2	0.0385	0.0715	0.0547
27	8	1	0.0372	0.0638	0.0504	2	0.0614	0.0950	0.0772
28	8	1	0.0386	0.0632	0.0517	2	0.0654	0.0946	0.0777
29	8	1	0.0412	0.0627	0.0524	2	0.0690	0.0937	0.0799
30	8	1	0.0387	0.0646	0.0516	2	0.0646	0.0966	0.0788
31	8	1	0.0451	0.0817	0.0631	2	0.0795	0.1283	0.1048
32	8	1	0.0416	0.0844	0.0620	2	0.0732	0.1328	0.1032
33	8	1	0.0488	0.0806	0.0654	2	0.0870	0.1266	0.1085

Cul-vert	D (ft)	No. of axles	S1 (k-ft/ft)	S2 (k-ft/ft)	S3 (k-ft/ft)	No. of axles	S1 (k-ft/ft)	S2 (k-ft/ft)	S3 (k-ft/ft)
34	8	1	0.0515	0.0801	0.0662	2	0.0920	0.1257	0.1095
1	2	3	0.1478	0.2354	0.1476	4	0.1478	0.2366	0.1473
2	2	3	0.1255	0.2580	0.1253	4	0.1255	0.2592	0.1250
3	2	3	0.1088	0.2750	0.1085	4	0.1088	0.2763	0.1081
4	2	3	0.0957	0.2882	0.0953	4	0.0957	0.2895	0.0952
5	2	3	0.1575	0.3617	0.1565	4	0.1575	0.3617	0.1567
6	2	3	0.1350	0.3843	0.1342	4	0.1350	0.3843	0.1343
7	2	3	0.1500	0.3733	0.1498	4	0.1500	0.3746	0.1496
8	2	3	0.1351	0.3883	0.1350	4	0.1351	0.3896	0.1346
9	2	3	0.2177	0.4786	0.2175	4	0.2191	0.4942	0.2191
10	2	3	0.1944	0.5016	0.1943	4	0.1950	0.5186	0.1950
11	2	3	0.2324	0.4480	0.2324	4	0.2356	0.4655	0.2381
12	2	3	0.2162	0.4640	0.2161	4	0.2185	0.4827	0.2209
13	2	3	0.3052	0.5117	0.3051	4	0.3218	0.5448	0.3202
14	2	3	0.2717	0.5441	0.2716	4	0.2851	0.5815	0.2833
15	2	3	0.3142	0.4934	0.3123	4	0.3344	0.5241	0.3344
16	2	3	0.2925	0.5141	0.2907	4	0.3104	0.5478	0.3104
1	4	3	0.0918	0.1457	0.0916	4	0.0944	0.1497	0.0942
2	4	3	0.0780	0.1598	0.0777	4	0.0801	0.1642	0.0800
3	4	3	0.0676	0.1704	0.0673	4	0.0695	0.1751	0.0693
4	4	3	0.0595	0.1787	0.0592	4	0.0611	0.1836	0.0610
5	4	3	0.1002	0.2322	0.1002	4	0.1030	0.2386	0.1027
6	4	3	0.0859	0.2468	0.0859	4	0.0883	0.2536	0.0880
7	4	3	0.0958	0.2410	0.0956	4	0.0984	0.2476	0.0981
8	4	3	0.0863	0.2507	0.0861	4	0.0887	0.2576	0.0883
9	4	3	0.1367	0.3097	0.1365	4	0.1402	0.3236	0.1399
10	4	3	0.1215	0.3249	0.1213	4	0.1245	0.3395	0.1243
11	4	3	0.1544	0.3009	0.1541	4	0.1585	0.3151	0.1584
12	4	3	0.1433	0.3120	0.1431	4	0.1471	0.3268	0.1470
13	4	3	0.2065	0.3473	0.2061	4	0.2162	0.3747	0.2159
14	4	3	0.1835	0.3700	0.1831	4	0.1914	0.4000	0.1911
15	4	3	0.2201	0.3442	0.2201	4	0.2309	0.3714	0.2304
16	4	3	0.2048	0.3592	0.2048	4	0.2143	0.3882	0.2139
1	6	3	0.0666	0.1056	0.0665	4	0.0708	0.1122	0.0707
2	6	3	0.0565	0.1158	0.0564	4	0.0601	0.1231	0.0601
3	6	3	0.0490	0.1235	0.0489	4	0.0521	0.1313	0.0521
4	6	3	0.0431	0.1295	0.0430	4	0.0458	0.1377	0.0458
5	6	3	0.0727	0.1685	0.0726	4	0.0773	0.1792	0.0770

Cul-vert	D (ft)	No. of axles	S1 (k-ft/ft)	S2 (k-ft/ft)	S3 (k-ft/ft)	No. of axles	S1 (k-ft/ft)	S2 (k-ft/ft)	S3 (k-ft/ft)
6	6	3	0.0623	0.1791	0.0623	4	0.0663	0.1904	0.0660
7	6	3	0.0695	0.1749	0.0694	4	0.0739	0.1860	0.0736
8	6	3	0.0626	0.1820	0.0625	4	0.0666	0.1934	0.0663
9	6	3	0.0992	0.2289	0.0991	4	0.1054	0.2433	0.1054
10	6	3	0.0881	0.2402	0.0881	4	0.0937	0.2553	0.0937
11	6	3	0.1122	0.2229	0.1118	4	0.1192	0.2370	0.1190
12	6	3	0.1041	0.2312	0.1037	4	0.1106	0.2457	0.1104
13	6	3	0.1533	0.2628	0.1531	4	0.1629	0.2821	0.1628
14	6	3	0.1357	0.2805	0.1355	4	0.1442	0.3012	0.1441
15	6	3	0.1634	0.2601	0.1633	4	0.1737	0.2797	0.1738
16	6	3	0.1517	0.2718	0.1517	4	0.1612	0.2923	0.1614
1	8	3	0.0504	0.0800	0.0504	4	0.0551	0.0873	0.0549
2	8	3	0.0429	0.0878	0.0428	4	0.0468	0.0958	0.0467
3	8	3	0.0371	0.0936	0.0371	4	0.0405	0.1022	0.0404
4	8	3	0.0326	0.0981	0.0327	4	0.0356	0.1071	0.0355
5	8	3	0.0552	0.1278	0.0551	4	0.0602	0.1395	0.0599
6	8	3	0.0473	0.1359	0.0472	4	0.0516	0.1483	0.0514
7	8	3	0.0527	0.1327	0.0526	4	0.0576	0.1448	0.0573
8	8	3	0.0475	0.1380	0.0474	4	0.0519	0.1507	0.0516
9	8	3	0.0753	0.1738	0.0751	4	0.0822	0.1897	0.0820
10	8	3	0.0669	0.1824	0.0667	4	0.0730	0.1991	0.0728
11	8	3	0.0852	0.1693	0.0851	4	0.0930	0.1848	0.0926
12	8	3	0.0790	0.1756	0.0790	4	0.0863	0.1916	0.0859
13	8	3	0.1165	0.2018	0.1165	4	0.1271	0.2202	0.1267
14	8	3	0.1031	0.2154	0.1031	4	0.1126	0.2351	0.1121
15	8	3	0.1242	0.2000	0.1243	4	0.1356	0.2183	0.1354
16	8	3	0.1153	0.2091	0.1154	4	0.1258	0.2282	0.1257
17	2	3	0.0589	0.0902	0.1100	4	0.0597	0.0908	0.1387
18	2	3	0.0439	0.0980	0.1137	4	0.0446	0.0988	0.1442
19	2	3	0.0354	0.1025	0.1149	4	0.0359	0.1033	0.1468
20	2	3	0.0697	0.1607	0.1329	4	0.0640	0.1611	0.2105
21	2	3	0.0810	0.1658	0.1305	4	0.0746	0.1650	0.2057
22	2	3	0.0711	0.1720	0.1290	4	0.0640	0.1712	0.2074
23	2	3	0.1842	0.2118	0.1924	4	0.1771	0.2128	0.2072
24	2	3	0.1620	0.2263	0.1872	4	0.1533	0.2273	0.2091
25	2	3	0.1458	0.2368	0.1834	4	0.1365	0.2378	0.2099
26	2	3	0.1335	0.2449	0.1805	4	0.1237	0.2459	0.2102
27	2	3	0.1903	0.3142	0.2584	4	0.2046	0.3133	0.2559

Cul-vert	D (ft)	No. of axles	S1 (k-ft/ft)	S2 (k-ft/ft)	S3 (k-ft/ft)	No. of axles	S1 (k-ft/ft)	S2 (k-ft/ft)	S3 (k-ft/ft)
28	2	3	0.2021	0.3113	0.2597	4	0.2148	0.3118	0.2620
29	2	3	0.2105	0.3071	0.2670	4	0.2262	0.3064	0.2675
30	2	3	0.1973	0.3167	0.2637	4	0.2112	0.3160	0.2643
31	2	3	0.2553	0.4222	0.3229	4	0.2952	0.4323	0.3358
32	2	3	0.2359	0.4371	0.3170	4	0.2725	0.4480	0.3297
33	2	3	0.2564	0.3984	0.3316	4	0.2974	0.4116	0.3533
34	2	3	0.2760	0.3824	0.3434	4	0.3223	0.3902	0.3587
17	4	3	0.0315	0.0539	0.0778	4	0.0326	0.0554	0.0799
18	4	3	0.0227	0.0591	0.0808	4	0.0236	0.0608	0.0830
19	4	3	0.0179	0.0621	0.0822	4	0.0185	0.0639	0.0844
20	4	3	0.0401	0.1017	0.0918	4	0.0374	0.1045	0.1421
21	4	3	0.0440	0.1018	0.0920	4	0.0412	0.1047	0.1436
22	4	3	0.0383	0.1056	0.0918	4	0.0347	0.1087	0.1455
23	4	3	0.1148	0.1311	0.1220	4	0.1055	0.1347	0.1488
24	4	3	0.1004	0.1401	0.1189	4	0.0893	0.1441	0.1518
25	4	3	0.0900	0.1467	0.1166	4	0.0783	0.1509	0.1535
26	4	3	0.0821	0.1518	0.1147	4	0.0705	0.1561	0.1545
27	4	3	0.1302	0.2016	0.1614	4	0.1327	0.2069	0.1744
28	4	3	0.1365	0.2004	0.1657	4	0.1408	0.2057	0.1760
29	4	3	0.1438	0.1985	0.1704	4	0.1500	0.2038	0.1778
30	4	3	0.1346	0.2047	0.1682	4	0.1398	0.2103	0.1773
31	4	3	0.1646	0.2698	0.2198	4	0.1840	0.2808	0.2273
32	4	3	0.1516	0.2792	0.2166	4	0.1686	0.2907	0.2238
33	4	3	0.1800	0.2659	0.2271	4	0.2041	0.2774	0.2343
34	4	3	0.1996	0.2567	0.2317	4	0.2249	0.2674	0.2430
17	6	3	0.0230	0.0390	0.0562	4	0.0243	0.0414	0.0598
18	6	3	0.0166	0.0428	0.0584	4	0.0175	0.0454	0.0621
19	6	3	0.0131	0.0450	0.0594	4	0.0137	0.0477	0.0631
20	6	3	0.0263	0.0736	0.0880	4	0.0279	0.0782	0.1064
21	6	3	0.0289	0.0737	0.0875	4	0.0304	0.0782	0.1075
22	6	3	0.0244	0.0765	0.0882	4	0.0256	0.0812	0.1090
23	6	3	0.0800	0.0950	0.0930	4	0.0795	0.1011	0.1354
24	6	3	0.0692	0.1016	0.0937	4	0.0673	0.1081	0.1396
25	6	3	0.0617	0.1064	0.0940	4	0.0586	0.1132	0.1422
26	6	3	0.0559	0.1101	0.0940	4	0.0520	0.1172	0.1440
27	6	3	0.0963	0.1463	0.1175	4	0.0914	0.1553	0.1501
28	6	3	0.1016	0.1454	0.1204	4	0.0978	0.1545	0.1501
29	6	3	0.1077	0.1441	0.1235	4	0.1051	0.1531	0.1500

Cul-vert	D (ft)	No. of axles	S1 (k-ft/ft)	S2 (k-ft/ft)	S3 (k-ft/ft)	No. of axles	S1 (k-ft/ft)	S2 (k-ft/ft)	S3 (k-ft/ft)
30	6	3	0.1005	0.1486	0.1219	4	0.0974	0.1579	0.1508
31	6	3	0.1288	0.1988	0.1593	4	0.1378	0.2114	0.1730
32	6	3	0.1184	0.2058	0.1568	4	0.1263	0.2188	0.1719
33	6	3	0.1395	0.1960	0.1679	4	0.1526	0.2085	0.1773
34	6	3	0.1513	0.1920	0.1701	4	0.1648	0.2039	0.1825
17	8	3	0.0173	0.0294	0.0425	4	0.0187	0.0321	0.0464
18	8	3	0.0125	0.0323	0.0442	4	0.0135	0.0352	0.0482
19	8	3	0.0098	0.0340	0.0449	4	0.0106	0.0370	0.0490
20	8	3	0.0199	0.0557	0.0758	4	0.0217	0.0608	0.0827
21	8	3	0.0220	0.0558	0.0766	4	0.0237	0.0608	0.0836
22	8	3	0.0185	0.0579	0.0776	4	0.0200	0.0631	0.0847
23	8	3	0.0566	0.0721	0.0834	4	0.0614	0.0786	0.1188
24	8	3	0.0480	0.0771	0.0854	4	0.0520	0.0840	0.1226
25	8	3	0.0417	0.0807	0.0866	4	0.0452	0.0880	0.1252
26	8	3	0.0370	0.0835	0.0873	4	0.0400	0.0910	0.1271
27	8	3	0.0701	0.1109	0.0961	4	0.0666	0.1209	0.1385
28	8	3	0.0746	0.1103	0.0967	4	0.0715	0.1203	0.1377
29	8	3	0.0796	0.1093	0.0974	4	0.0771	0.1192	0.1367
30	8	3	0.0741	0.1128	0.0973	4	0.0706	0.1230	0.1382
31	8	3	0.0992	0.1508	0.1222	4	0.1015	0.1646	0.1495
32	8	3	0.0910	0.1561	0.1203	4	0.0922	0.1704	0.1497
33	8	3	0.1100	0.1490	0.1259	4	0.1135	0.1624	0.1505
34	8	3	0.1153	0.1477	0.1291	4	0.1210	0.1613	0.1503

APPENDIX C BAYESIAN LINEAR REGRESSION

Regression seeks the relationship between an outcome variable (y) and one or several explanatory variables ($\mathbf{x}$), as expressed by the following equation:

$$y = f(\boldsymbol{x}; \boldsymbol{w}) + \epsilon$$

Equation C.1 Regression analysis

where $f(\mathbf{x}; \mathbf{w})$ = regression function, parameterized by $\mathbf{w}$, of explanatory variable(s) $\mathbf{x}$; ϵ = normally distributed random variable to account for the unexplained variance. Conventional regression analysis focuses on the determination of the regression function. It also assumes that (a) the function parameters $\mathbf{w}$ are deterministic and inferred from sufficient examples of $(\mathbf{x}, y)$ pairs called training data, and (b) the unexplained uncertainty ϵ is constant regardless of $\mathbf{x}$ values.

Uncertainty quantification, on the other hand, is concerned not only with the parameters of $f(\mathbf{x})$, but also and perhaps more importantly, models of the residual variable ϵ. Bayesian regression is an effective tool to overcome the limiting assumptions related to convention regression analysis. Instead of more complex models, linear regression is considered in this project to avoid overfitting. Accordingly, the regression function $f(\mathbf{x}; \mathbf{w})$ can be expressed as $f(\mathbf{x}; \mathbf{w}) = \mathbf{w}^{\mathrm{T}}\mathbf{x}$.

Bayesian linear regression considers a prior distribution for the function parameters. In practice, a multivariate normal distribution shown below is usually adopted as the prior distribution:

$$\boldsymbol{w} \sim \mathcal{N}(\mathbf{0}, \lambda^{-1}\boldsymbol{I})$$

Equation C.2 Prior distribution of parameters

where λ = precision of the parameter distribution; $\mathbf{I}$ = identity matrix. This prior gives rise to the so-called Bayesian ridge regression. The training data are used to obtain the posterior distribution of $\mathbf{w}$ based on Bayes' theorem. The marginal distribution of the outcome variable y, also known as the predictive distribution, is then derived using the law of total probability. Specifically, the predictive distribution of y given a specific $\mathbf{x}$ can be expressed as

$$y|\boldsymbol{x} \sim \mathcal{N}\left(\mu_y = \boldsymbol{w}^{*T}\boldsymbol{x}, \sigma_y^2 = 1/\alpha^* + \boldsymbol{x}^T(\alpha^*\boldsymbol{X}^T\boldsymbol{X} + \lambda^*\boldsymbol{I})^{-1}\boldsymbol{x}\right)$$

Equation C.3 Predictive distribution of the outcome variable

where μ_y and σ_y = the mean and STD of the outcome variable; $\mathbf{X}$ = matrix containing all explanatory variables used for training (each row $\mathbf{x}_i$ includes a dummy variable equal to 1 and the explanatory variables of a training instance); $\mathbf{y}$ = vector containing all the corresponding outcome variables (the ith entry is y_i associated with $\mathbf{x}_i$); $\mathbf{w}^*$ = posterior function parameters given training data $\mathbf{X}$ and $\mathbf{y}$; α^* = posterior precision of the residual variable ϵ; λ^* = posterior precision of the function parameters.

The variance term in Equation C.3 indicates that (a) the residual uncertainty reflects the limited amount of training data available to the regression via the inclusion of $\mathbf{X}$ and $\mathbf{y}$ in the variance, and (b) the variance is linked to the value of $\mathbf{x}$ and is higher for extrapolation than interpolation within

the range of explanatory variables used in training. In this project, Bayesian linear regression formulated above is implemented using scikit-learn[1], a Python package for machine learning.

[1] The U.S. Government does not endorse products or manufacturers. They are included for informational purposes only and are not intended to reflect a preference, approval, or endorsement of any one product or entity.

APPENDIX D UNCERTAINTY OF LIVE LOAD EFFECTS

Table D.1 lists the uncertainty parameters of the projected live load effect (i.e., midspan moment in k-ft/ft) and site-to-site variation. Two reference periods, 5 years and 75 years, are included in the results. Table D.2 provides the total uncertainty of the live load effect combining all compositions of live load uncertainty. Table D.3 provides the nominal live load effect and the back-calculated nominal resistance under different rating vehicles. The latter is obtained using the existing live load factors in the MBE (and 2.0 for FAST Act emergency vehicles as surrogate loads) for the factored live load effect. These nominal resistance values may change during the calibration of live load factors to ensure that the reliability index is always associated with RF = 1.

Table D.1 Projected live load effects (LL_{FR}) and site-to-site variation

Cul-vert	D (ft)	Reference period = 5 years			Reference period = 75 years		
		Projected mean	Projected COV	Site-to-site COV	Projected mean	Projected COV	Site-to-site COV
1	2	7.6550	0.0309	0.1692	8.1322	0.0269	0.1712
2	2	8.3436	0.0309	0.1686	8.8629	0.0269	0.1706
3	2	8.8758	0.0309	0.1678	9.4281	0.0269	0.1698
4	2	9.2882	0.0309	0.1682	9.8655	0.0268	0.1702
5	2	10.9686	0.0308	0.1671	11.6491	0.0268	0.1690
6	2	11.6153	0.0308	0.1677	12.3358	0.0268	0.1697
7	2	11.2762	0.0308	0.1674	11.9756	0.0268	0.1694
8	2	11.7005	0.0308	0.1677	12.4262	0.0268	0.1697
9	2	13.9113	0.0308	0.1674	14.7741	0.0268	0.1694
10	2	14.5204	0.0308	0.1674	15.4202	0.0268	0.1694
11	2	13.0220	0.0308	0.1674	13.8299	0.0268	0.1694
12	2	13.4409	0.0308	0.1667	14.2740	0.0268	0.1686
13	2	14.5797	0.0308	0.1673	15.4836	0.0268	0.1692
14	2	15.4189	0.0308	0.1665	16.3748	0.0268	0.1685
15	2	14.2938	0.0308	0.1675	15.1800	0.0268	0.1695
16	2	14.8546	0.0309	0.1672	15.7774	0.0268	0.1691
1	4	4.8286	0.0308	0.1679	5.1282	0.0268	0.1699
2	4	5.2936	0.0309	0.1675	5.6225	0.0268	0.1695
3	4	5.6389	0.0308	0.1681	5.9890	0.0268	0.1701
4	4	5.9145	0.0309	0.1677	6.2819	0.0268	0.1697
5	4	7.2780	0.0308	0.1675	7.7297	0.0268	0.1695
6	4	7.7156	0.0308	0.1678	8.1942	0.0268	0.1699
7	4	7.5057	0.0308	0.1675	7.9711	0.0268	0.1695
8	4	7.8004	0.0308	0.1683	8.2843	0.0268	0.1703
9	4	9.2117	0.0308	0.1670	9.7831	0.0268	0.1689
10	4	9.6356	0.0308	0.1663	10.2331	0.0268	0.1682
11	4	8.9466	0.0308	0.1679	9.5019	0.0268	0.1699
12	4	9.2522	0.0308	0.1672	9.8266	0.0268	0.1692
13	4	10.1411	0.0308	0.1668	10.7702	0.0268	0.1687
14	4	10.7512	0.0308	0.1671	11.4185	0.0268	0.1691
15	4	9.9838	0.0308	0.1669	10.6025	0.0268	0.1689

Cul-vert	D (ft)	Reference period = 5 years			Reference period = 75 years		
		Projected mean	Projected COV	Site-to-site COV	Projected mean	Projected COV	Site-to-site COV
16	4	10.3852	0.0308	0.1670	11.0294	0.0268	0.1690
1	6	3.3660	0.0308	0.1676	3.5749	0.0268	0.1696
2	6	3.6927	0.0308	0.1673	3.9220	0.0268	0.1693
3	6	3.9398	0.0309	0.1674	4.1847	0.0268	0.1694
4	6	4.1313	0.0309	0.1670	4.3880	0.0268	0.1689
5	6	5.2947	0.0308	0.1677	5.6230	0.0268	0.1697
6	6	5.6332	0.0308	0.1664	5.9830	0.0268	0.1683
7	6	5.4932	0.0308	0.1667	5.8339	0.0268	0.1686
8	6	5.7140	0.0308	0.1667	6.0685	0.0268	0.1686
9	6	6.9079	0.0308	0.1677	7.3367	0.0268	0.1697
10	6	7.2413	0.0308	0.1677	7.6908	0.0268	0.1697
11	6	6.7018	0.0308	0.1664	7.1172	0.0268	0.1684
12	6	6.9507	0.0308	0.1671	7.3822	0.0268	0.1690
13	6	7.6643	0.0308	0.1679	8.1401	0.0268	0.1700
14	6	8.1422	0.0308	0.1670	8.6470	0.0268	0.1690
15	6	7.5995	0.0308	0.1671	8.0708	0.0268	0.1691
16	6	7.9261	0.0308	0.1676	8.4182	0.0268	0.1696
1	8	2.4440	0.0308	0.1678	2.5958	0.0268	0.1698
2	8	2.6816	0.0308	0.1683	2.8482	0.0268	0.1704
3	8	2.8602	0.0309	0.1676	3.0379	0.0268	0.1695
4	8	2.9986	0.0308	0.1680	3.1848	0.0268	0.1700
5	8	3.9028	0.0308	0.1668	4.1453	0.0268	0.1688
6	8	4.1471	0.0308	0.1677	4.4047	0.0268	0.1697
7	8	4.0465	0.0308	0.1671	4.2974	0.0268	0.1691
8	8	4.2133	0.0308	0.1672	4.4750	0.0268	0.1692
9	8	5.2525	0.0308	0.1669	5.5784	0.0268	0.1689
10	8	5.5108	0.0308	0.1668	5.8528	0.0268	0.1687
11	8	5.1061	0.0308	0.1668	5.4227	0.0268	0.1687
12	8	5.2968	0.0308	0.1670	5.6255	0.0268	0.1689
13	8	5.9339	0.0308	0.1680	6.3019	0.0268	0.1700
14	8	6.3233	0.0308	0.1669	6.7153	0.0268	0.1689
15	8	5.8698	0.0308	0.1670	6.2341	0.0268	0.1690
16	8	6.1245	0.0308	0.1670	6.5043	0.0268	0.1690
17	2	3.5952	0.0336	0.1813	3.8386	0.0290	0.1840
18	2	3.9052	0.0335	0.1808	4.1691	0.0290	0.1834
19	2	4.0938	0.0335	0.1814	4.3705	0.0290	0.1840
20	2	5.7771	0.0313	0.1725	6.1418	0.0272	0.1747
21	2	5.8959	0.0313	0.1719	6.2680	0.0272	0.1741
22	2	6.1358	0.0313	0.1722	6.5223	0.0272	0.1744
23	2	6.9782	0.0310	0.1698	7.4143	0.0270	0.1719
24	2	7.4209	0.0310	0.1693	7.8837	0.0269	0.1714
25	2	7.7552	0.0310	0.1695	8.2387	0.0269	0.1716
26	2	8.0273	0.0310	0.1690	8.5277	0.0269	0.1711

Cul-vert	D (ft)	Reference period = 5 years			Reference period = 75 years		
		Projected mean	Projected COV	Site-to-site COV	Projected mean	Projected COV	Site-to-site COV
27	2	9.7683	0.0308	0.1682	10.3751	0.0268	0.1702
28	2	9.5833	0.0309	0.1684	10.1795	0.0268	0.1704
29	2	9.4993	0.0308	0.1677	10.0893	0.0268	0.1697
30	2	9.7732	0.0308	0.1680	10.3801	0.0268	0.1700
31	2	12.4886	0.0308	0.1675	13.2641	0.0268	0.1694
32	2	12.8857	0.0308	0.1677	13.6854	0.0268	0.1697
33	2	11.7872	0.0308	0.1668	12.5190	0.0268	0.1687
34	2	11.4306	0.0308	0.1687	12.1402	0.0268	0.1707
17	4	1.8862	0.0316	0.1744	2.0065	0.0275	0.1768
18	4	2.0685	0.0316	0.1738	2.2002	0.0274	0.1761
19	4	2.1769	0.0316	0.1745	2.3157	0.0274	0.1768
20	4	3.4643	0.0310	0.1704	3.6808	0.0270	0.1725
21	4	3.4715	0.0310	0.1697	3.6883	0.0269	0.1718
22	4	3.6072	0.0311	0.1698	3.8329	0.0270	0.1719
23	4	4.3727	0.0308	0.1681	4.6442	0.0268	0.1701
24	4	4.6700	0.0308	0.1676	4.9600	0.0268	0.1696
25	4	4.8885	0.0308	0.1685	5.1920	0.0268	0.1705
26	4	5.0561	0.0308	0.1676	5.3698	0.0268	0.1696
27	4	6.4038	0.0308	0.1669	6.8013	0.0268	0.1688
28	4	6.3350	0.0308	0.1666	6.7278	0.0268	0.1685
29	4	6.2901	0.0308	0.1676	6.6804	0.0268	0.1696
30	4	6.4838	0.0308	0.1671	6.8864	0.0268	0.1690
31	4	8.1582	0.0308	0.1675	8.6639	0.0268	0.1695
32	4	8.4345	0.0308	0.1676	8.9580	0.0268	0.1696
33	4	8.0236	0.0308	0.1677	8.5217	0.0268	0.1697
34	4	7.7709	0.0308	0.1670	8.2530	0.0268	0.1689
17	6	1.2501	0.0310	0.1703	1.3281	0.0269	0.1724
18	6	1.3722	0.0310	0.1693	1.4578	0.0269	0.1713
19	6	1.4418	0.0310	0.1699	1.5317	0.0269	0.1720
20	6	2.3588	0.0309	0.1698	2.5057	0.0269	0.1719
21	6	2.3618	0.0310	0.1700	2.5092	0.0269	0.1721
22	6	2.4502	0.0310	0.1701	2.6029	0.0269	0.1722
23	6	3.0316	0.0308	0.1679	3.2197	0.0268	0.1699
24	6	3.2432	0.0308	0.1682	3.4446	0.0268	0.1702
25	6	3.4009	0.0309	0.1683	3.6123	0.0268	0.1703
26	6	3.5162	0.0308	0.1682	3.7345	0.0268	0.1702
27	6	4.6113	0.0308	0.1678	4.8975	0.0268	0.1698
28	6	4.5901	0.0308	0.1677	4.8751	0.0268	0.1697
29	6	4.5349	0.0308	0.1676	4.8161	0.0268	0.1696
30	6	4.6796	0.0308	0.1672	4.9699	0.0268	0.1691
31	6	6.0606	0.0308	0.1671	6.4362	0.0268	0.1690
32	6	6.2749	0.0308	0.1670	6.6642	0.0268	0.1689
33	6	5.9691	0.0308	0.1670	6.3394	0.0268	0.1690

Cul-vert	D (ft)	Reference period = 5 years			Reference period = 75 years		
		Projected mean	Projected COV	Site-to-site COV	Projected mean	Projected COV	Site-to-site COV
34	6	5.8208	0.0308	0.1672	6.1818	0.0268	0.1692
17	8	0.8992	0.0308	0.1678	0.9551	0.0268	0.1698
18	8	0.9865	0.0308	0.1676	1.0478	0.0268	0.1695
19	8	1.0368	0.0308	0.1680	1.1012	0.0268	0.1700
20	8	1.7036	0.0309	0.1681	1.8095	0.0268	0.1700
21	8	1.7045	0.0309	0.1674	1.8104	0.0268	0.1693
22	8	1.7689	0.0309	0.1682	1.8788	0.0268	0.1702
23	8	2.1996	0.0308	0.1670	2.3361	0.0268	0.1689
24	8	2.3547	0.0309	0.1675	2.5011	0.0268	0.1694
25	8	2.4641	0.0308	0.1684	2.6171	0.0268	0.1704
26	8	2.5489	0.0308	0.1674	2.7072	0.0268	0.1693
27	8	3.3798	0.0308	0.1674	3.5893	0.0268	0.1694
28	8	3.3686	0.0308	0.1673	3.5776	0.0268	0.1693
29	8	3.3369	0.0308	0.1672	3.5440	0.0268	0.1691
30	8	3.4402	0.0308	0.1678	3.6536	0.0268	0.1698
31	8	4.5635	0.0308	0.1670	4.8464	0.0268	0.1689
32	8	4.7224	0.0308	0.1667	5.0152	0.0268	0.1686
33	8	4.5046	0.0308	0.1671	4.7840	0.0268	0.1691
34	8	4.4729	0.0308	0.1677	4.7505	0.0268	0.1697

Table D.2 Total uncertainty of live load effect (*LL*)

Culvert	D (ft)	Reference period = 5 years		Reference period = 75 years	
		LL mean (k-ft/ft)	LL COV	LL mean (k-ft/ft)	LL COV
1	2	6.3625	0.2407	6.7591	0.2402
2	2	6.9348	0.2407	7.3665	0.2402
3	2	7.3772	0.2407	7.8362	0.2402
4	2	7.7199	0.2407	8.1998	0.2402
5	2	8.3385	0.2381	8.8558	0.2376
6	2	8.8301	0.2381	9.3778	0.2376
7	2	8.5723	0.2381	9.1040	0.2376
8	2	8.8949	0.2381	9.4466	0.2376
9	2	9.7448	0.2362	10.3492	0.2357
10	2	10.1715	0.2362	10.8018	0.2357
11	2	9.1219	0.2362	9.6878	0.2357
12	2	9.4153	0.2362	9.9989	0.2357
13	2	9.4698	0.2346	10.0569	0.2341
14	2	10.0149	0.2346	10.6358	0.2341
15	2	9.2841	0.2346	9.8598	0.2341
16	2	9.6484	0.2346	10.2478	0.2341
1	4	3.8780	0.2334	4.1186	0.2329
2	4	4.2515	0.2334	4.5156	0.2329
3	4	4.5288	0.2334	4.8100	0.2329
4	4	4.7501	0.2334	5.0452	0.2329

Culvert	D (ft)	Reference period = 5 years		Reference period = 75 years	
		LL mean (k-ft/ft)	LL COV	LL mean (k-ft/ft)	LL COV
5	4	5.3464	0.2308	5.6782	0.2303
6	4	5.6678	0.2308	6.0193	0.2303
7	4	5.5136	0.2308	5.8555	0.2303
8	4	5.7301	0.2308	6.0856	0.2303
9	4	6.2353	0.2288	6.6220	0.2283
10	4	6.5222	0.2288	6.9266	0.2283
11	4	6.0558	0.2288	6.4317	0.2283
12	4	6.2626	0.2288	6.6515	0.2283
13	4	6.3648	0.2272	6.7597	0.2267
14	4	6.7478	0.2272	7.1666	0.2267
15	4	6.2661	0.2272	6.6544	0.2267
16	4	6.5180	0.2272	6.9224	0.2267
1	6	2.6091	0.2285	2.7710	0.2280
2	6	2.8623	0.2285	3.0401	0.2280
3	6	3.0539	0.2285	3.2437	0.2280
4	6	3.2023	0.2285	3.4013	0.2280
5	6	3.7538	0.2258	3.9865	0.2253
6	6	3.9937	0.2258	4.2417	0.2253
7	6	3.8945	0.2258	4.1360	0.2253
8	6	4.0510	0.2258	4.3023	0.2253
9	6	4.5127	0.2238	4.7928	0.2232
10	6	4.7305	0.2238	5.0242	0.2232
11	6	4.3781	0.2237	4.6494	0.2232
12	6	4.5407	0.2238	4.8226	0.2232
13	6	4.6425	0.2221	4.9307	0.2216
14	6	4.9320	0.2221	5.2378	0.2216
15	6	4.6033	0.2221	4.8888	0.2216
16	6	4.8011	0.2221	5.0992	0.2216
1	8	1.8259	0.2266	1.9393	0.2261
2	8	2.0035	0.2266	2.1279	0.2261
3	8	2.1369	0.2266	2.2696	0.2261
4	8	2.2403	0.2266	2.3794	0.2261
5	8	2.6670	0.2240	2.8326	0.2234
6	8	2.8339	0.2240	3.0099	0.2234
7	8	2.7651	0.2239	2.9366	0.2234
8	8	2.8791	0.2240	3.0579	0.2234
9	8	3.3073	0.2219	3.5125	0.2214
10	8	3.4699	0.2219	3.6853	0.2214
11	8	3.2151	0.2219	3.4144	0.2213
12	8	3.3352	0.2219	3.5421	0.2214
13	8	3.4644	0.2202	3.6793	0.2197
14	8	3.6918	0.2202	3.9207	0.2197
15	8	3.4271	0.2202	3.6397	0.2197
16	8	3.5757	0.2202	3.7974	0.2197

Culvert	D (ft)	Reference period = 5 years		Reference period = 75 years	
		LL mean (k-ft/ft)	LL COV	LL mean (k-ft/ft)	LL COV
17	2	3.6760	0.2489	3.9249	0.2483
18	2	3.9930	0.2489	4.2628	0.2483
19	2	4.1859	0.2489	4.4688	0.2483
20	2	5.2968	0.2441	5.6311	0.2436
21	2	5.4056	0.2441	5.7468	0.2436
22	2	5.6256	0.2440	5.9799	0.2436
23	2	5.8000	0.2407	6.1624	0.2402
24	2	6.1679	0.2407	6.5526	0.2402
25	2	6.4458	0.2407	6.8477	0.2402
26	2	6.6719	0.2407	7.0879	0.2402
27	2	7.4260	0.2381	7.8873	0.2376
28	2	7.2854	0.2381	7.7386	0.2376
29	2	7.2215	0.2381	7.6700	0.2376
30	2	7.4297	0.2381	7.8911	0.2376
31	2	8.7482	0.2362	9.2914	0.2357
32	2	9.0264	0.2362	9.5866	0.2357
33	2	8.2569	0.2362	8.7695	0.2357
34	2	8.0071	0.2362	8.5042	0.2357
17	4	1.8636	0.2416	1.9825	0.2411
18	4	2.0437	0.2416	2.1738	0.2411
19	4	2.1509	0.2416	2.2880	0.2411
20	4	3.0692	0.2369	3.2610	0.2364
21	4	3.0755	0.2369	3.2677	0.2364
22	4	3.1958	0.2369	3.3958	0.2364
23	4	3.5119	0.2334	3.7300	0.2329
24	4	3.7507	0.2334	3.9836	0.2329
25	4	3.9261	0.2334	4.1699	0.2329
26	4	4.0607	0.2334	4.3127	0.2329
27	4	4.7041	0.2308	4.9962	0.2303
28	4	4.6536	0.2308	4.9422	0.2303
29	4	4.6207	0.2308	4.9074	0.2303
30	4	4.7630	0.2308	5.0587	0.2303
31	4	5.5221	0.2288	5.8645	0.2283
32	4	5.7092	0.2288	6.0635	0.2283
33	4	5.4311	0.2288	5.7682	0.2283
34	4	5.2600	0.2288	5.5863	0.2283
17	6	1.1920	0.2368	1.2664	0.2363
18	6	1.3084	0.2368	1.3901	0.2363
19	6	1.3748	0.2368	1.4605	0.2363
20	6	2.0168	0.2320	2.1425	0.2315
21	6	2.0194	0.2320	2.1454	0.2315
22	6	2.0950	0.2320	2.2256	0.2315
23	6	2.3498	0.2285	2.4957	0.2280
24	6	2.5139	0.2285	2.6700	0.2280

Culvert	D (ft)	Reference period = 5 years		Reference period = 75 years	
		LL mean (k-ft/ft)	LL COV	LL mean (k-ft/ft)	LL COV
25	6	2.6361	0.2285	2.8000	0.2280
26	6	2.7255	0.2285	2.8947	0.2280
27	6	3.2692	0.2258	3.4722	0.2253
28	6	3.2542	0.2258	3.4562	0.2253
29	6	3.2151	0.2258	3.4144	0.2253
30	6	3.3177	0.2258	3.5235	0.2253
31	6	3.9592	0.2237	4.2046	0.2232
32	6	4.0992	0.2237	4.3535	0.2232
33	6	3.8995	0.2238	4.1414	0.2232
34	6	3.8026	0.2237	4.0384	0.2232
17	8	0.8265	0.2350	0.8778	0.2345
18	8	0.9067	0.2350	0.9630	0.2345
19	8	0.9529	0.2350	1.0121	0.2345
20	8	1.4040	0.2302	1.4913	0.2297
21	8	1.4047	0.2302	1.4920	0.2297
22	8	1.4578	0.2302	1.5484	0.2297
23	8	1.6433	0.2266	1.7453	0.2261
24	8	1.7592	0.2266	1.8686	0.2261
25	8	1.8409	0.2266	1.9553	0.2261
26	8	1.9043	0.2266	2.0226	0.2261
27	8	2.3095	0.2239	2.4527	0.2234
28	8	2.3019	0.2240	2.4447	0.2234
29	8	2.2802	0.2240	2.4218	0.2234
30	8	2.3508	0.2239	2.4966	0.2234
31	8	2.8735	0.2219	3.0516	0.2213
32	8	2.9735	0.2219	3.1579	0.2213
33	8	2.8364	0.2219	3.0123	0.2213
34	8	2.8164	0.2219	2.9912	0.2214

Table D.3 Nominal live load effect and resistance

Culvert	D (ft)	Design Load	LL Design (k-ft/ft)	R (inv) Design (k-ft/ft)	R (op) Design (k-ft/ft)	Legal Load	LL Legal (k-ft/ft)	R Legal (k-ft/ft)	FAST Act Load	LL Fast Act (k-ft/ft)	RFast Act (k-ft/ft)
1	2	Tandem	7.991	19.727	16.175	NRL	4.697	14.626	EV3	8.258	20.285
2	2	Tandem	8.727	21.287	17.408	NRL	5.133	15.726	EV3	9.018	21.921
3	2	Tandem	9.289	22.162	18.033	NRL	5.465	16.243	EV3	9.599	22.887
4	2	Tandem	9.732	22.416	18.090	NRL	5.724	16.213	EV3	10.056	23.256
5	2	Tandem	11.525	29.104	23.982	NRL	7.132	22.543	EV3	11.828	29.681
6	2	Tandem	12.209	30.307	24.881	NRL	7.562	23.372	EV3	12.525	30.961
7	2	Tandem	11.847	28.776	23.511	NRL	7.389	22.159	EV3	12.242	29.650
8	2	Tandem	12.297	28.759	23.293	NRL	7.675	21.904	EV3	12.707	29.777
9	2	Tandem	14.631	37.893	31.390	NRL	8.982	29.404	EV3	14.488	37.475
10	2	Tandem	15.286	38.809	32.015	NRL	9.406	29.989	EV3	15.135	38.447
11	2	Tandem	13.693	34.354	28.268	NRL	8.861	27.419	EV3	14.147	35.249
12	2	Tandem	14.144	34.169	27.883	NRL	9.171	27.047	EV3	14.614	35.229
13	2	Tandem	15.343	41.600	34.781	NRL	10.087	34.182	EV3	15.641	41.873
14	2	Tandem	16.229	43.627	36.414	NRL	10.723	35.900	EV3	16.537	43.938

Culvert	D (ft)	Design Load	LL Design (k-ft/ft)	R (inv) Design (k-ft/ft)	R (op) Design (k-ft/ft)	Legal Load	LL Legal (k-ft/ft)	R Legal (k-ft/ft)	FAST Act Load	LL Fast Act (k-ft/ft)	RFast Act (k-ft/ft)
15	2	Tandem	15.040	40.006	33.322	NRL	9.920	32.808	EV3	15.541	40.768
16	2	Tandem	15.610	40.697	33.759	NRL	10.336	33.313	EV3	16.130	41.571
1	4	Tandem	4.736	16.559	14.454	T3	2.684	13.316	EV3	4.895	16.405
2	4	Tandem	5.187	17.783	15.478	T3	2.940	14.230	EV3	5.362	17.650
3	4	Tandem	5.529	18.318	15.861	T3	3.134	14.531	EV3	5.715	18.240
4	4	Tandem	5.798	18.215	15.638	T3	3.286	14.244	EV3	5.993	18.233
5	4	Tandem	7.145	25.528	22.352	T3	4.035	20.600	EV3	7.358	25.185
6	4	Tandem	7.580	26.408	23.039	T3	4.279	21.179	EV3	7.804	26.109
7	4	Tandem	7.374	24.913	21.636	T3	4.182	19.868	EV3	7.625	24.768
8	4	Tandem	7.661	24.551	21.146	T3	4.344	19.308	EV3	7.922	24.533
9	4	Tandem	9.052	33.658	29.635	T3	5.098	27.386	EV3	9.297	33.044
10	4	Tandem	9.469	34.255	30.046	T3	5.332	27.692	EV3	9.724	33.705
11	4	Tandem	8.785	30.960	27.055	T3	4.978	24.940	EV3	9.078	30.646
12	4	Tandem	9.084	30.474	26.437	T3	5.148	24.250	EV3	9.387	30.303
13	4	Tandem	9.964	39.014	34.585	SU4	5.664	32.226	EV3	10.219	38.113
14	4	Tandem	10.561	40.885	36.191	SU4	6.035	33.759	EV3	10.829	39.972
15	4	Tandem	9.818	37.447	33.084	SU4	5.600	30.802	EV3	10.074	36.669
16	4	Tandem	10.207	37.953	33.417	SU4	5.844	31.092	EV3	10.472	37.239
1	6	Tandem	3.065	16.679	15.317	T3	1.737	14.579	EV3	3.167	15.982
2	6	Tandem	3.362	17.838	16.344	T3	1.905	15.534	EV3	3.474	17.118
3	6	Tandem	3.585	18.245	16.652	T3	2.032	15.789	EV3	3.705	17.556
4	6	Tandem	3.760	17.953	16.282	T3	2.131	15.377	EV3	3.885	17.349
5	6	Tandem	4.832	26.250	24.102	T3	2.739	22.940	EV3	4.994	25.157
6	6	Tandem	5.135	27.055	24.773	T3	2.911	23.538	EV3	5.308	25.978
7	6	Tandem	5.013	25.447	23.219	T3	2.838	22.006	EV3	5.175	24.479
8	6	Tandem	5.215	24.900	22.583	T3	2.952	21.320	EV3	5.383	24.050
9	6	Tandem	6.303	35.254	32.453	T3	3.562	30.913	EV3	6.495	33.688
10	6	Tandem	6.607	35.790	32.853	T3	3.733	31.239	EV3	6.808	34.264
11	6	Tandem	6.123	32.246	29.525	T3	3.470	28.051	EV3	6.327	30.960
12	6	Tandem	6.343	31.612	28.793	T3	3.594	27.266	EV3	6.554	30.460
13	6	Tandem	6.994	41.451	38.343	SU4	3.980	36.696	EV3	7.195	39.457
14	6	Tandem	7.437	43.449	40.144	SU4	4.247	38.428	EV3	7.649	41.388
15	6	Tandem	6.940	39.777	36.693	SU4	3.941	35.042	EV3	7.140	37.935
16	6	Tandem	7.232	40.278	37.063	SU4	4.119	35.368	EV3	7.440	38.473
1	8	Tandem	2.056	18.292	17.378	T3	1.165	16.883	EV3	2.125	17.114
2	8	Tandem	2.255	19.517	18.514	T3	1.278	17.971	EV3	2.331	18.279
3	8	Tandem	2.405	19.899	18.830	T3	1.363	18.251	EV3	2.486	18.671
4	8	Tandem	2.523	19.502	18.381	T3	1.429	17.773	EV3	2.607	18.350
5	8	Tandem	3.286	28.745	27.284	T3	1.862	26.493	EV3	3.395	26.911
6	8	Tandem	3.492	29.561	28.009	T3	1.979	27.168	EV3	3.608	27.710
7	8	Tandem	3.411	27.745	26.229	T3	1.933	25.408	EV3	3.524	26.050
8	8	Tandem	3.548	27.067	25.490	T3	2.010	24.636	EV3	3.666	25.483
9	8	Tandem	4.428	38.878	36.910	T3	2.509	35.844	EV3	4.575	36.392
10	8	Tandem	4.646	39.421	37.356	T3	2.633	36.237	EV3	4.801	36.950
11	8	Tandem	4.308	35.492	33.578	T3	2.440	32.538	EV3	4.449	33.303
12	8	Tandem	4.467	34.758	32.773	T3	2.530	31.694	EV3	4.613	32.692
13	8	Tandem	5.006	46.138	43.913	T3	2.831	42.696	EV3	5.162	43.089
14	8	Tandem	5.336	48.369	45.997	T3	3.018	44.699	EV3	5.503	45.199
15	8	Tandem	4.950	44.165	41.965	T3	2.799	40.762	EV3	5.105	41.296
16	8	Tandem	5.167	44.718	42.422	T3	2.922	41.165	EV3	5.329	41.862
17	2	HS20	4.135	9.190	7.352	SU4	1.942	5.466	EV2	3.560	8.154
18	2	HS20	4.496	9.894	7.896	SU4	2.115	5.853	EV2	3.864	8.766
19	2	HS20	4.713	10.245	8.150	SU4	2.214	6.000	EV2	4.046	9.066

Culvert	D (ft)	Design Load	LL Design (k-ft/ft)	R (inv) Design (k-ft/ft)	R (op) Design (k-ft/ft)	Legal Load	LL Legal (k-ft/ft)	R Legal (k-ft/ft)	FAST Act Load	LL Fast Act (k-ft/ft)	RFast Act (k-ft/ft)
20	2	HS20	6.292	14.320	11.523	SU4	3.455	9.763	EV3	6.261	14.399
21	2	HS20	6.313	14.293	11.487	SU5	3.451	9.685	EV3	6.242	14.298
22	2	HS20	6.526	14.579	11.678	SU5	3.590	9.867	EV3	6.505	14.711
23	2	Tandem	7.263	17.162	13.934	SU5	4.240	12.463	EV3	7.511	17.758
24	2	Tandem	7.739	18.101	14.661	SU5	4.524	13.107	EV3	8.004	18.757
25	2	Tandem	8.092	18.704	15.107	SU5	4.735	13.491	EV3	8.368	19.407
26	2	Tandem	8.381	19.081	15.356	SU5	4.899	13.672	EV3	8.666	19.838
27	2	Tandem	10.250	24.488	19.933	SU6	6.140	18.203	EV3	10.433	24.967
28	2	Tandem	10.039	23.961	19.500	SU6	6.140	18.085	EV3	10.382	24.761
29	2	Tandem	9.961	23.633	19.206	SU6	5.987	17.568	EV3	10.298	24.433
30	2	Tandem	10.252	23.956	19.399	SU6	6.166	17.723	EV3	10.598	24.814
31	2	Tandem	13.123	32.077	26.244	SU6	7.857	24.020	EV3	12.947	31.798
32	2	Tandem	13.546	32.765	26.744	SU6	8.117	24.462	EV3	13.356	32.494
33	2	Tandem	12.386	30.204	24.699	SU6	7.786	23.421	EV3	12.773	31.054
34	2	Tandem	12.009	29.453	24.116	SU6	7.650	23.101	EV3	12.630	30.751
17	4	HS20	1.932	5.785	4.926	T3	1.013	4.278	EV3	1.846	5.518
18	4	HS20	2.120	6.170	5.228	T3	1.111	4.517	EV3	2.026	5.895
19	4	HS20	2.230	6.298	5.306	T3	1.167	4.555	EV3	2.129	6.022
20	4	Tandem	3.366	10.159	8.663	T3	1.910	7.859	EV3	3.484	10.220
21	4	Tandem	3.374	10.092	8.592	T3	1.913	7.783	EV3	3.488	10.156
22	4	Tandem	3.501	10.187	8.632	T3	1.985	7.792	EV3	3.620	10.283
23	4	Tandem	4.284	13.566	11.662	T3	2.430	10.636	EV3	4.431	13.575
24	4	Tandem	4.576	14.191	12.157	T3	2.596	11.061	EV3	4.733	14.230
25	4	Tandem	4.791	14.530	12.401	T3	2.718	11.254	EV3	4.956	14.605
26	4	Tandem	4.958	14.648	12.444	T3	2.813	11.258	EV3	5.129	14.765
27	4	Tandem	6.283	19.968	17.175	T3	3.545	15.627	EV3	6.464	19.903
28	4	Tandem	6.221	19.707	16.943	T3	3.528	15.452	EV3	6.434	19.718
29	4	Tandem	6.174	19.404	16.660	T3	3.500	15.176	EV3	6.382	19.422
30	4	Tandem	6.361	19.507	16.680	T3	3.606	15.151	EV3	6.576	19.575
31	4	Tandem	8.018	26.477	22.913	T3	4.513	20.915	EV3	8.229	26.256
32	4	Tandem	8.283	26.870	23.189	T3	4.660	21.120	EV3	8.498	26.684
33	4	Tandem	7.877	25.689	22.188	T3	4.462	20.290	EV3	8.137	25.611
34	4	Tandem	7.632	25.161	21.769	T3	4.294	19.864	EV3	7.831	24.950
17	6	Tandem	1.130	5.152	4.649	T3	0.641	4.378	EV3	1.169	4.995
18	6	Tandem	1.241	5.406	4.855	T3	0.703	4.557	EV3	1.283	5.260
19	6	Tandem	1.304	5.428	4.848	T3	0.740	4.535	EV3	1.349	5.300
20	6	Tandem	2.137	9.365	8.415	T3	1.209	7.897	EV3	2.205	9.099
21	6	Tandem	2.137	9.269	8.320	T3	1.212	7.807	EV3	2.210	9.022
22	6	Tandem	2.218	9.252	8.266	T3	1.258	7.734	EV3	2.293	9.033
23	6	Tandem	2.760	12.877	11.650	T3	1.563	10.983	EV3	2.850	12.459
24	6	Tandem	2.952	13.352	12.040	T3	1.671	11.325	EV3	3.047	12.945
25	6	Tandem	3.093	13.553	12.179	T3	1.750	11.429	EV3	3.192	13.169
26	6	Tandem	3.201	13.536	12.114	T3	1.811	11.337	EV3	3.302	13.186
27	6	Tandem	4.203	19.212	17.343	T3	2.386	16.340	EV3	4.351	18.636
28	6	Tandem	4.184	19.013	17.153	T3	2.366	16.134	EV3	4.314	18.417
29	6	Tandem	4.138	18.675	16.836	T3	2.346	15.841	EV3	4.277	18.120
30	6	Tandem	4.268	18.649	16.752	T3	2.419	15.726	EV3	4.412	18.138
31	6	Tandem	5.535	26.087	23.627	T3	3.127	22.273	EV3	5.702	25.195
32	6	Tandem	5.727	26.351	23.806	T3	3.234	22.403	EV3	5.898	25.489
33	6	Tandem	5.448	25.332	22.910	T3	3.087	21.599	EV3	5.630	24.524
34	6	Tandem	5.313	24.833	22.471	T3	3.015	21.201	EV3	5.498	24.047
17	8	Tandem	0.756	5.399	5.062	T3	0.429	4.881	EV3	0.782	5.099
18	8	Tandem	0.830	5.604	5.235	T3	0.470	5.036	EV3	0.858	5.307

Culvert	D (ft)	Design Load	LL Design (k-ft/ft)	R (inv) Design (k-ft/ft)	R (op) Design (k-ft/ft)	Legal Load	LL Legal (k-ft/ft)	R Legal (k-ft/ft)	FAST Act Load	LL Fast Act (k-ft/ft)	RFast Act (k-ft/ft)
19	8	Tandem	0.872	5.570	5.183	T3	0.494	4.974	EV3	0.902	5.291
20	8	Tandem	1.432	9.657	9.020	T3	0.810	8.673	EV3	1.477	9.140
21	8	Tandem	1.433	9.549	8.912	T3	0.813	8.568	EV3	1.482	9.050
22	8	Tandem	1.487	9.458	8.797	T3	0.843	8.441	EV3	1.538	8.986
23	8	Tandem	1.851	13.458	12.635	T3	1.049	12.191	EV3	1.913	12.700
24	8	Tandem	1.979	13.857	12.978	T3	1.122	12.503	EV3	2.046	13.101
25	8	Tandem	2.072	13.977	13.056	T3	1.175	12.559	EV3	2.143	13.239
26	8	Tandem	2.144	13.870	12.917	T3	1.216	12.403	EV3	2.218	13.166
27	8	Tandem	2.849	19.961	18.695	T3	1.616	18.013	EV3	2.947	18.874
28	8	Tandem	2.837	19.753	18.492	T3	1.606	17.805	EV3	2.928	18.669
29	8	Tandem	2.810	19.416	18.167	T3	1.593	17.492	EV3	2.904	18.366
30	8	Tandem	2.899	19.296	18.008	T3	1.643	17.311	EV3	2.996	18.286
31	8	Tandem	3.850	27.361	25.650	T3	2.181	24.721	EV3	3.977	25.841
32	8	Tandem	3.984	27.527	25.757	T3	2.257	24.796	EV3	4.115	26.033
33	8	Tandem	3.799	26.600	24.912	T3	2.152	23.995	EV3	3.924	25.139
34	8	Tandem	3.770	26.065	24.389	T3	2.133	23.475	EV3	3.890	24.641

APPENDIX E RESULTS OF RELIABILITY ANALYSIS AND CALIBRATION

Results of reliability analysis and calibration are presented in Table E.1 to Table E.3 for operating rating, AASHTO legal loads, and FAST Act emergency vehicles as surrogate loads, respectively. For calibration, both the calibrated live load factor (with and without scaling) and the associated reliability index are reported.

Table E.1 Reliability index and calibrated reliability index for operating rating

Cul-vert	D (ft)	Reliability (with γ_{LL}=1.35)	Calibrated factor γ_{LL}	Calibrated reliability	Scaled factor γ_{LL}	Scaled reliability
1	2	2.9600	1.9038	3.9446	1.1423	2.4960
2	2	2.9498	1.9038	3.9402	1.1423	2.4822
3	2	2.9222	1.9038	3.9233	1.1423	2.4476
4	2	2.8783	1.9038	3.8966	1.1423	2.3924
5	2	3.2807	1.7333	3.9922	1.0400	2.5662
6	2	3.2600	1.7333	3.9776	1.0400	2.5371
7	2	3.2301	1.7333	3.9555	1.0400	2.4963
8	2	3.1810	1.7333	3.9203	1.0400	2.4278
9	2	3.5559	1.5898	4.0180	0.9539	2.6185
10	2	3.5338	1.5898	4.0006	0.9539	2.5833
11	2	3.5113	1.5898	3.9814	0.9539	2.5519
12	2	3.4644	1.5898	3.9438	0.9539	2.4788
13	2	3.8329	1.4674	4.0639	0.8804	2.7136
14	2	3.8225	1.4674	4.0546	0.8804	2.6962
15	2	3.8091	1.4674	4.0425	0.8804	2.6744
16	2	3.7807	1.4674	4.0165	0.8804	2.6296
1	4	3.2467	1.1166	4.1408	1.0325	2.6429
2	4	3.2186	1.7209	3.8412	1.0325	2.6064
3	4	3.1746	1.7209	3.8196	1.0325	2.5473
4	4	3.0991	1.7209	3.7871	1.0325	2.4472
5	4	3.5054	1.7209	3.7301	0.9286	2.6778
6	4	3.4757	1.5477	3.8370	0.9286	2.6329
7	4	3.4350	1.5477	3.8122	0.9286	2.5730
8	4	3.3613	1.5477	3.7775	0.9286	2.4648
9	4	3.7353	1.5477	3.7145	0.8418	2.7206
10	4	3.7024	1.4030	3.8270	0.8418	2.6667
11	4	3.6679	1.4030	3.7956	0.8418	2.6120
12	4	3.6007	1.4030	3.7625	0.8418	2.5046
13	4	3.9583	1.4030	3.6982	0.7681	2.7977
14	4	3.9436	1.2802	3.8355	0.7681	2.7728
15	4	3.9317	1.2802	3.8199	0.7681	2.7477
16	4	3.9000	1.2802	3.8069	0.7681	2.6931
1	6	3.3602	1.2802	3.7733	0.9031	2.7182
2	6	3.3306	0.9342	3.6495	0.9031	2.6758
3	6	3.2770	1.5051	3.5653	0.9031	2.6010

Cul-vert	D (ft)	Reliability (with γ_{LL}=1.35)	Calibrated factor γ_{LL}	Calibrated reliability	Scaled factor γ_{LL}	Scaled reliability
4	6	3.1866	1.5051	3.5391	0.9031	2.4777
5	6	3.5146	1.5051	3.4915	0.8002	2.6999
6	6	3.4785	1.5051	3.4103	0.8002	2.6439
7	6	3.4347	1.3337	3.4921	0.8002	2.5754
8	6	3.3493	1.3337	3.4555	0.8002	2.4494
9	6	3.6296	1.3337	3.4112	0.7157	2.6940
10	6	3.5944	1.3337	3.3247	0.7157	2.6343
11	6	3.5619	1.1929	3.4112	0.7157	2.5801
12	6	3.4841	1.1929	3.3707	0.7157	2.4604
13	6	3.7507	1.1929	3.3336	0.6454	2.7501
14	6	3.7359	1.1929	3.2468	0.6454	2.7234
15	6	3.7240	1.0756	3.3795	0.6454	2.6942
16	6	3.6903	1.0756	3.3606	0.6454	2.6364
1	8	3.2288	1.0756	3.3427	0.7776	2.7220
2	8	3.1967	1.0756	3.3006	0.7776	2.6785
3	8	3.1394	0.7581	3.1837	0.7776	2.6027
4	8	3.0416	1.2961	3.1826	0.7776	2.4775
5	8	3.3004	1.2961	3.1495	0.6816	2.6936
6	8	3.2623	1.2961	3.0906	0.6816	2.6393
7	8	3.2133	1.2961	2.9904	0.6816	2.5705
8	8	3.1190	1.1359	3.1118	0.6816	2.4455
9	8	3.3589	1.1359	3.0689	0.6048	2.6802
10	8	3.3190	1.1359	3.0140	0.6048	2.6215
11	8	3.2820	1.1359	2.9105	0.6048	2.5685
12	8	3.1999	1.0080	3.0556	0.6048	2.4558
13	8	3.4414	1.0080	3.0076	0.5426	2.7349
14	8	3.4233	1.0080	2.9637	0.5426	2.7071
15	8	3.4060	1.0080	2.8684	0.5426	2.6805
16	8	3.3697	0.9043	3.0603	0.5426	2.6264
17	2	2.4673	0.9043	3.0371	1.4184	2.6122
18	2	2.4582	0.9043	3.0149	1.4184	2.6038
19	2	2.4418	0.9043	2.9693	1.4184	2.5885
20	2	2.6856	0.6372	2.9950	1.2659	2.4988
21	2	2.6261	2.3641	4.1339	1.2659	2.4384
22	2	2.5878	2.3641	4.1315	1.2659	2.3984
23	2	2.9066	2.3641	4.1238	1.1423	2.4308
24	2	2.9008	2.1099	4.0065	1.1423	2.4219
25	2	2.8881	2.1099	3.9494	1.1423	2.4055
26	2	2.8708	2.1099	3.9188	1.1423	2.3836
27	2	3.2276	1.9038	3.9091	1.0400	2.4900
28	2	3.2198	1.9038	3.9080	1.0400	2.4814
29	2	3.2148	1.9038	3.9007	1.0400	2.4733
30	2	3.1975	1.9038	3.8905	1.0400	2.4485
31	2	3.5105	1.7333	3.9555	0.9539	2.5420

Cul-vert	D (ft)	Reliability (with γ_{LL}=1.35)	Calibrated factor γ_{LL}	Calibrated reliability	Scaled factor γ_{LL}	Scaled reliability
32	2	3.5002	1.7333	3.9481	0.9539	2.5250
33	2	3.5028	1.7333	3.9455	0.9539	2.5315
34	2	3.5077	1.7333	3.9335	0.9539	2.5398
17	4	2.6053	1.5898	3.9835	1.3153	2.5401
18	4	2.5714	1.5898	3.9756	1.3153	2.5051
19	4	2.5297	1.5898	3.9768	1.3153	2.4620
20	4	2.7962	1.5898	3.9805	1.1588	2.4174
21	4	2.7830	2.1921	3.8819	1.1588	2.4017
22	4	2.7428	2.1921	3.8648	1.1588	2.3543
23	4	3.1657	2.1921	3.8420	1.0325	2.5243
24	4	3.1444	1.9313	3.7342	1.0325	2.4942
25	4	3.1196	1.9313	3.7256	1.0325	2.4595
26	4	3.0888	1.9313	3.6986	1.0325	2.4167
27	4	3.4343	1.7209	3.7873	0.9286	2.5458
28	4	3.4299	1.7209	3.7724	0.9286	2.5389
29	4	3.4170	1.7209	3.7547	0.9286	2.5204
30	4	3.3875	1.7209	3.7325	0.9286	2.4754
31	4	3.6967	1.5477	3.7837	0.8418	2.6064
32	4	3.6781	1.5477	3.7801	0.8418	2.5743
33	4	3.6732	1.5477	3.7688	0.8418	2.5718
34	4	3.6820	1.5477	3.7439	0.8418	2.5882
17	6	2.8007	1.4030	3.7933	1.1907	2.5629
18	6	2.7530	1.4030	3.7756	1.1907	2.5077
19	6	2.6955	1.4030	3.7706	1.1907	2.4421
20	6	3.0512	1.4030	3.7788	1.0303	2.5328
21	6	3.0299	1.9844	3.6211	1.0303	2.5074
22	6	2.9849	1.9844	3.5933	1.0303	2.4474
23	6	3.3389	1.9844	3.5576	0.9031	2.6130
24	6	3.3180	1.7171	3.5710	0.9031	2.5752
25	6	3.2887	1.7171	3.5531	0.9031	2.5284
26	6	3.2543	1.7171	3.5200	0.9031	2.4734
27	6	3.5360	1.5051	3.5644	0.8002	2.5929
28	6	3.5248	1.5051	3.5475	0.8002	2.5775
29	6	3.5115	1.5051	3.5225	0.8002	2.5589
30	6	3.4815	1.5051	3.4932	0.8002	2.5050
31	6	3.7139	1.3337	3.5107	0.7157	2.6160
32	6	3.7005	1.3337	3.4995	0.7157	2.5810
33	6	3.6844	1.3337	3.4860	0.7157	2.5750
34	6	3.6753	1.3337	3.4555	0.7157	2.5711
17	8	2.9680	1.1929	3.4642	1.0593	2.6590
18	8	2.9310	1.1929	3.4467	1.0593	2.6069
19	8	2.8732	1.1929	3.4323	1.0593	2.5343
20	8	3.1270	1.1929	3.4240	0.9001	2.6067
21	8	3.1038	1.7655	3.3823	0.9001	2.5791

Cul-vert	D (ft)	Reliability (with γ_{LL}=1.35)	Calibrated factor γ_{LL}	Calibrated reliability	Scaled factor γ_{LL}	Scaled reliability
22	8	3.0599	1.7655	3.3632	0.9001	2.5143
23	8	3.2806	1.7655	3.3229	0.7776	2.6519
24	8	3.2684	1.5001	3.2907	0.7776	2.6166
25	8	3.2486	1.5001	3.2688	0.7776	2.5741
26	8	3.2150	1.5001	3.2309	0.7776	2.5157
27	8	3.4008	1.2961	3.2239	0.6816	2.6257
28	8	3.3851	1.2961	3.2097	0.6816	2.6069
29	8	3.3646	1.2961	3.1881	0.6816	2.5830
30	8	3.3391	1.2961	3.1524	0.6816	2.5311
31	8	3.4928	1.1359	3.1625	0.6048	2.6299
32	8	3.4838	1.1359	3.1458	0.6048	2.5973
33	8	3.4569	1.1359	3.1243	0.6048	2.5861
34	8	3.4315	1.1359	3.0912	0.6048	2.5532

Table E.2 Reliability and calibrated reliability for AASHTO legal loads

Cul-vert	D (ft)	Reliability (with γ_{LL}=2.0)	Calibrated factor γ_{LL}	Calibrated reliability	Scaled factor γ_{LL}	Scaled reliability
1	2	2.5752	2.7789	3.4996	1.9453	2.4986
2	2	2.5643	2.7789	3.4953	1.9453	2.4871
3	2	2.5312	2.7789	3.4743	1.9453	2.4527
4	2	2.4778	2.7789	3.4404	1.9453	2.3972
5	2	3.0399	2.5300	3.6988	1.7710	2.7078
6	2	3.0192	2.5300	3.6845	1.7710	2.6831
7	2	3.0055	2.5300	3.6796	1.7710	2.6640
8	2	2.9535	2.5300	3.6420	1.7710	2.6029
9	2	3.2943	2.3205	3.7062	1.6244	2.7355
10	2	3.2756	2.3205	3.6925	1.6244	2.7085
11	2	3.3921	2.3205	3.8158	1.6244	2.8155
12	2	3.3482	2.3205	3.7810	1.6244	2.7564
13	2	3.7607	2.1418	3.9491	1.4993	2.9992
14	2	3.7637	2.1418	3.9533	1.4993	2.9969
15	2	3.7453	2.1418	3.9359	1.4993	2.9734
16	2	3.7267	2.1418	3.9196	1.4993	2.9437
1	4	2.8468	1.6299	4.4579	1.7583	2.5676
2	4	2.8134	2.5119	3.3731	1.7583	2.5298
3	4	2.7599	2.5119	3.3466	1.7583	2.4686
4	4	2.6690	2.5119	3.3054	1.7583	2.3650
5	4	3.0957	2.5119	3.2342	1.5814	2.5983
6	4	3.0588	2.2592	3.3725	1.5814	2.5513
7	4	3.0196	2.2592	3.3404	1.5814	2.4985
8	4	2.9307	2.2592	3.3076	1.5814	2.3867
9	4	3.3217	2.2592	3.2295	1.4335	2.6412
10	4	3.2808	2.0478	3.3740	1.4335	2.5850
11	4	3.2535	2.0478	3.3342	1.4335	2.5407

Cul-vert	D (ft)	Reliability (with γ_{LL}=2.0)	Calibrated factor γ_{LL}	Calibrated reliability	Scaled factor γ_{LL}	Scaled reliability
12	4	3.1724	2.0478	3.3079	1.4335	2.4301
13	4	3.5708	2.0478	3.2288	1.3081	2.7408
14	4	3.5643	1.8687	3.4256	1.3081	2.7243
15	4	3.5450	1.8687	3.4176	1.3081	2.6955
16	4	3.5153	1.8687	3.3969	1.3081	2.6464
1	6	3.0589	1.8687	3.3642	1.5379	2.6697
2	6	3.0236	1.3636	3.5601	1.5379	2.6263
3	6	2.9605	2.1969	3.2163	1.5379	2.5496
4	6	2.8555	2.1969	3.1841	1.5379	2.4236
5	6	3.2081	2.1969	3.1261	1.3627	2.6554
6	6	3.1651	2.1969	3.0289	1.3627	2.5982
7	6	3.1104	1.9468	3.1640	1.3627	2.5265
8	6	3.0105	1.9468	3.1199	1.3627	2.3979
9	6	3.3217	1.9468	3.0640	1.2189	2.6509
10	6	3.2788	1.9468	2.9619	1.2189	2.5897
11	6	3.2446	1.7412	3.1075	1.2189	2.5378
12	6	3.1542	1.7412	3.0591	1.2189	2.4161
13	6	3.4660	1.7412	3.0196	1.0990	2.7194
14	6	3.4539	1.7412	2.9197	1.0990	2.6959
15	6	3.4284	1.5700	3.1205	1.0990	2.6605
16	6	3.3928	1.5700	3.1033	1.0990	2.6046
1	8	3.0414	1.5700	3.0734	1.3243	2.6970
2	8	3.0051	1.5700	3.0288	1.3243	2.6528
3	8	2.9412	1.1066	3.1442	1.3243	2.5761
4	8	2.8336	1.8918	2.9874	1.3243	2.4495
5	8	3.1095	1.8918	2.9499	1.1607	2.6709
6	8	3.0665	1.8918	2.8841	1.1607	2.6160
7	8	3.0115	1.8918	2.7735	1.1607	2.5464
8	8	2.9079	1.6581	2.9342	1.1607	2.4202
9	8	3.1683	1.6581	2.8866	1.0300	2.6599
10	8	3.1233	1.6581	2.8259	1.0300	2.6006
11	8	3.0816	1.6581	2.7135	1.0300	2.5468
12	8	2.9912	1.4714	2.8959	1.0300	2.4331
13	8	3.2568	1.4714	2.8434	0.9240	2.7165
14	8	3.2362	1.4714	2.7953	0.9240	2.6884
15	8	3.2167	1.4714	2.6927	0.9240	2.6615
16	8	3.1759	1.3200	2.9202	0.9240	2.6070
17	2	1.3971	1.3200	2.8950	2.4155	1.9573
18	2	1.3844	1.3200	2.8710	2.4155	1.9492
19	2	1.3526	1.3200	2.8218	2.4155	1.9238
20	2	2.0859	0.9301	2.9537	2.1558	2.3040
21	2	2.0095	3.4507	3.0041	2.1558	2.2290
22	2	1.9839	3.4507	3.0020	2.1558	2.2057
23	2	2.4933	3.4507	2.9845	1.9453	2.4145

Cul-vert	D (ft)	Reliability (with γ_{LL}=2.0)	Calibrated factor γ_{LL}	Calibrated reliability	Scaled factor γ_{LL}	Scaled reliability
24	2	2.4887	3.0798	3.3450	1.9453	2.4093
25	2	2.4753	3.0798	3.2736	1.9453	2.3953
26	2	2.4513	3.0798	3.2588	1.9453	2.3705
27	2	2.8880	2.7789	3.4377	1.7710	2.5459
28	2	2.9386	2.7789	3.4384	1.7710	2.5955
29	2	2.8829	2.7789	3.4315	1.7710	2.5387
30	2	2.8646	2.7789	3.4155	1.7710	2.5167
31	2	3.1712	2.5300	3.5614	1.6244	2.5951
32	2	3.1611	2.5300	3.6141	1.6244	2.5807
33	2	3.2999	2.5300	3.5595	1.6244	2.7187
34	2	3.3430	2.5300	3.5470	1.6244	2.7629
17	4	1.9862	2.3205	3.5927	2.2398	2.2590
18	4	1.9400	2.3205	3.5851	2.2398	2.2189
19	4	1.8810	2.3205	3.7256	2.2398	2.1667
20	4	2.3672	2.3205	3.7684	1.9733	2.3346
21	4	2.3490	3.1997	3.1603	1.9733	2.3161
22	4	2.3007	3.1997	3.1353	1.9733	2.2672
23	4	2.7440	3.1997	3.1000	1.7583	2.4449
24	4	2.7173	2.8190	3.2321	1.7583	2.4135
25	4	2.6865	2.8190	3.2189	1.7583	2.3776
26	4	2.6486	2.8190	3.1859	1.7583	2.3333
27	4	2.9959	2.5119	3.3003	1.5814	2.4567
28	4	3.0030	2.5119	3.2807	1.5814	2.4612
29	4	2.9862	2.5119	3.2577	1.5814	2.4408
30	4	2.9503	2.5119	3.2293	1.5814	2.3943
31	4	3.2562	2.2592	3.2913	1.4335	2.5174
32	4	3.2321	2.2592	3.2996	1.4335	2.4831
33	4	3.2444	2.2592	3.2845	1.4335	2.4956
34	4	3.2394	2.2592	3.2533	1.4335	2.4983
17	6	2.4743	2.0478	3.3121	2.0276	2.4989
18	6	2.4166	2.0478	3.2886	2.0276	2.4420
19	6	2.3480	2.0478	3.3009	2.0276	2.3744
20	6	2.7050	2.0478	3.2954	1.7545	2.4675
21	6	2.6848	2.8966	3.2010	1.7545	2.4451
22	6	2.6305	2.8966	3.1646	1.7545	2.3832
23	6	3.0008	2.8966	3.1191	1.5379	2.5557
24	6	2.9722	2.5064	3.1535	1.5379	2.5159
25	6	2.9350	2.5064	3.1372	1.5379	2.4670
26	6	2.8913	2.5064	3.0951	1.5379	2.4096
27	6	3.1907	2.1969	3.1775	1.3627	2.5417
28	6	3.1706	2.1969	3.1528	1.3627	2.5202
29	6	3.1604	2.1969	3.1196	1.3627	2.5052
30	6	3.1227	2.1969	3.0807	1.3627	2.4496
31	6	3.3601	1.9468	3.1399	1.2189	2.5632

Culvert	D (ft)	Reliability (with γ_{LL}=2.0)	Calibrated factor γ_{LL}	Calibrated reliability	Scaled factor γ_{LL}	Scaled reliability
32	6	3.3402	1.9468	3.1197	1.2189	2.5265
33	6	3.3330	1.9468	3.1091	1.2189	2.5258
34	6	3.3276	1.9468	3.0701	1.2189	2.5240
17	8	2.7398	1.7412	3.1098	1.8039	2.6188
18	8	2.6920	1.7412	3.0851	1.8039	2.5649
19	8	2.6237	1.7412	3.0796	1.8039	2.4904
20	8	2.8803	1.7412	3.0751	1.5327	2.5670
21	8	2.8578	2.5770	3.0817	1.5327	2.5412
22	8	2.8046	2.5770	3.0502	1.5327	2.4750
23	8	3.0504	2.5770	2.9977	1.3243	2.6209
24	8	3.0303	2.1896	3.0029	1.3243	2.5845
25	8	3.0028	2.1896	2.9816	1.3243	2.5409
26	8	2.9608	2.1896	2.9332	1.3243	2.4813
27	8	3.1610	1.8918	2.9835	1.1607	2.5972
28	8	3.1413	1.8918	2.9610	1.1607	2.5764
29	8	3.1216	1.8918	2.9311	1.1607	2.5535
30	8	3.0884	1.8918	2.8864	1.1607	2.5005
31	8	3.2527	1.6581	2.9371	1.0300	2.6034
32	8	3.2375	1.6581	2.9170	1.0300	2.5700
33	8	3.2146	1.6581	2.8961	1.0300	2.5593
34	8	3.1860	1.6581	2.8553	1.0300	2.5254

Table E.3 Reliability and calibrated reliability for FAST Act emergency vehicles as surrogate loads

Culvert	D (ft)	Reliability (with γ_{LL}=2.0)	Calibrated factor γ_{LL}	Calibrated reliability	Scaled factor γ_{LL}	Scaled reliability
1	2	4.1877	1.5545	3.4518	1.0881	2.4526
2	2	4.1845	1.5545	3.4448	1.0881	2.4383
3	2	4.1696	1.5545	3.4230	1.0881	2.4030
4	2	4.1462	1.5545	3.3887	1.0881	2.3466
5	2	4.4926	1.4152	3.4859	0.9907	2.5055
6	2	4.4802	1.4152	3.4660	0.9907	2.4744
7	2	4.4845	1.4152	3.4594	0.9907	2.4525
8	2	4.4571	1.4152	3.4152	0.9907	2.3826
9	2	4.6640	1.2981	3.4201	0.9086	2.4660
10	2	4.6518	1.2981	3.3961	0.9086	2.4279
11	2	4.7664	1.2981	3.4925	0.9086	2.5088
12	2	4.7415	1.2981	3.4455	0.9086	2.4345
13	2	5.0217	1.1981	3.5612	0.8387	2.6406
14	2	5.0147	1.1981	3.5482	0.8387	2.6215
15	2	5.0496	1.1981	3.5711	0.8387	2.6344
16	2	5.0321	1.1981	3.5399	0.8387	2.5888
1	4	4.3206	1.4051	3.4209	0.9836	2.6097
2	4	4.3032	1.4051	3.3948	0.9836	2.5727

Cul-vert	D (ft)	Reliability (with γ_{LL}=2.0)	Calibrated factor γ_{LL}	Calibrated reliability	Scaled factor γ_{LL}	Scaled reliability
3	4	4.2782	1.4051	3.3546	0.9836	2.5126
4	4	4.2330	1.4051	3.2851	0.9836	2.4111
5	4	4.5798	1.2637	3.4188	0.8846	2.6384
6	4	4.5633	1.2637	3.3874	0.8846	2.5923
7	4	4.5518	1.2637	3.3557	0.8846	2.5407
8	4	4.5083	1.2637	3.2792	0.8846	2.4309
9	4	4.8066	1.1455	3.4183	0.8019	2.6787
10	4	4.7880	1.1455	3.3793	0.8019	2.6235
11	4	4.7852	1.1455	3.3540	0.8019	2.5803
12	4	4.7464	1.1455	3.2765	0.8019	2.4714
13	4	5.0206	1.0453	3.4449	0.7317	2.7567
14	4	5.0115	1.0453	3.4257	0.7317	2.7310
15	4	5.0095	1.0453	3.4103	0.7317	2.7067
16	4	4.9912	1.0453	3.3694	0.7317	2.6508
1	6	4.2409	1.2289	3.2509	0.8602	2.6965
2	6	4.2246	1.2289	3.2193	0.8602	2.6537
3	6	4.1934	1.2289	3.1623	0.8602	2.5781
4	6	4.1380	1.2289	3.0668	0.8602	2.4535
5	6	4.4165	1.0890	3.1964	0.7623	2.6802
6	6	4.3971	1.0890	3.1531	0.7623	2.6237
7	6	4.3711	1.0890	3.0981	0.7623	2.5528
8	6	4.3199	1.0890	2.9976	0.7623	2.4256
9	6	4.5237	0.9740	3.1369	0.6818	2.6730
10	6	4.5064	0.9740	3.0892	0.6818	2.6125
11	6	4.4974	0.9740	3.0504	0.6818	2.5612
12	6	4.4511	0.9740	2.9519	0.6818	2.4406
13	6	4.6156	0.8782	3.1351	0.6148	2.7302
14	6	4.6087	0.8782	3.1130	0.6148	2.7031
15	6	4.6091	0.8782	3.0912	0.6148	2.6738
16	6	4.5917	0.8782	3.0431	0.6148	2.6153
1	8	3.8143	1.0582	3.0064	0.7408	2.7108
2	8	3.7941	1.0582	2.9693	0.7408	2.6670
3	8	3.7562	1.0582	2.9042	0.7408	2.5908
4	8	3.6868	1.0582	2.7946	0.7408	2.4650
5	8	3.8964	0.9275	2.9514	0.6493	2.6834
6	8	3.8727	0.9275	2.9043	0.6493	2.6289
7	8	3.8411	0.9275	2.8441	0.6493	2.5598
8	8	3.7738	0.9275	2.7326	0.6493	2.4342
9	8	3.9542	0.8231	2.9114	0.5762	2.6711
10	8	3.9292	0.8231	2.8593	0.5762	2.6121
11	8	3.9040	0.8231	2.8116	0.5762	2.5586
12	8	3.8457	0.8231	2.7097	0.5762	2.4455
13	8	4.0105	0.7384	2.9336	0.5169	2.7261
14	8	3.9993	0.7384	2.9086	0.5169	2.6982

Cul-vert	D (ft)	Reliability (with γ_{LL}=2.0)	Calibrated factor γ_{LL}	Calibrated reliability	Scaled factor γ_{LL}	Scaled reliability
15	8	3.9890	0.7384	2.8848	0.5169	2.6715
16	8	3.9653	0.7384	2.8359	0.5169	2.6172
17	2	3.1817	1.9303	3.0769	1.3512	2.0302
18	2	3.1714	1.9303	3.0663	1.3512	2.0137
19	2	3.1562	1.9303	3.0505	1.3512	1.9903
20	2	3.8299	1.7228	3.3851	1.2059	2.3434
21	2	3.7531	1.7228	3.3082	1.2059	2.2631
22	2	3.7467	1.7228	3.2992	1.2059	2.2458
23	2	4.1581	1.5545	3.4108	1.0881	2.3884
24	2	4.1582	1.5545	3.4079	1.0881	2.3796
25	2	4.1511	1.5545	3.3974	1.0881	2.3620
26	2	4.1423	1.5545	3.3841	1.0881	2.3396
27	2	4.4395	1.4152	3.4141	0.9907	2.4037
28	2	4.4811	1.4152	3.4525	0.9907	2.4395
29	2	4.4787	1.4152	3.4473	0.9907	2.4302
30	2	4.4694	1.4152	3.4315	0.9907	2.4045
31	2	4.6306	1.2981	3.3605	0.9086	2.3729
32	2	4.6234	1.2981	3.3475	0.9086	2.3526
33	2	4.7614	1.2981	3.4786	0.9086	2.4827
34	2	4.8240	1.2981	3.5394	0.9086	2.5447
17	4	3.5073	1.7899	3.2123	1.2529	2.3075
18	4	3.4867	1.7899	3.1880	1.2529	2.2684
19	4	3.4561	1.7899	3.1535	1.2529	2.2173
20	4	3.9244	1.5769	3.2841	1.1038	2.3827
21	4	3.9141	1.5769	3.2712	1.1038	2.3646
22	4	3.8894	1.5769	3.2388	1.1038	2.3167
23	4	4.2856	1.4051	3.3503	0.9836	2.4902
24	4	4.2749	1.4051	3.3313	0.9836	2.4596
25	4	4.2619	1.4051	3.3089	0.9836	2.4245
26	4	4.2454	1.4051	3.2812	0.9836	2.3812
27	4	4.5550	1.2637	3.3404	0.8846	2.5007
28	4	4.5679	1.2637	3.3489	0.8846	2.5055
29	4	4.5579	1.2637	3.3340	0.8846	2.4854
30	4	4.5416	1.2637	3.3036	0.8846	2.4398
31	4	4.8121	1.1455	3.3593	0.8019	2.5588
32	4	4.8008	1.1455	3.3363	0.8019	2.5253
33	4	4.8146	1.1455	3.3487	0.8019	2.5377
34	4	4.7992	1.1455	3.3428	0.8019	2.5399
17	6	3.7163	1.6203	3.2436	1.1342	2.5348
18	6	3.6908	1.6203	3.2081	1.1342	2.4791
19	6	3.6575	1.6203	3.1638	1.1342	2.4128
20	6	4.0040	1.4020	3.1953	0.9814	2.5024
21	6	3.9934	1.4020	3.1793	0.9814	2.4803
22	6	3.9687	1.4020	3.1382	0.9814	2.4196

Cul-vert	D (ft)	Reliability (with γ_{LL}=2.0)	Calibrated factor γ_{LL}	Calibrated reliability	Scaled factor γ_{LL}	Scaled reliability
23	6	4.2882	1.2289	3.2161	0.8602	2.5868
24	6	4.2808	1.2289	3.1921	0.8602	2.5478
25	6	4.2659	1.2289	3.1598	0.8602	2.4999
26	6	4.2490	1.2289	3.1218	0.8602	2.4435
27	6	4.5220	1.0890	3.1772	0.7623	2.5715
28	6	4.5045	1.0890	3.1571	0.7623	2.5500
29	6	4.5024	1.0890	3.1467	0.7623	2.5352
30	6	4.4887	1.0890	3.1087	0.7623	2.4806
31	6	4.6959	0.9740	3.1443	0.6818	2.5900
32	6	4.6933	0.9740	3.1203	0.6818	2.5540
33	6	4.6828	0.9740	3.1146	0.6818	2.5531
34	6	4.6754	0.9740	3.1100	0.6818	2.5511
17	8	3.6648	1.4416	3.1113	1.0091	2.6413
18	8	3.6566	1.4416	3.0811	1.0091	2.5886
19	8	3.6269	1.4416	3.0300	1.0091	2.5153
20	8	3.8661	1.2248	3.0309	0.8574	2.5881
21	8	3.8526	1.2248	3.0098	0.8574	2.5626
22	8	3.8335	1.2248	2.9626	0.8574	2.4972
23	8	3.9899	1.0582	3.0070	0.7408	2.6383
24	8	3.9999	1.0582	2.9854	0.7408	2.6026
25	8	4.0019	1.0582	2.9563	0.7408	2.5597
26	8	3.9917	1.0582	2.9126	0.7408	2.5008
27	8	4.1421	0.9275	2.9592	0.6493	2.6135
28	8	4.1242	0.9275	2.9392	0.6493	2.5927
29	8	4.1094	0.9275	2.9183	0.6493	2.5699
30	8	4.1053	0.9275	2.8783	0.6493	2.5176
31	8	4.2279	0.8231	2.9264	0.5762	2.6179
32	8	4.2360	0.8231	2.9024	0.5762	2.5850
33	8	4.1978	0.8231	2.8854	0.5762	2.5739
34	8	4.1760	0.8231	2.8542	0.5762	2.5402